universität wien

MASTERARBEIT / MASTER'S THESIS

Titel der Masterarbeit / Title of the Master's Thesis

„Surface dynamics of a landslide in Gresten, Lower Austria – Structure from Motion (SfM) analysis of UAV-based Digital Surface Models“

verfasst von / submitted by

Bastian Lindemair, B.Sc.

angestrebter akademischer Grad / in partial fulfilment of the requirements for the degree of

Master of Science (MSc)

Wien, 2021 / Vienna 2021

Studienkennzahl lt. Studienblatt / degree programme code as it appears on the student record sheet:	UA 066 855
Studienrichtung lt. Studienblatt / degree programme as it appears on the student record sheet:	Masterstudium Geographie
Betreut von / Supervisor:	Univ.-Prof. Dipl.-Geogr. Dr. Thomas Glade

Statutory Declaration | Eidesstattliche Erklärung

I hereby declare,

- that I have written this master's thesis independently, have not used any sources or references other than those indicated, and have not made use of any other unauthorized assistance,
- that I have not previously submitted the topic of this master's thesis in any form as an examination paper neither in Austria nor abroad
- and that this thesis is in complete agreement with the thesis assessed by the supervisor.

Hiermit versichere ich,

- dass ich die vorliegende Masterarbeit selbstständig verfasst, andere als die angegebenen Quellen und Hilfsmittel nicht benutzt und mich auch sonst keiner unerlaubter Hilfe bedient habe,
- dass ich dieses Masterarbeitsthema bisher weder im In- noch im Ausland in irgendeiner Form als Prüfungsarbeit vorgelegt habe
- und dass diese Arbeit mit der vom Begutachter beurteilten Arbeit vollständig übereinstimmt.

Wien, am 17.08.2021

Acknowledgements

In the very beginning, I want to thank my supervisor Professor Dr. Thomas Glade for guiding me through my studies in Vienna over the last years. Thank you for your advices, critical suggestions, and your constant encouragement – you helped me to find my direction in the field of Geography like no one else.

I also would like to express my great appreciation to Margherita Stumvoll for the constant accompaniment of my master thesis from the very beginning to the end. Thank you very much for the interesting times in the field and your suggestions for improvement as well as your continual feedback as soon as things became unclear for me. I wish you all the best for your time after your PhD.

Thank you, Robert Kanta, for your friendly support with my data acquisition – you saved me a lot of time and frustration with your technical knowledge. The countless conversations we had during my studies have been very enriching. May the Metal-Bus live on.

I also want to thank William Ries for giving me valuable hints and tips regarding my data acquisition. Really wishing you and your family all the best for your future.

Finally, I would like to thank all the people around me. Beginning with my two flatmates who made corona lockdowns at least a little more bearable. Thanks for the great times, enriching conversations, and motivation you two gave me. You will soon finish your masters as well so all the best for that. A big thank you to the ones who read and commented my thesis – I owe you.

And the last but most important thank you goes out for my parents, without whom none of this would have ever happened. Thank you for everything!

Summary

People and infrastructure are affected by various forms of landslides and their impacts in various regions of the Federal State of Lower Austria. Among other things, responsible for their frequent occurrence is the highly weathered geology of the Grestner Klippen Zone and the Flysch Zone. In addition, changing precipitation patterns due to the global environmental change, as well as the tendency of urban sprawl in previously less populated areas will presumably lead to an increase of landslide occurrences affecting humans in the future.

In parallel, enhanced technologies and innovations are enabling the investigation of landslides and their associated processes and dynamics in order to better understand, analyze, monitor and forecast them. Unmanned aerial vehicles (UAV), often called drones, have now entered the commercial market for a while and offer a low-cost alternative to more traditional remote sensing methods.

The landslide under investigation is embedded in the NoeSLIDE Project, which was launched in 2015 through a cooperation of Austrian Universities and various natural science agencies of Austria. The aim is to better understand and investigate different gravitational mass movements in Lower Austria through long-term monitoring. This master thesis was written in cooperation with the ENGAGE working group of the University of Vienna. Previous findings and knowledge from their studies on the landslide were thus incorporated into this thesis.

This master thesis investigates the surface dynamics of a landslide in Gresten in the district of Scheibbs, Lower Austria over the winter of 2020/2021. The study area is about 4000 m^2 in size and is located at about 430-470 meters above sea level.

For the investigation, three aerial surveys were carried out with a drone, and several analyses were performed based on the acquired images. Here, the image processing method "*Structure-from-Motion*" was used, in which topographic structures can be reconstructed from overlapping, two-dimensional images. A three-dimensional point clouds as well as digital terrain models of the study area were generated and compared with each other in order to determine surface changes caused by landslide movements. The surface analysis is complemented by the inclusion of surface data

from 2007, 2009, and 2014 to display the evolution of the main scarps and other landslide features over more than 13 years.

The results of the surface analysis over the winter of 2020/2021 indicate surface movements within double-digit centimeter ranges and confirm previously assumed movement rates of the landslides main body. Areas of depletion as well as accumulation were identified, displacement of the main scarps due to surface movements were mapped, and cross-sectional profiles as well as so-called DEMs of Difference (DoD) illustrate temporal elevation loss, and gain.

Thus, this work not only shows that UAV remote sensing can be used as a surface sensing method even for shorter observation periods, but also that many different methodological approaches exist to process the acquired data.

The final analysis of the data showed that the landslide moved in phases/episodically over the observation period. The lower part of the landslide is affected by its use as a horse pasture, while in the upper part experienced more movements, especially along the main scarps. In addition, the knowledge gained about landslide movements reinforces the theories that the body moves on multiple shear surfaces and therefore has complex characteristics for a rotational landslide.

Finally, this paper points out uncertainties of the study as well as of the landslide itself, so that further knowledge and data about the landslide in Gresten can be gathered in subsequent investigations.

Zusammenfassung

In vielen Regionen im Land Niederösterreich sind Menschen-, und Infrastruktur durch verschiedene Formen von gravitativen Massenbewegungen und deren Auswirkungen betroffen. Das häufige Auftreten ist unter anderem auf die stark verwitterte Geologie der Grestner Klippenzone und der Flysch Zone zurückzuführen. Hinzukommen veränderte Niederschlagsmuster durch den globalen Umweltwandel, sowie zunehmende Tendenzen der Zersiedelung in bisher weniger bewohnten Landstrichen. Dadurch ist auch in Zukunft mit einem vermehrten Auftreten von Hangrutschungen zu rechnen.

Parallel dazu ermöglichen verbesserte Technologien und Innovation die Untersuchung von gravitativen Massenbewegungen und den damit verbunden Prozessen und Dynamiken, um diese zu verstehen und dadurch auch besser vorherzusagen. Unbemannte Luftfahrzeuge (UAV), oftmals Drohne genannt, sind mittlerweile auf dem kommerziellen Markt weit verbreitet und bieten eine preiswerte Alternative zu den traditionellen Fernerkundungsmethoden.

Die untersuchte Hangrutschung ist Teil des NoeSLIDE Projects, welches 2015 durch die Kooperation von einigen österreichischen Universitäten und naturwissenschaftlichen Behörden ins Leben gerufen wurde. Ziel ist es durch ein Langzeit-Monitoring Projekt von verschiedenen gravitativen Massenbewegungen in Niederösterreich, die Prozesse zu verstehen und zu erforschen. Hierbei wurde diese Masterarbeit in Abstimmung mit der Arbeitsgruppe ENGAGE der Universität Wien erstellt. Bisherige Erkenntnisse und Wissensstände aus vorherigen Untersuchungen über die Rutschung wurden auf diese Weise in dieser Arbeit miteinbezogen.

Diese Masterarbeit untersucht die Oberflächendynamiken einer gravitativen Massenbewegung in Gresten im Bezirk Scheibbs, NÖ über den Winter 2020/2021. Das Untersuchungsgebiet ist ca. 4000 m^2 groß und liegt auf ca. 430-470 m über dem Meeresspiegel.

Für die Untersuchung wurden drei Befliegungen mit einer Drohne durchgeführt, und auf Basis der Aufnahmen mehrere Auswertungen durchgeführt. Zum Einsatz kam die Bildverarbeitungsmethodik „*Structure-from-Motion*“, bei der topographische Gegebenheiten aus durch überschneidenden, zwei-dimensionalen Bilder,

rekonstruiert werden. Dadurch können dreidimensionale Punktwolken sowie Digitale Geländemodelle des Untersuchungsgebiets erzeugt, sowie miteinander verglichen werden, um Veränderungen der Oberfläche durch Rutschungsbewegungen zu ermitteln. Ergänzt wird die Oberflächenanalyse durch das Einbeziehen von Daten aus 2007, 2009 und 2014, um somit die Entwicklung von Abrisskanten und der Topographie über mehr als 13 Jahre darzustellen.

Die Ergebnisse der Oberflächenanalyse über den Winter 2020/2021 zeigen flächenhaft verteilte Bewegungen in zweistelligen Zentimeterbereichen auf und decken sich mit bisher angenommen Bewegungsraten der Rutschung. Veränderung des Reliefs sind durch Querschnittsprofile sowie sog. DEMs of Difference (DoD) nachweisbar und Bereiche der Abtragung, sowie Akkumulation konnten dadurch identifiziert und die Verschiebung der Abrisskanten durch Bewegungen der Oberfläche kartiert werden.

Einerseits zeigt diese Arbeit auf, dass die UAV-Fernerkundung für kürzere Beobachtungszeiträume als Oberflächenerkundungsmethode einsetzbar ist, und andererseits, dass es viele unterschiedliche methodischen Ansätze zur Auswertung der gewonnen Daten gibt.

Zusätzlich ergaben die Untersuchungen, dass die gravitative Massenbewegung sich über den Beobachtungszeitraum phasenweise bewegt hat. Der untere Bereich der Rutschung ist durch die Nutzung als Pferdeweide beeinflusst, während es im oberen Bereich vermehrt zu Dynamiken der Oberfläche, insbesondere entlang der Abrisskanten, kam. Des Weiteren wurden Bewegungen entlang der angrenzenden steileren Hänge im Westen festgestellt. Außerdem bestärken die gewonnen Erkenntnisse die Theorien über die gravitative Massenbewegung, dass diese sich auf mehreren unterirdischen Gleitflächen bewegt und dadurch komplexe Charakteristiken für eine eigentliche Rotationsrutschung aufweist. Abschließend wird auf neu entdeckte, sowie auf bereits bekannte Unklarheiten hingewiesen, sodass künftige Untersuchungen direkt, an die hier präsentierten Ergebnisse anknüpfen können.

Contents

List of abbreviations

ALS	airborne laser scanning
BBA	Bundle Block Adjustment
C2C	Cloud-to-cloud comparison
C2M	Cloud-to-mesh comparison
CMOS	complementary metal-oxide semiconductor
CSF	Cloth Simulation Filter
DEM	digital elevation model
DoD	digital terrain model of difference
DP	dynamic probing
DSM	digital surface model
DTM	digital terrain model
ERT	electrical resistivity tomography
GBA	Geological Survey of Austria
GCP	ground control points
GKZ	Gresten Klippen Zone
GNSS	global navigation satellite system
LiDAR	light detection and ranging
M3C2	Multiscale Model to Model Cloud Comparison
PBIA	pixel-based image analysis
RGB	red green blue
RTK	real time kinematic
SfM	structure from motion
TDR	time domain reflectometry
(p)TLS	terrestrial laser scanner (p – permanent)
UAV	unmanned aerial vehicle

List of Figures

List of Tables

1 Introduction

The basis for nearly every landslide is a topographical difference in elevation, possibly displaced material, and the earth's gravitational force. These conditions apply to almost every region in the world, which is the reason why landslides are among the most common, most distributed, and therefore deadliest natural hazards to exist (PETLEY 2012a). Landslides cause areas to be uninhabitable and shape the Earth's surface in its appearance on land as well as under water (KORUP 2012). They are defined as "*movements of a mass of rock, earth or debris down a slope*" (CRUDEN 1991: 28).

Between 1998-2017 landslides affected more than 4.8 M. people worldwide resulting in more than 18.000 casualties and causing economic losses worth more than 8 billion USD (UNDRR 2018). Usually, landslides occur if the gravitational force is greater than the friction force, or simply said, if the internal stability is no longer given, the slope fails (CROZIER 1986). What mainly triggers this movement in Austria is heavy rainfall followed by an oversaturation of the soil resulting in an unstable slope and the landslide itself (DIKAU & GLADE 2005; SCHWEIGL & HERVAS 2009).

Repeatedly proven and undisputed, the effects of environmental change affect the internal stability of natural and engineered slopes which has direct consequences on landslide occurrences (GARIANO & GUZZETTI 2016). According to the World Disasters Report 2020, climate and weather-related landslides occurred more than 16 times more often than "geophysical" landslides (e.g. triggered by an earthquake) since 1960 (IFRC 2020). Particularly changing air currents, more intense rainfalls and storms combined with an increasing altitude of temperatures will become more present especially for high mountainous regions and probably affect the susceptibility for landslides (HUGGEL et al. 2012).

For Austria, a decrease in average precipitation is predicted, while the intensity of rainfall is expected to increase. Such heavy rainfall events are responsible for many landslides and multiple forecasts point to the fact that they will be more common in the future due to the environmental change (GARIANO & GUZZETTI 2016).

Accordingly, the changing environment with all its various impacts will increase the frequency of landslides at a time where the world is becoming more and more populated.

At the same time, the number of new innovations and patents filed is increasing as humans constantly strive for technical improvements (ELLIS 2020). This master thesis makes use of unmanned aerial vehicles (=UAV) as a platform to survey the surface of a landslide in Gresten, Lower Austria. UAVs, also called drones, are a comparatively new addition to science and research fields because the technology and software behind it evolved a lot over the last decade. To illustrate the emerging role of UAVs in landslide research, Fig. 1 presents the rising numbers of papers published with the tags "*UAV*" and "*landslide*", based on usearch online library service from 2010 until 2020.

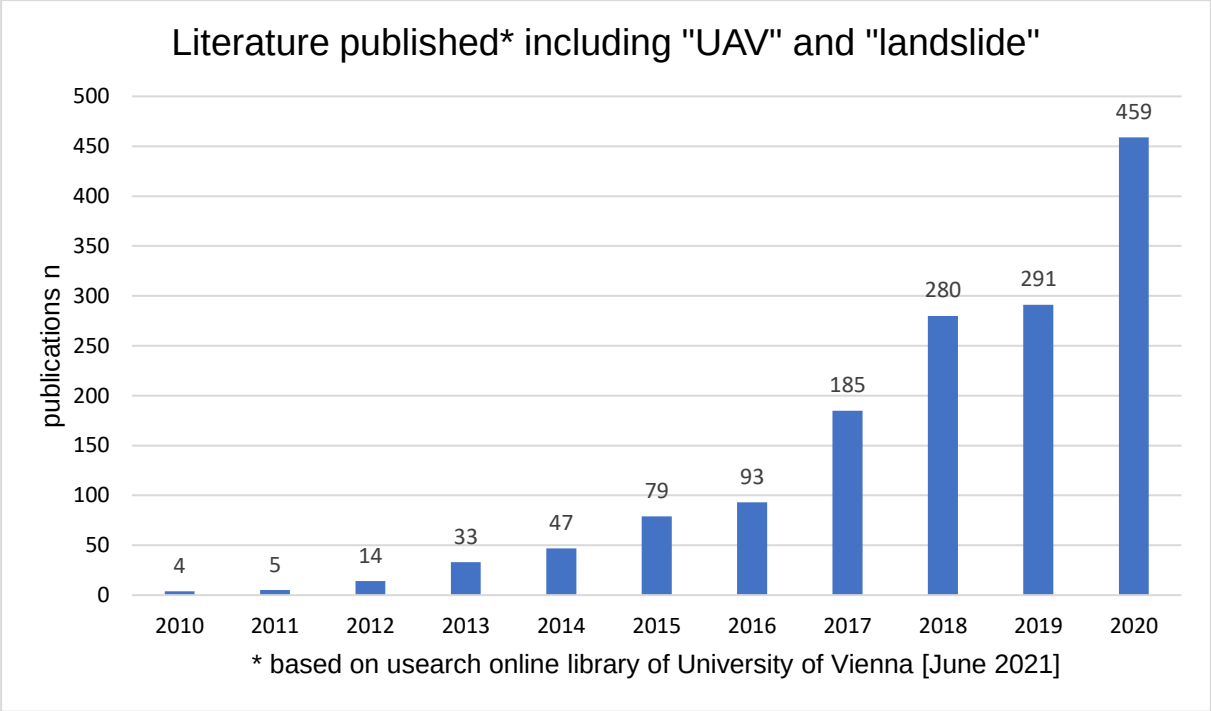

Figure 1: Peer-reviewed papers published with keywords "UAV" and "landslide" from 2010-2020

The diagram (Fig 1) shows how the number of papers published about landslide investigation with UAVs nearly reached exponential growth over 10 years. The absolute numbers show the amount of search hits on the usearch online library of the University of Vienna. This is only a selective choice of all published papers, so the absolute numbers do not represent the "true" number of publications, but it does show a certain trend.

So, the two developments, environmental change and technical improvements have and will certainly influence future landslide investigations.

This master thesis aims to analyze surface dynamics of a landslide in Lower Austria, a region prone for landslides due to the complex lithological background of the area with lots of weathered and therefore unstable rocks. A total of three UAV-surveys have been carried out between autumn 2020 and spring 2021 to determine surface changes. Data acquired in the process is used for Structure-from-Motion processing, which uses 2D images to recreate a 3D representation of the research area. Using these intermediate results, various calculations can be performed to accurately determine changes of the surface.

The thesis provides the reader with necessary background information and starts off by presenting important characteristics and attributes of landslides before going over to present various methods to determine landslide dynamics. This theoretical background is needed to understand surface processes and the discussion. The research area, including the geographic setting, land use, soil and climate will be described along with previous results of investigations at the Salcher landslide. Afterwards, the carried-out research is explained, and a differentiation is made between the methodological part, how the data was acquired and processed, and a part where results of the surface analysis are presented. The results of this investigation are discussed along with three hypotheses. Additionally, further interpretations are done for weather-, and subsurface data.

The thesis concludes with an overall summary of the most important results and a final chapter about the future development and research of the landslide.

2 Objectives and research questions

This master thesis links to previous research activities at the Salcher landslide in Lower Austria. The ENGAGE working group of the Institute of Geography and Regional Research from the University of Vienna is embedded in the NoeSLIDE project, along with the Geological Survey of Austria (GBA), the Provincial Government of Lower Austria, the Technical University of Vienna and the Austrian Service for Torrent and Avalanche Control (WLV). NoeSLIDE aims to investigate multiple landslides in Lower Austria, with a special focus on implementing long-term monitoring systems. Therefore, established as well as new, innovative methods of investigation and monitoring are applied on multiple sites for different types of landslides.

Within the NoeSLIDE project, the following master thesis carries out a UAV-based surface investigation of the Salcher landslide. Various studies and investigations have already been conducted here, but so far, - no Structure from Motion (SfM) analysis of UAV-based Digital Surface Models has been performed at this site.

In total three UAV-surveys have been carried out between the 18th of November 2020 and the 23rd of April 2021 to detect elevation changes and surface movements of the landslide. Additionally, laser scanning data from previous surface investigations was embedded in the final analysis and interpretation of the results. The focus is primarily on surface characteristics and movement patterns, however insights of the subsurface are indispensable for a more comprehensive understanding of the processes and will be addressed as well.

The surface analysis is based on three hypotheses with each being supported by at least two research questions:

> H1: "***Repeated SfM methodology can be used to investigate short-period surface dynamics of landslides.***"

Firstly, it will be tested if surface movements at a smaller scale can be detected, since the Salcher landslide is known for slow movement rates and UAV remote sensing is only an emerging methodological approach over the last decade. The approach pursues the possibility of a surface investigation in a comparably short-period (total 156 days). This hypothesis is accompanied by two research questions:

Q1.1: "*Can surface dynamics of a landslide be identified by comparing two- or more SfM-generated elevation models?"*

Question 1.1. refers directly to the first hypothesis 1 and aims to investigate surface dynamics with a DEM of Difference (DoD) analysis. Two elevation models of the same research area are superimposed to determine eventual height differences. Since there are three data acquisitions, three elevation models are available for an investigation of surface dynamics.

Q1.2: "*Did certain parts of the surface experience greater movements than others?*".

The second question aims to find out whether the applied SfM-method can also be used to determine different rates of movement. This differentiation is important for understanding surface dynamics and further interpretation.

H2: "***Digital Terrain model- and point cloud analysis are both suitable methods to gain information about landslide-surface dynamics.***"

The second hypothesis is more methodological and compares features of two different analytical approaches of surface change detection. Results of the DoD-analysis will be compared with the results of two different point cloud comparison methods with the aim to determine which method is more suitable and how they differ in terms of uncertainties, computation, and results.

Q2.1: "*How do the results of the elevation model- and dense point cloud analysis differ?*"

Q2.2: "*Is one of the approaches more suitable for surface investigations of landslides?"*

Question 2.1 ties with the hypothesis and compares the generated results of the surface analysis while question 2.2 evaluates these along with literature-based information to determine which approach is more suitable for a surface investigation. To answer these two questions, an insight into the plugins and algorithms of point cloud and DoD-analysis will be given and main differences as well as advantages and disadvantages of each methodological approach are elaborated. In addition, examples of suitable applications of the respective methods will be presented.

H3: "***The landslide has been continuously moving for more than a decade since the last reactivation.***"

The third and final hypothesis focus lies on the actual movements of the surface itself and is not limited to the observation period and therefore includes data from previous research activities. Because according to the characteristics known so far, the Salcher landslide is a slow rotational landslide moving at very slow rates. However, it is unclear if there are any spatiotemporal patterns or continuous movements. To verify or falsify this statement, three research questions have been set up, whereas the Q 3.3 even investigates one step further.

Q3.1: *"To what extent did the main scarps and features of the landslide change?".*

The first research question here aims to investigate how much and in what eventual patterns the main scarps and features change since the beginning of the long-term monitoring. For this purpose, geomorphological mapping is done on the basis of the gathered data from 2020/2021 as well as previous data set in order to both visually represent and calculate occurred changes.

Q3.2: "*Are there any differences in surface movement during winter and spring?".*

Question 3.2 is limited to the observation period and compares results of the surface analysis between the first and second UAV-survey with the results of the second and third UAV-survey. Here it is expected to determine the effects snow and its melting during spring has on the landslide.

Q3.3: "*Can the processes, mainly responsible for movements in Gresten, be identified with a surface analysis?".*

The final research question deals with how the results of the surface analysis can be used further and to what extent it can be used to draw conclusions about the subsurface. This intradisciplinary approach includes subsurface data to visually compare them with surface movement results.

3 Characteristics of landslides

Since the term "*landslide*" is included in the title of this master thesis, the following chapter provides a general overview of this natural phenomenon. Multiple other terms like slope failure, mass wasting, mass movement and slope movement have been used in literature and research to describe a landslide (CROZIER 1986). For a better understanding, the most important definition and classifications of this natural phenomenon will be explained. Furthermore, a detailed insight into the factors causing landslides, split in predisposing-, triggering-, and controlling- factors, will conclude this chapter.

3.1 Classification of landslides

By now, there is no unique definition of what a landslide exactly is. One of the reasons for this is that the definition is often directly associated with specific characteristics, and the variety of manifestations of landslides is immense (HIGHLAND & BOBROWSKY 2008). Multiple definitions of the term "*landslide*" exist in literature, while the one from CRUDEN (1991: 28) "*movements of a mass of rock, earth or debris down a slope*" is one of the most cited. This definition already distinguishes between three types of displaced material. These three material types are included in most classifications along the type of process and the degree of disruption of the displaced material (GLADE et al. 2005).

DIKAU & GLADE (2002: 45) added that, "*landslides are fractioned or non-fractioned gravitational driven*", which indicates the different mechanisms involved. Many of today's definitions are based on a paper published by DAVID J. VARNES in 1954 (20), defining landslides as a "*downward and outward movement of slope-forming materials composed of natural rock, soils, artificial fills or combinations of these*". Several years later in 1978, VARNES (11) stated that he prefers the term "*slope movements, rather than landslides*" since the process of "*falling*" does not suit with "*sliding"*. On this basis, VARDEN (1978) published one of the well-known classifications of landslides in which he distinguishes between the type of movement and material (Tab. 1).

Type of Movement			Type of Material		
			Bedrock	Engineering Soils	
				Predominantly coarse	*Predominantly fine*
Falls			Rock fall	Debris fall	Earth fall
Topples			Rock topple	Debris topple	Earth topple
Slides	Rotational	Few units	Rock slump	Debris slump	Earth slump
	Translational	Few units	Rock block slide	Debris block slide	Earth block slide
		Many units	Rock slide	Debris slide	Earth slide
Lateral Spreads			Rock spread	Debris spread	Earth spread
Flows			Rock flow (deep creep)	Debris flow (soil creep)	Earth flow
Complex	Combination of two or more principal types of movement				

Table 1: Classification of landslides (after VARNES 1978: 11)

Other than that, classifications of a landslide often include several criteria, besides the type of movement and material to differentiate between the morphometric characteristics, the degree of displacement, disruption and potential hazard, geologic setting, and causes (CROZIER 1986).

The development of such classifications has come a long way. In the 19th century, BALTZER (1875) published his book "*Ueber Bergstürze in den Alpen*" in which he distinguishes between the modes of motion: falling, sliding, and toppling, based on historical landslides that occurred in the alpine region. The publications of VARNES (1954; 1978) specified the classifications while CROZIER (1986) published a book about the causes and consequences of landslides and CRUDEN (1991) rewrote the definition. These publications are amongst the most cited ones in the field of landslide research. Their work was the basis for the UNESCO Working Party on World Landslide Inventory in the 90s. Over the span of five years, multiple documents were published, which provided methodologies for landslide investigations and reports (HUNGR et al. 2014). The overall aim was to establish generally accepted standards and terminologies for landslides (UNESCO-WP/WLI 1990; 1991; 1993a; 1993b). The importance of different velocities and materials spread within the scientific consensus through the publication of DIKAU et al. (1996) and CRUDEN & VARNES (1996). Other than that, classifications of landslide often include several criteria to differentiate between them.

Another "milestone" in the history of landslide classifications is the publication from HUNGR et al. 2014 in which he and his colleagues present an updated classification system based on VARNES's version from 1978. The updated version distinguishes

between six types of movement: fall, topple, slide, spread, flow and slope deformation, while VARNES (1978) listed seven types: fall, topple, rotational sliding, translational sliding, lateral spreading, flow and complex (HUNGR et al. 2014; Fig X.). Besides combining rotational-, and translational sliding as one type, HUNGR et al (2014) dispensed the landslide type “complex” and extended the type of “slope deformation” instead. This new type of landslide describes (extremely) slow and partly very large movements of masses consistent of solid and loose material (HUNGR et al. 2014). If, and to what extent this new classification will be accepted and prevail in future landslide research is yet unclear (GLADE & ZANGERL 2020).

Due to this uncertainty, the six types of movement, *fall-, topple-, slide-, spread-, flow-* and *complex*, according to VARNES (1978) UNCESO-WP/WLI (1993) and CRUDEN & VARNES (1996) are described in the following.

Movement-type: **Fall**

The process of falling in landslide research refers to material detached along surfaces where little to no shear motion occurs (DIKAU et al. 2019; CRUDEN & VARNES 1996). Due to this, there is only little dynamic interaction between the displaced fragments and the surface below along the path (HUNGR et al. 2014). The material "falls" mostly through the air by free fall, bounding or rolling (VARNES 1978) (Fig. 2 & 3). The falling material may break into fragments upon impact on the surface below and may continue rolling until, either the terrain flattens, or obstacles block the path (HIGHLAND & BOBROWSKY 2008). This type of landslide usually occurs if material beneath the surface has been eroded along steep slopes or cliffs (CRUDEN & VARNES 1996). Falling is one of the fastest moving types of landslide (VARNES 1978).

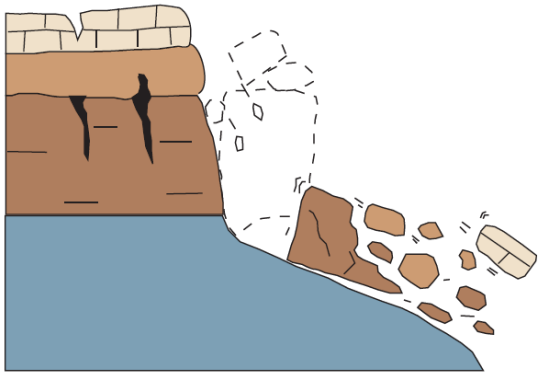

Figure 2: Topple movement (HIGHLAND & BOBROWSKY 2008: 9)

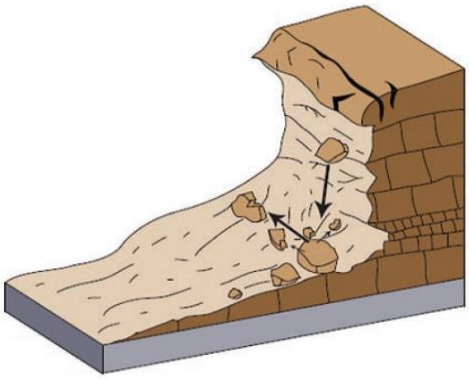

Figure 3: Rockfall movement HIGHLAND & BOBROWSKY 2008: 7)

Movement-type: **Topple**

With similar velocities, toppling landslides are also among the fastest types, but mainly due to acceleration shortly after toppling over (VARNES 1978; CRUDEN & VARNES 1996). The term "topple" refers to a forward, downslope rotation of material on a slope by one point or an axis below its center of gravity (DIKAU et al. 2019) (Fig. 2). This type of movement is mainly triggered by exerted material upslope transferring energy on the displaced mass below or by water and ice inside the cracks of the mass leading to a failure of the slope (CRUDEN & VARNES 1996). Toppling landslides are not limited to consist of rock, but also soil and debris (HUNGR et al. 2014).

Movement-type: **Slide**

Sliding "*is a downslope movement of a soil or rock mass occurring dominantly on surfaces of rupture or on relatively thin zones of intense shear strain*" (CRUDEN & VARNES 1996: 56). Varnes (1978) originally differentiated between rotational (Fig. 4) - and translational slides (Fig .5) since there are major differences in stability analysis and control methods (CRUDEN & VARNES 1996). Nevertheless, both types of landslides are characterised by a downhill sliding mass of material.

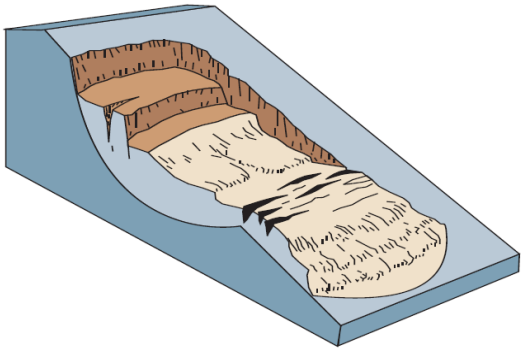

Figure 4: Rotational landslide (HIGHLAND & BOBROWSKY 2008: 11)

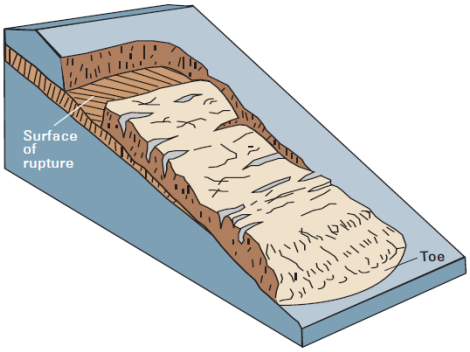

Figure 5: Translational landslide (HIGHLAND & BOBROWSKY 2008: 13)

a) Rotational landslide

As the name suggests, rotational landslides move along a subsurface that is curved and concave leading to a rotational movement as the mass is driven downslope (CRUDEN & VARNES 1996). Characteristic for rotational slides is the low degree of internal deformation of the displaced material, even though the mass can break into several clods during the rotational process (DIKAU et al. 2019). While the lower end of the landslide often moves almost completely downslope, the upper end commonly tilts upslope towards the scarp (HIGHLAND & BOBROWSKY 2008; VARNES 1978).

The slide can be divided into a zone of depletion and a zone of accumulation. The depletion zone encompasses the entire upper area of the slide which subsides due to the rotational movement. The displaced material is deposited in the accumulation zone resulting in an increasing topography here (CRUDEN & VARNES 1996).

Rotational landslides mainly occur in regions with homogeneous materials and are among the most widespread type there (CRUDEN & VARNES 1996). The rate

of movement can range from extremely slow to rapid (VARNES 1978). If a larger rotational landslide has slow movement rates, buildings and infrastructure can still be built on it (GLADE et al. 2005).

b) Translational landslide

Compared to the rotational type of movement, the translational landslide is defined by, a more or less, planar surface with little to no rotary movement (VARNES 1978). Due to a relatively flat surface of rapture, the translational slide can move on for longer distances than rotational slides (ROTARU et al. 2007). They also tend to be more shallow than rotational landslides, but can still reach a thickness of up to 100 meters in case of block slides (CRUDEN & VARNES 1996; HUNGR et al. 2014).

Movement-type: **Spread**

Spreads usually occur on flat terrain or on gentle slopes (ROTARU et al. 2007). According to HUNGR et al. (2014: 179) the movement-type "*spread should be applied where a large and well-defined part of the slope has undergone distinct displacements so that a rupture surface can be defined*". Spreads can be defined as subsided material from a fractured mass in combination with an extension of soil or rock material into mostly softer subsurface material (CRUDEN & VARNES 1996). There are various forms of spreads depending on the involved type of material like block-, rock-, liquefaction-, and clay- spreads (HIGHLAND & BOBROWSKY 2008; HUNGR et al. 2014). In the 1978 classification of VARNES (Tab. 3), the term "lateral spreads" was used for this type of movement. Fig. 6 displays a schematic lateral spread.

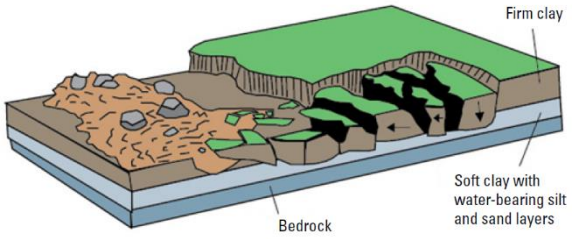

Figure 6: Lateral spread (HIGHLAND & BOBROWSKY 2008: 15)

Movement-type: **Flow**

The landslide type of “flow” can be described as a continuous, irreversible deformation of material moving with similar velocity characteristics like a viscous liquid (DIKAU & GLADE 2002). Various types of landslides fall under this movement-type like rock/ice and debris avalanches (Fig. 8) as well as mud-, earth-, peat-, and debris- flows (Fig. 7.) (HUNGR et al. 2014). Depending on the involved materials and slope angle, flows range from being slow to extremely rapid and disastrous (CRUDEN & VARNES 1996).

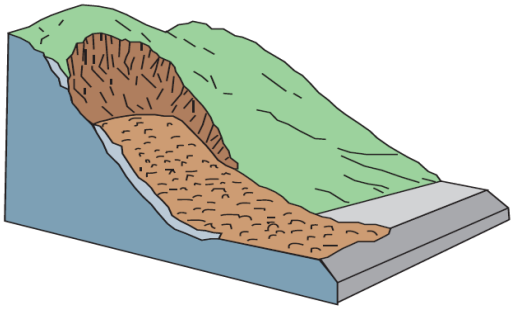

Figure 7: Debris avalanche (HIGHLAND & BOBROWSKY 2008: 21)

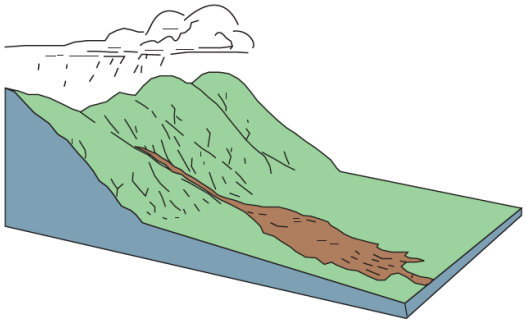

Figure 8: Flow scheme (HIGHLAND & BOBROWSKY 2008: 17)

Movement-type: **Complex**

The sixth and last type of landslides according to various classifications are complex landslides. Complex movements involve more than one of the mentioned movement-types, rather than being an independent process (ROTARU et al. 2005; DIKAU & GLADE 2002). The different types of movement are involved either during the different stages of development of an occurring landslide - a rotational landslide can turn into an earthflow under certain conditions (HUNGR et al. 2014), or within parts of the displaced mass (VARNES 1978). An example of a complex landslide happened in 2017 near Bondo in Switzerland. An initial rockslide/rockfall occurred, entrained parts of a glacier resulting in a rock-ice avalanche which then evolved into a debris flow (MERGILI et al. 2020).

It is evident that the majority of occurring landslides does not correspond to only one type of motion and material and are usually a combination of processes and materials (GLADE & ZANGERL 2020).

3.2 Features of landslides

Along with the differentiation of the various types of landslides comes the usage of landslide terminology. This master thesis makes use of landslide-related terms to describe specific parts of a landslide. The establishment of nomenclature for landslide features is important for landslide research since it provides generally accepted terms.

The most important terminology based on VARNES 1978 and CRUDEN & VARNES adaption from 1996 are listed in Tab. 2 along with a schematic representation of which parts the terms describe (Fig. 9) can be seen in the following.

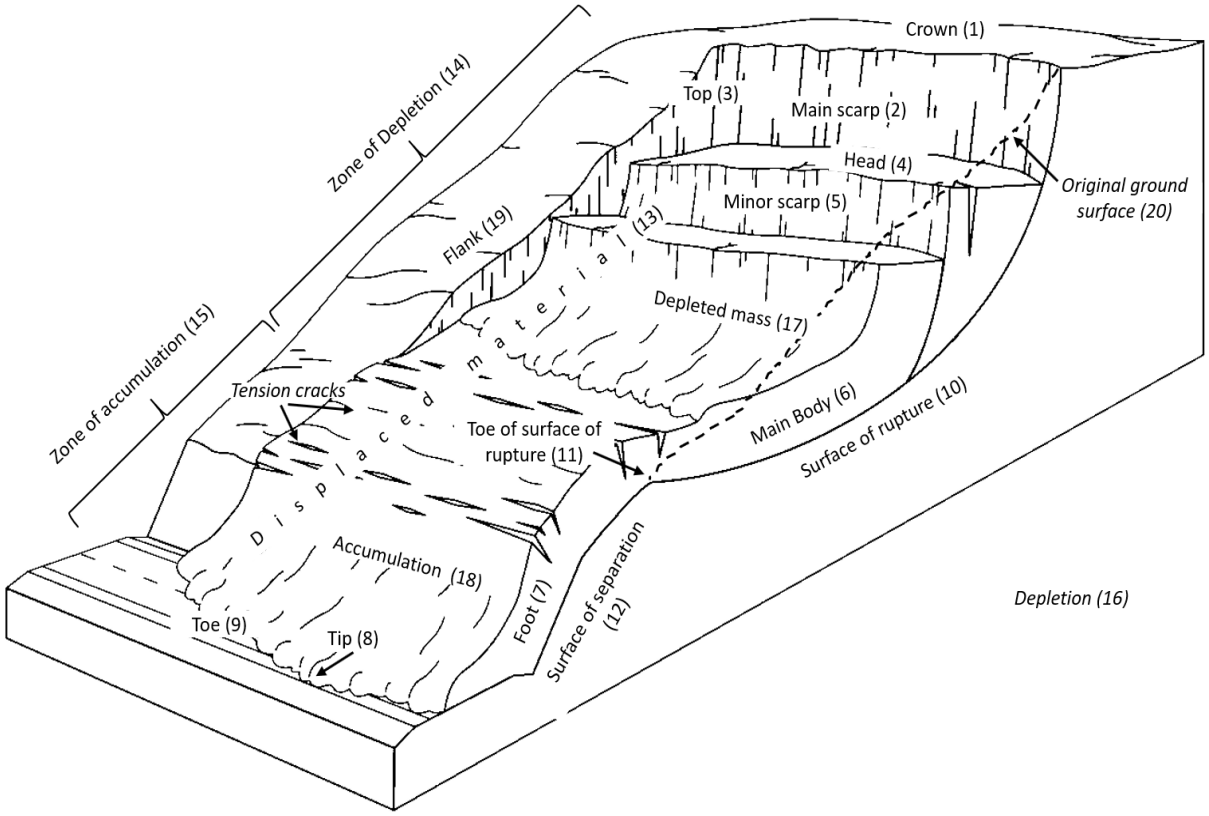

Figure 9: Landslide features, (after CRUDEN & VARNES 1996; landslide scheme taken from JOHNSON et al. 2017)

The term “depletion”, referring to the displaced volume of material between the original ground surface, main scarp, and depleted mass (CRUDEN & VARNES 1996), is excluded for graphical reasons in Fig. 9.

Number	Name	Definition
1	Crown	Practically un-displaced material adjacent to highest parts of main scarp
2	Main Scarp	Steep surface on undisturbed ground at the upper edge of landslide caused by movement of displaced material (13, stippled area) away from undisturbed ground; it is visible part of surface of rupture (10)
3	Top	Highest point of contact between displaced material (13) and main scarp (2)
4	Head	Upper parts of landslide along contact between displaced material and main scam (2)
5	Minor scarp	Steep surface on displaced material of landslide produced by differential movements within displaced material
6	Main body	Part of displaced material of landslide that overlies surface of rupture between main scam (2) and toe of surface of rupture (11)
7	Foot	Portion of landslide that has moved beyond toe of surface of rupture (11) and overlies original ground surface (20)
8	Tip	Point on toe (9) farthest from top (3) of landslide
9	Toe	Lower, usually curved margin of displaced material of a landslide, most distant from main scarp (2)
10	Surface of rupture	Surface that forms (or that has formed) lower boundary of displaced material (13) below original ground surface (20)
11	Toe of surface of rupture	Intersection (usually buried) between lower part of surface of rupture (10) of a landslide and original ground surface (20)
12	Surface of separation	Part of original ground surface (20) now overlain by foot (7) of landslide
13	Displaced material	Material displaced from its original position on slope by movement in landslide; forms both depleted mass (17) and accumulation (18)
14	Zone of depletion	Area of landslide within which displaced material (13) lies below original ground surface (20)
15	Zone of accumulation	Area of landslide within which displaced material lies above original ground surface (20)
16	Depletion	Volume bounded by main scarp (2), depleted mass (17), and original ground surface (20)
17	Depleted mass	Volume of displaced material that overlies surface of rupture (10) but underlies original ground surface (20)
18	Accumulation	Volume of displaced material (13) that lies above original ground surface (20)
19	Flank	Un-displaced material adjacent to sides of surface of rupture; compass directions are preferable in describing flanks, but if left and right are used, they refer to flanks as viewed from crown
20	Original ground surface	Surface of slope that existed before landslide took place

Table 2: Landslide features and their definition (after CRUDEN & VARNES 1996)

3.3 Slope (in-)stability and thresholds

"*Slope instability is the condition which gives rise to slope movements*" (CROZIER 1986: 32). Since landslides can affect human lives, buildings and infrastructure, multiple disciplines try to determine at which point a slope changes from a stable to an unstable state. GLADE & DIKAU (2005: 43f.) defined slope (in-)stability as "*the propensity for a slope to undergo morphologically and structurally disruptive landslide processes*" but added, that slower types of movement like soil creep are not included in this definition since their structural disruption isn't adequate enough to be considered as an unstable slope. Inside every slope are gravitationally driven driving forces, which promote downward movement and counteracting resisting forces which resist movement and are therefore, partly, responsible for the slope stability. These forces are directly and indirectly influenced by various factors, which will be discussed in the following subchapter 3.4. The driving and resisting forces are often referred to as shear- "stress" and "strength" (GLADE & DIKAU 2005). If the shear stress gets larger than the sheer strength, the slope becomes unstable and the landslide process occurs (PREUTH et al. 2010). This transition from a stable to unstable state is referred to as "*slope failure*" (CRUDEN & VARNES 1996; CLAGUE & ROBERTS 2012). According to CROZIER 1986, slopes can therefore be defined into three different stages: (i) *stable* to (ii) *marginally stable* to (iii) *unstable* (Fig. 10).

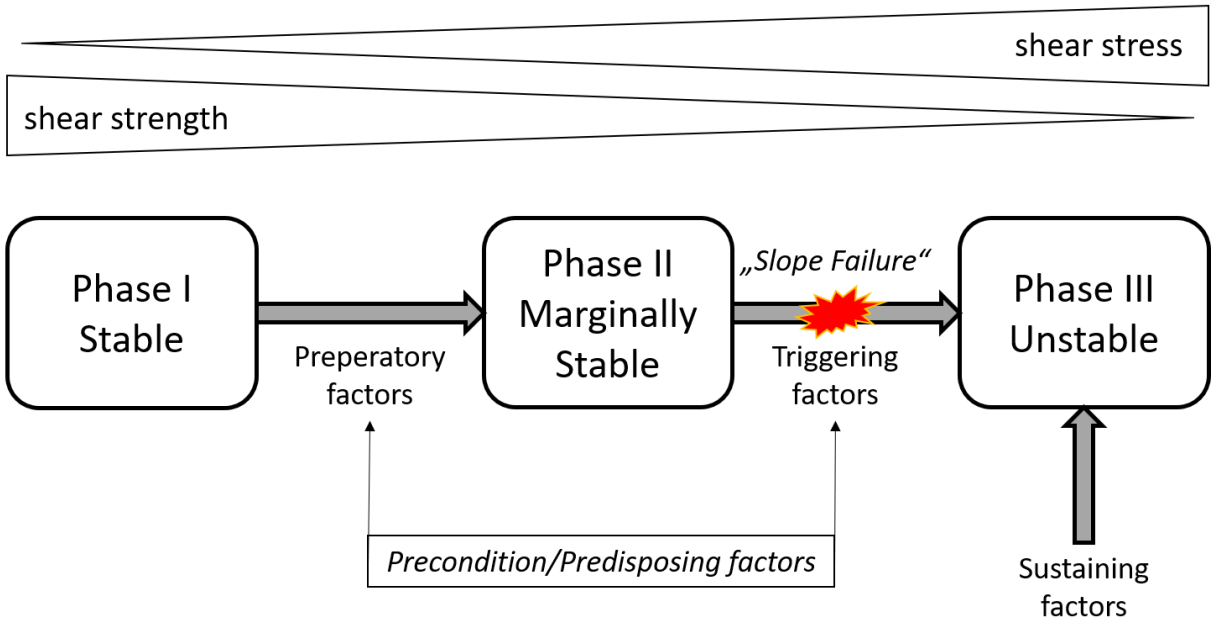

Figure 10: Different stability phases and destabilizing factors (after CROZIER 1989 and DIKAU & GLADE 2005)

Phase I describes a state in which the shear strength of a slope is sufficiently large to withstand any gravitational movements and destabilizing factors. The slope is stable. Phase II is named marginally stable since the slope is still stable as long as there is an equilibrium between the gravitational and resisting force – but susceptible to fail as soon as a trigger factor leads to higher shear stress. While it might seem easy to differentiate between these two states in theory, in practice it is difficult because the predisposing factors often only have temporary effects on the slope (CROZIER 1986). The third phase is an actively unstable state. The slope fails due to one or multiple triggers and depleted material moves downslope. The downward displacement of material is then determined by sustaining factors, affecting the rate, form, and duration of movement (CROZIER 1986).

3.4 Factors influencing landslides

After differentiating the different phases that slopes can undergo, different factors affecting these phases have already been shortly addressed in the chapter before. In the event of a landslide, four factors play an important role to promote slope instability. In the following predisposing-, preparatory-, triggering-, and sustaining factors (see Fig. 10) are explained. The differentiation is based on the factor's influence on the slope and not on the factor itself.

a) **Predisposing** factors are inherent and static. They act more as a catalyst for other destabilizing factors rather than directly affecting the slope (DIKAU & GLADE 2005). Also called preconditioning factors, they influence the inherent shear strength and are considered to not change over comparably short time periods (human timescales) (MCCOLL 2015).

b) **Preparatory** factors, on the other hand, are actively increasing the shear stress of slopes. These factors are responsible for the transition from a stable to a marginally stable slope (see Fig. 10). They make slopes susceptible to movement but do not initiate the movement (CROZIER 1986). Some preparatory factors like tectonic uplift or environmental change operate over long periods of time while others like deforestation and anthropogenic disturbance can lead to quick and direct responses (DIKAU & GLADE 2005).

c) **Triggering** factors are the ones that initiate the slope failure and therefore the downward movement. They shift the slope from a marginally stable to an actively unstable state (CROZIER 1989). Trigger factors are easier to identify than preparatory factors (see Chapter 3.3) because it is possible to determine threshold values for triggering factors, responsible for the initiating movement. Nevertheless, movement can still be initiated without identifiable external triggering forces in certain cases if internal thresholds are surpassed inside the slope (DIKAU & GLADE 2005).

d) **Sustaining** factors or sometimes **controlling** factors, dictate the condition and sequence of movement and control the form, rate, and duration of the movement (CROZIER 1986). They can either be dynamic, like rainfall or static, like the terrain encountered in the path of the landslide (DIKAU & GLADE 2005).

A broader selection of specific preparatory-, triggering- and sustaining factors for landslides, split in different categories; geology, climate, soil, vegetation, hydrology, topography anthropogenic was published by DIKAU & GLADE (2002: 39), which can be seen in the following table 3. This selection shows that various external factors can have different influences on slopes and are therefore listed in more than one column and can be preparatory-, triggering- and sustaining factors. These factors are displayed *cursively.*

Preparatory factors	Triggering factors	Sustaining factors
Geology		
Discontinuities Weathering Isotasy Tectonic faults	Earthquakes Volcanic eruption	Type of rock *Discontinuity* Tectonic faults
Climate		
Extended antecedent rain Snow melt Freeze-Thaw cycles	*Precipitation* (intensity & amount) (quick) snow melt	*Precipitation* (intensity & amount)
Soil		
Weathering Geotechnical properties of the soil material Soil type / class Subterranean erosion	-	State of saturation Soil thickness
Vegetation		
Natural change in land cover (forest fire, drought)	-	Vegetation e.g. trees can block the path
Hydrology		
Thawing permafrost	Fluctuating hydraulic head & pore-water pressure	Channel roughness Further transport of displaced material
Topography		
Slope exposition *Height of the slope*	-	*Slope inclination* *Slope curvature* *Depression line*
Anthropogenic		
Deforestation Dam construction Slope toe removal Irrigation Mining Leaking pipes / drainages	*Slope cut* *Slope undercutting* *Loading*	Obstructions Dams Levelling Changes of channel in width

Table 3: Factors influencing landslides (after DIKAU & GLADE 2002:39)

4 Methods to determine landslide dynamics

The following chapter provides an overview of existing methods to analyze landslides and their dynamics. It builds on the theory about landslides from the previous chapter and is intended to bring the reader closer to the current state of landslide research and investigation. The “state of art” is divided between subsurface and surface investigation measures. Some of the described surface- and subsurface investigation methods in the following are not only used to collect data and gain insights of the present state of a landslide but rather repeatedly over longer time periods. This is called monitoring, which is the basis for many landslide hazard assessments and early warning systems (EBERHARDT 2012). Collecting the same type of data over a longer time allows to detect changes in various desired categories like kinematic, hydrology and climate (THIEBES et al. 2013). Especially the determination of movement rate and the velocity of a slope are among the purposes of monitoring (EBERHARDT 2012). Knowledge about slope stability is also important for predicting slope behaviour and forecasting (THIEBES et al. 2014).

To fully understand the dynamics of a landslide, a multidisciplinary research approach is almost indispensable (PERRONE et al. 2014). For the study of this master thesis, an aerial based survey of the surface was carried out with the results being interpreted using existing results from previous subsurface and surface investigations. Since there is a broad option of different methods for analyzing landslide dynamics, researchers can theoretically select their preferred approach. Nevertheless - in reality, research is often limited by budgets, access to specific measures and instruments as well as time shortages.

The focus of this master thesis is about the surface dynamics so the basics of subsurface investigations will be addressed briefly. The selection of the following presented investigation methods is based on the measurements used by the ENGAGE working group.

4.1 Subsurface investigation methods

Investigating the subsurface of a landslide means gathering as much information about the underground as possible. Knowledge about sub-surface properties, soil composition, water content, slope gradient and other physical features can be gained and further used for research regarding slope stability, equilibrium, early warning systems, monitoring and hazard risk research (PERRONE ET AL. 2014; THIEBES ET al. 2014; STUMVOLL ET AL. 2020; SUPPER et al. 2014). A selection of subsurface investigation methods is described in the following.

a) **ERT** (=Electrical Resistivity Tomography): As the name suggests, the ERT measures the electrical resistivity of the ground and is mainly used to investigate the near-surface area, especially for landslides with complex geological settings (PERRONE et al. 2014).

   It is an indirect geophysical method, which means that the results purely show the distribution of electrical resistivity. Nevertheless, these results allow further interpretation about the mineralogy of particles, ground water content and porosity (PERRONE et al. 2014). ERT (Fig. 11) is often used combined with other direct subsurface investigation methods for interpretation and validation reasons (BELL et al. 2006).

Figure 11: ERT cables along the Hofermühle, NÖ (March 2019)

b) **TDR** (=Time Domain Reflectometry): TDR-devices are sensors, directly measuring the moisture content of the ground via electrical conductivity (STANGL et al. 2009). It measures the travel time of an electronic pulse surrounded by a medium to be investigated (soil for landslides) and relates the duration of the signal to the soil water content (NUR et al. 2016).

c) **DP** (=Dynamic Probing) is an indirect mechanical exploration method to measure ground resistance. Usually, one-meter-long sectional rods equipped with a cone are hammered into the ground. The “hammer” consists of a specific weight which is lifted and then dropped on the rods, sometimes powered by a fuel operated chain hoist (Fig. 12) or a simpler hydraulic pump (Fig 13). According to the European Committee for Standardization (2005) DP is categorized into four groups, depending on the weight used for the penetration: DP-light (DPL), -medium (DPM), -heavy (DPH), -superheavy (DPSH). The number of blows the hammer needs to penetrate the attached rods into the ground for every 10 cm is counted and can be plotted afterwards (AVANZI et al. 2013).

Additionally, a probe core can be attached to the rods to collect samples of the soil, which can be analyzed regarding material, particle size, water and carbonate content as well as consistency (SALAS-ROMERO et al. 2016).

Figure 12: Fuel operated hydraulic Drill at the Hofermühle, NÖ (March 2019)

Figure 13: Dynamic penetration test (March 2019)

d) **Piezometer**: A Piezometer is an instrument to measure the groundwater level by a direct measurement of the pressure from pore water (HIGHLAND & BOBROWSKY 2008). Piezometers in combination with TDR-devices enable researchers to get an overview of ground humidity and water content, which is often a triggering factor for landslides (see Chapter 3.4).

e) **Inclinometer**: An inclinometer is a device to measure local subsurface movements which makes it possible to create profiles of horizontal deformations inside the ground (STARK & CHOI 2008). The setup requires installing a tube with inside-grooves (Fig. 14) vertically in the ground. The inclinometer itself has four guiding wheels and is lowered along these grooves inside the tube so that the deformation can be measured in multiple depths. This can be done manually or automatically. Ideally, the installation of the guiding tube is perfectly vertical, so the first inclination measurement would be zero. After movements in the ground occur, the tube is most likely to be bent to a certain degree, which then can be measured. Inclinometers are mainly used for monitoring aspects so analyze the subsurface deformation changes over time (STARK & CHOI 2008).

Figure 14: Inclinometer shorty before installation (March 2019)

4.2 Surface investigation methods

Surface investigation methods aim to collect information about the slopes surface, which then can be either analyzed on its own or in combination with subsurface information for a deeper understanding of landslide characteristics. Techniques in this category vary a lot, ranging from simple manual mappings of surface characteristics over electronic distance measurement to aerial and satellite photography.

4.2.1 Mapping

Landslide mapping can have different meanings in research and literature and makes use of various techniques depending on the scale and desired results (PARISE 2000). For this master thesis, a mapping of the surface characteristics was done based on orthophotos, recorded with an UAV. Landslide inventory maps, a method to mark the location, type, and date of multiple landslide occurrences (GUZZETTI et al. 2012) are not addressed here.

Landslide mapping can cover landslide characteristics like slope inclination, surface attributes (Fig. 15), sediments, geology, hydrology, and geomorphic processes (see LESER & STÄBLEIN 1975; DEMOULIN & GLADE 2004; WOLTER et al. 2016). By the time the first guidelines were published, the common method to map the surface of a landslide was by walking on the area of interest and note down geomorphic characteristics by hand; mainly referred to as a field survey. While this is still possible, nowadays mapping landslide characteristics can also be automated via GIS-software (MESSENZEHL et al. 2014) or hand based by sense of proportion on an orthophoto as a background layer. Regardless of the differences in the making, a landslide map needs to have a legend included, displaying 3D characteristics in 2D (see Fig. 15). There is no standardization for geomorphic maps, since it depends on the field use, however TERHORST & KIRSCHHAUSEN (2001); LESER & STÄBLEIN (1975) and DEMEK (1972) have published guidelines and manuals.

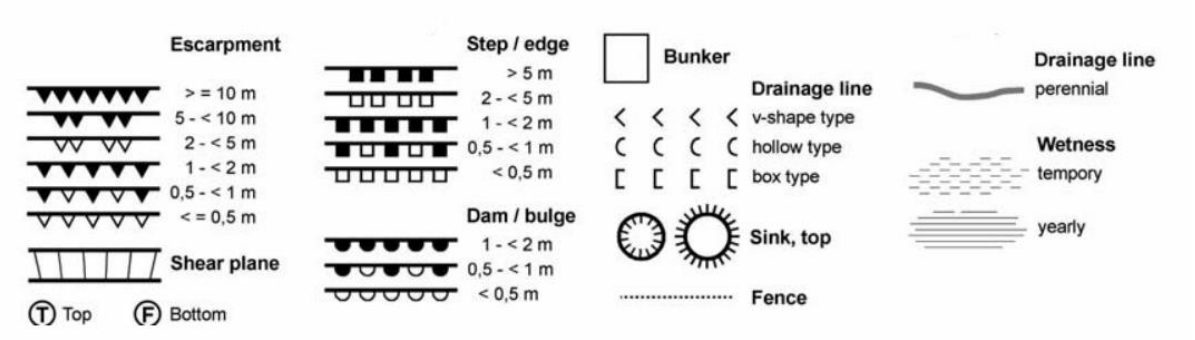

Figure 15: Legend of a geomorphic map (edited after DEMOULIN & GLADE 2004: 307)

Landslide mapping is a method to get an overview of spatial distribution of surface characteristics. It displays the state of a landslide at the time of investigation but can also be used for back-calculations (WOLTER et al. 2016) or for time series to detect changes like in this master thesis (see Chapter 6.4 and 7.2).

4.2.2 GNSS Survey

Another way to investigate and monitor surface changes of landslides is via GNSS surveys. GNSS stands for Global Network Satellite System and is a collective term for all existing satellite and positioning systems irrespective of their origin. For surveys with GNSS, characteristic points of the surface are selected and marked, or artificial points are installed. Then these points are measured via GNSS over a chosen period to determine dynamics of the surface. How often the survey is carried out can range from seconds to days to a few months (COE et al. 2003; GALI et al. 2000; STUMVOLL et al. 2020). The difference of the GNSS measurements reflects the changes of the surface and the velocity of a slope can be determined (WANG et al. 2014; HASTAOGLU et al. 2018). Due to GNSS being able to only measure movements for individual points, multiple points are needed for surveying whole areas (HASTAOGLU et al. 2018). For long-term monitoring it is recommended to use time resistant markings like steel pins or rock engravings (GALI et al. 2000)

However, this method is mainly suitable for slow(-er) moving landslides since the GNSS points still need to be detected after movements, which would not be possible if the surface gets disrupted and mixed with subsurface material (HASTAOGLU et al. 2018).

4.2.3 Remote Sensing

The term remote sensing encompasses all methods that acquire their data and information about an object of interest without having physical contact (KLEIN 2006). Different approaches regarding landslide research range from interpreting analog aerial and satellite images to the use of laser and radar technologies and AI-image processing (PETLEY 2012b). Regarding landslide investigation, different remote sensing approaches have been widely applied like SAR (TOFANI et al. 2014; RAUCOULES et al. 2020), LiDAR (JABOYEDOFF et al. 2012) and Optical Remote Sensing (EKER et al. 2017; LUCIEER et al. 2014), which all differ regarding the wavelengths of captured rays. Despite their different technical approaches, all these methods obtain elevation data of a research area. Due to this, a digital elevation model in a graphical information system (GIS) for further analysis is usually produced during post-processing steps. Different types of elevation models will be presented before describing the mentioned approaches to create them. FLORINSKY (2016: 78) defined a DEM as a "*two-dimensional (or bivariate) discrete function of elevation of the topographic surface*". A DEM (Digital Elevation Model) is the generic term for every digital reproduction of terrains and elevations (PECKHAM & JORDAN 2007). However various forms of DEMs exist, depending on what needs to be investigated.

- DSM: Digital Surface Model is a DTM with all objects situated on top of the surface including features like trees, buildings, and infrastructure. DSMs only describe the topographic surface for areas not covered with mentioned features (FLORINSKY 2016).
- DTM: Digital Terrain Models represent "tract of country considered with regarded to its natural features" (LI et al. 2005: 7). It displays the ground surface without (higher) vegetation, and any human made object, which can be removed digitally.
- DHM: Digital Height Models practically represent the (higher) vegetation and human made objects removed from DTMs but without displaying the ground surface. Only elevation above the ground, or any other set level is considered for DHMs (LI et al. 2005). DHMs are applied inter alia for forestry research and tree detections and are therefore referred as CHM (Canopy Height Model) (MATESE et al. 2016)

- An additional type of an elevation model is a DoD, which stands for "*DEM of difference".* DoDs are elevation models, created by subtracting an early elevation model from a later elevation model of the same extent (Eker et al. 2017). In this way, changes and deformations of a surface can be calculated and visually displayed. Any of the above-mentioned types of elevation models can be used to produce DoDs, depending on the wanted result (CLAPUYT et al. 2016; WARRICK et al. 2019). More details about DoDs are described in Chapter 7.4.3.

Regardless of the type of elevation model, elevation data in landslide research can be gathered with:

a) SAR

Synthetic Aperture Radar (SAR) is a radar investigation method using at least two different SAR images to measure displacements (RAUCOULES et al. 2020). Various forms of SAR exist like InSAR (interferometric SAR) which is usually applied for topographic mapping and landslide investigations (METTERNICHT et al. 2005). This remote sensing method is mainly attached to satellites like *ERS*, *Envisat ASAR*, *Sentinel* and *TerraSAR* (ZHAO & LU 2018), however ground-based InSAR (GBInSAR) approaches also exist (LISSAK et al. 2020) and can be combined for monitoring systems of landslides (TOFANI et al. 2014). The use of radar waves to detect surface changes has the advantage over optical sensors, that surveys are possible regardless of weather conditions and clouds (METTERNICHT et al. 2005; HERRERA et al. 2010).

b) LiDAR

LiDAR (=Light detection and ranging) is used to create high-resolution point clouds, which can be used to produce DEMs (JABOYEDOFF et al. 2012). LiDAR is a laser scanning technique which targets an object or area of interest with photons and measures the time for the reflected waves to return to the device (LARGE & HERITAGE 2009). Simplified, the longer the laser takes to return, the larger is the distance between the scanner and the point of interest. Even though it is just a small proportion of photons that is reflected directly back to the laser, it is enough to determine properties of the reflecting object including distance, texture, and color (LARGE & HERITAGE 2009).

LiDAR can be either attached to a flying object (UAV, plane, helicopter) which is summarised by the term ALS (*airborne laser scanner*) or be positioned on the ground as a TLS (*terrestrial laser scanner*) (Fig. 16) (METTERNICHT et al. 2015).

Figure 16: TLS - System at Hofermühle-Landslide (March 2019)

TLS-systems have the limitation that they cannot be positioned everywhere since the alignment plays an important role to ensure that even small features of a slope are captured (LARGE & HERITAGE 2009). Due to this, the TLS device in Fig. 16 is situated on the opposite slope of the study area to have the best possible position of view.

Advantages of LiDAR usage is that the method is, highly accurate (JABOYEDOFF et al. 2012), mostly not affected by topographic shadowing (METTERNICHT et al. 2015) and can even be applied for investigation of landslides, covered by vegetation and forest (EECKHAUT et al. 2007).

c) Optical remote sensing

Unlike radar and laser techniques, optical remote sensing makes use of visible and near infrared waves of solar radiation reflected from objects or areas of interest. A differentiation can be made between panchromatic-, multispectral-, superspectral-, and hyperspectral imaging systems (REES 2012), however multispectral and visible optical investigations of landslide are the most common (HELENO et al. 2016; LIN et al.

2017; ROSSI et al. 2018). The sensor for optical remote sensing can either be airborne (e.g. UAV) spaceborne (e.g. Landsat satellite) or terrestrial.

Also widely spread Red-Green-Blue (RGB) cameras are applied for landslide remote sensing investigation (see LINDER et al. 2016; TURNER et al. 2015; LUCIEER et al. 2014) and were used to analyze surface changes in this master thesis. RGB remote sensing makes use of camera sensors that are either charge-coupled devices (CCD) or complementary metal oxide semiconductors (CMOS). CMOS sensors are multidimensional sensors more resistant towards interpolation and sharpening artifacts and therefore continuously replace the “older” CCDs (ABER et al. 2012).

Gathered images of a research area can either be visually interpreted or processed further to generate a high-resolution point cloud and/or DEMs. Here, the methodology of Structure from Motion Photogrammetry is used to create 3D structures based on 2D images. This post-processing step will be explained into detail in Chapter 7.

5 Research Area

This chapter provides an overview of the research area, a landslide in Gresten. Starting with the geographic setting, the geological, hydrological, and geomorphological characteristics of the analyzed landslide are described in the following.

5.1 Geographic Setting

The research area is located in Gresten, a municipality within the district of Scheibbs in the western part of the Federal State of Lower Austria (see Fig. 17). The landslide is situated within the municipal boundaries of Gresten, has an active area of approximately 4000m2 ranging from 430 to 470m. above sea level (*if using MGI M34 Bessel-Ellipsoid; or 476-516m if using UTM84 WGS 33N*).

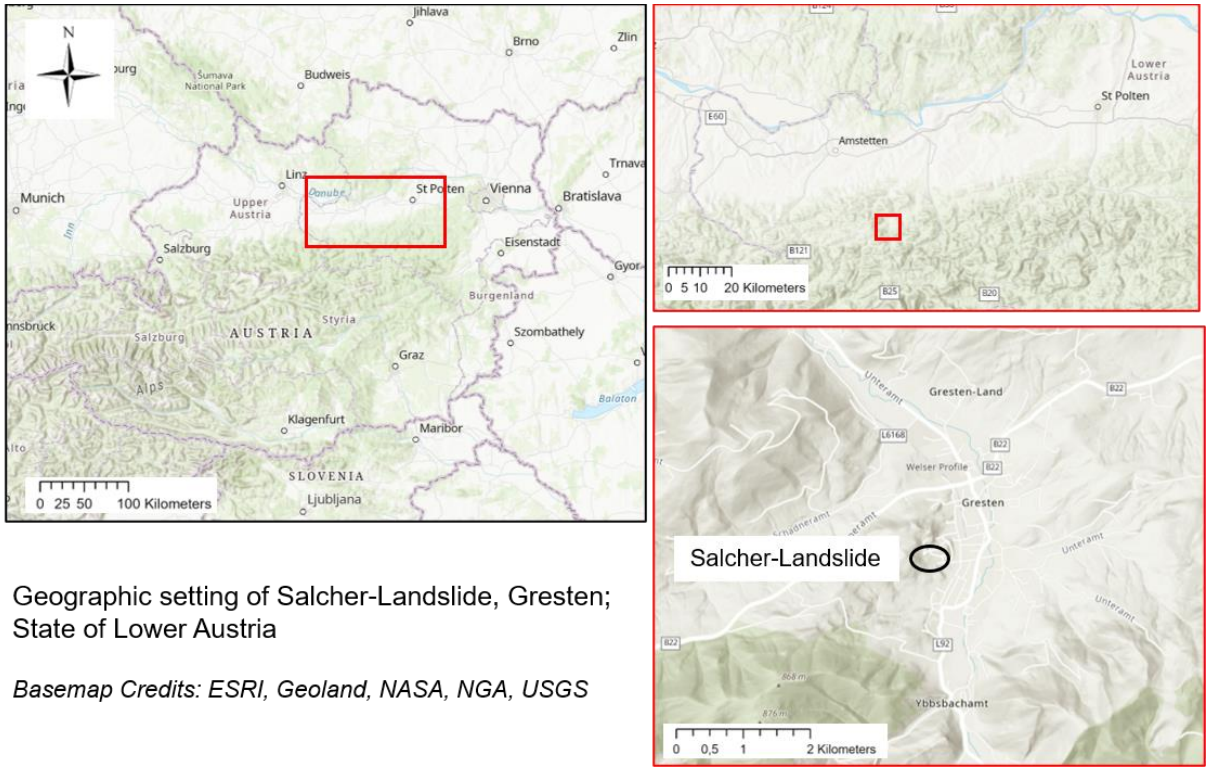

Geographic setting of Salcher-Landslide, Gresten; State of Lower Austria

Basemap Credits: ESRI, Geoland, NASA, NGA, USGS

Figure 17: Geographic setting of research area (created 12.05.2021; basemap: ESRI Geoland, NASA, NGA and USGS)

The slope is facing east with angles between 5 and 20°. The lower part of the landslide is delimited on three sides by two roads “Am Salcher” and “Salcherstraße” (see Fig. 18), which is the reason why this area is sometimes referred to as “Salcher” in literature (see SCHWEIGL 2013; STUMVOLL et al. 2020).

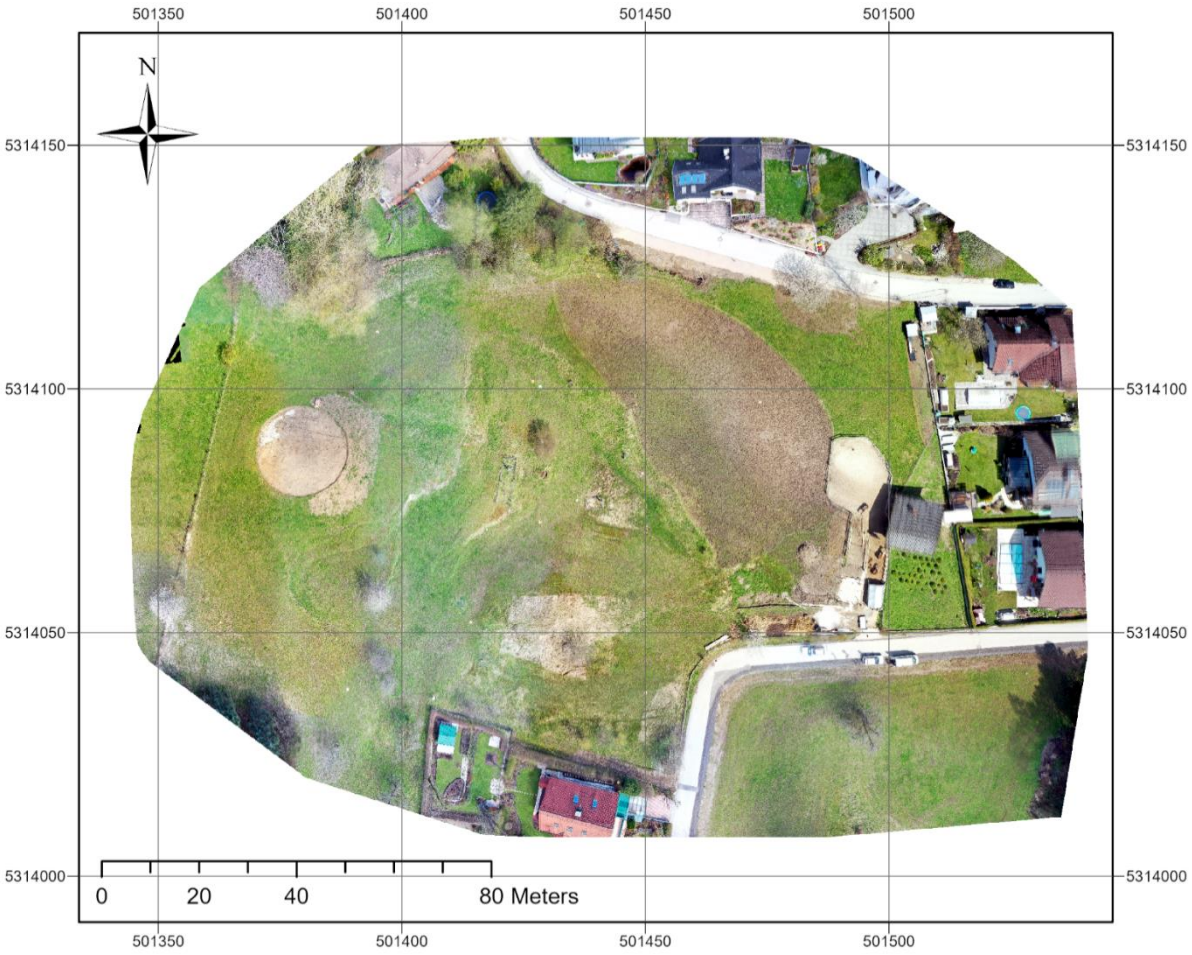

Figure 18: Salcher Landslide orthophoto (23.04) WGS84 UTM33N

Three residential buildings and one former lift shed are situated directly beneath the landslide toe. The shed is currently used for accommodating horses and hosting monitoring services of ENGAGE. Two of the three houses, west of the active landslide area, are directly influenced by ground movements (JOCHUM et al. 2008). There are two adjacent slopes in the periphery area of the landslide: one directly to the west, above the circular plane (see Fig. 18) and one southwest, covered by trees. The circular plane is planned to be used as a horse vaulting area according to the current land tenant. Both slopes have effects on the landslide in terms of hydrology and have steeper slopes than the active zones of the main landslide body.

5.2 Land Use and Vegetation

The research area was used as a skiing slope between the 1950s until the mid-1970s. A ski lift was built (Fig. 19), for which foundations had to be installed in the ground. Structural remains of the skiing infrastructure are still visible in the research area today. One foundation has tilted over the years due to the slow rotational sliding processes (Fig. 20).

Figure 19: Historical view of the Salcher landslide with ski lift in the 50s (Image by Marcel Mollik; taken from University Vienna 2021)

Figure 20: Ski lift foundation remains (05.11.2020)

After landslides occurred in 1975 (SCHWENK 1976) and 1978 (SCHWENK 1979) presumably due to heavy rainfall events, the skiing operation had to be stopped because the lowest ski lift pole was affected by the ground movement. Due to the movements, investigations by different organisations and authorities started, and the landslide has since been monitored, with a few gap years in between (see Chapter 6). The research area has become a pasture and is now used by horses with the old ski lift hut serving as a horse stable. It is covered with grass and partly surrounded by trees while on the landslide itself only a few trees have grown over the years.

So, regarding vegetation being a factor influencing slope movement (CROZIER 1986) the Salcher landslide has little to no deeper roots stabilising the soil which makes the area susceptible to movements.

5.3 Geology

The Geology of the Lower Austrian Alpine foreland is characterised by a complex geological background. The landslide under investigation is situated in the geologic transition zone of the GKZ and the Flysch Zone. On a comparably small scale, the region of Gresten is divided into three tectonic units, the Helvetic *Gresten Klippen Zone* (GKZ), located between the *Penninic* (Rhenodanubian) *Flysch Zone* in the north and the *Northern Calcareous Alps* in the south (RUTTNER & SCHNABEL 1988). As seen in Fig. 21 the tectonic units are all within a narrow zone in longitudinal direction and even on the small scale of the municipality of Gresten, different geological units characterise the research area. The spatial density of three tectonic units leads to diverse and complex successions of different lithological units which promotes landslide occurrence in the whole region (GALLISTL et al. 2018).

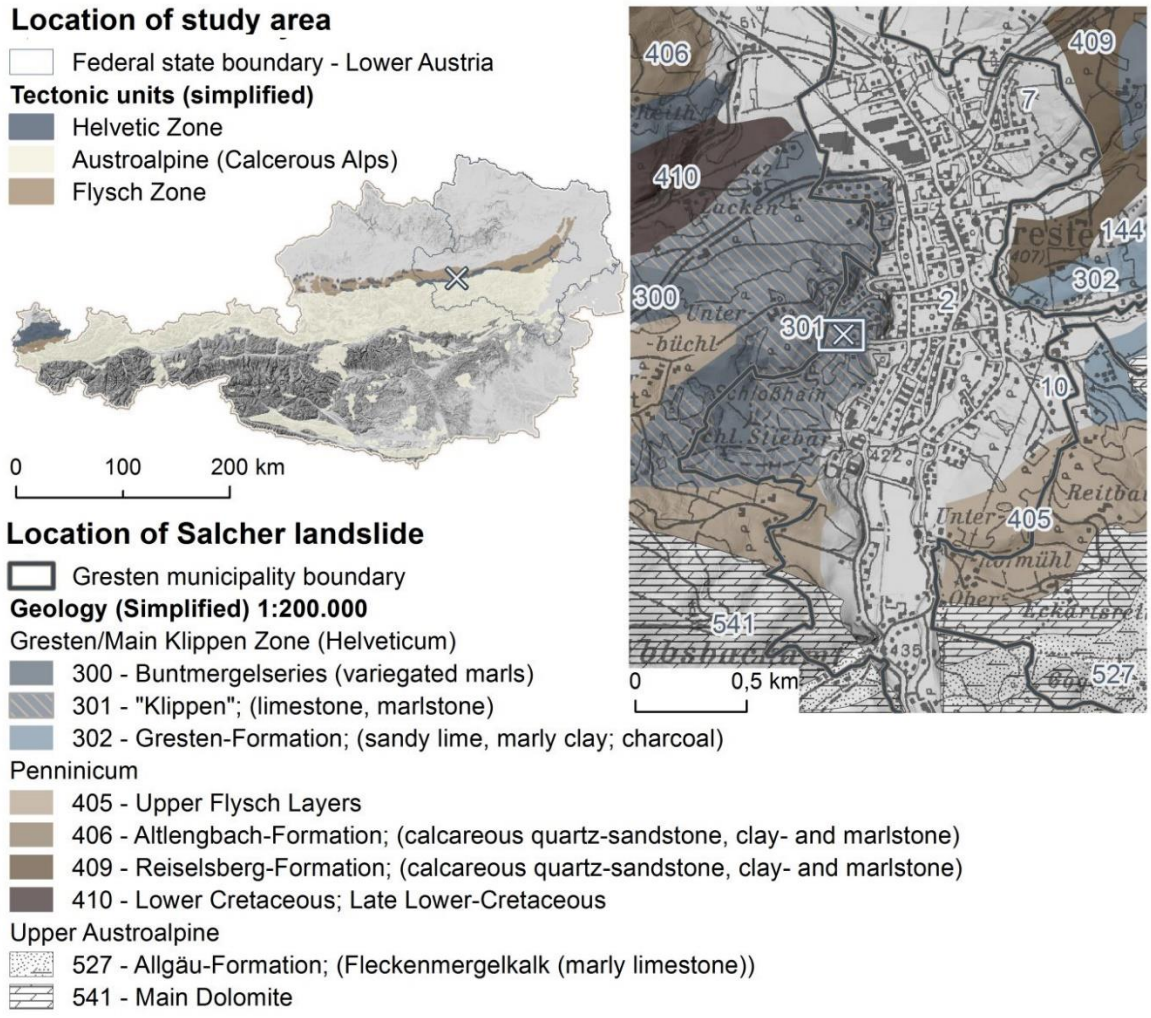

Figure 21: Location of Salcher landslide in a geological context (edited from Stumvoll et al. 2020: 1833)

During the Alpine orogenesis, the Flysch Zone over-thrusted the GKZ, which originally was situated north of it (SCHNABEL 1999). Parts of the local thrusting are only around 200m eastwards from the Salcher landslide (RUTTNER & SCHNABEL 1988). This transition with its axially diving movement formed several “klippen”, which developed upon Jurassic and Lower Cretaceous deposits (HÖCK et al. 2005). According to the geological map of Austria (RUTTNER & SCHNABEL 1988), the GKZ is characterised by marlstone, clayey shales, sandstones, conglomerates and breccia covered by variegated marls, while the Flysch Zone consists of marine sandstones, clays, clayey shales, quartzstones and marly limestones which makes them both extremely complex in terms of stratigraphy and lithology (WIDDER 1988). The lithology of this area acts as a predisposing factor for landslides due to tectonically strained and deeply weathered peltic layers as well as the high content of clay with the corresponding weathering products (STUMVOLL et al. 2020). The geology is susceptible and prone to landslides. This was also shown by SCHWENK (1992) who compiled an extensive inventory of landslides in Lower Austria that occurred between 1953 and 1990. Over a period of 37 years, 1138 landslides have been reported to the Geological Survey of Austria. More than half of them (61%) occurred in the Flysch Zone and the GKZ, while these areas only cover about 9 % of the whole Lower Austria. Most of them were characterised as having a sliding type of movement. The share of rock falls, -topples and creeps is comparatively low.

5.4 Soil

The composition of the soil is strongly related to the geological structure, terrain morphology and climatic conditions of the research area. As already stated, the complex geological background and the transitions between zones lead to a variety of weathered materials in the ground. The soil is therefore very heterogeneous and soil profiles vary, depending on the extraction site. Fig. 22 displays two soil profiles taken from the digital soil map for Austria (BFW 2021) – the left one (Soil I) from the upper western area and the right one (Soil II) from the main body of the landslide.

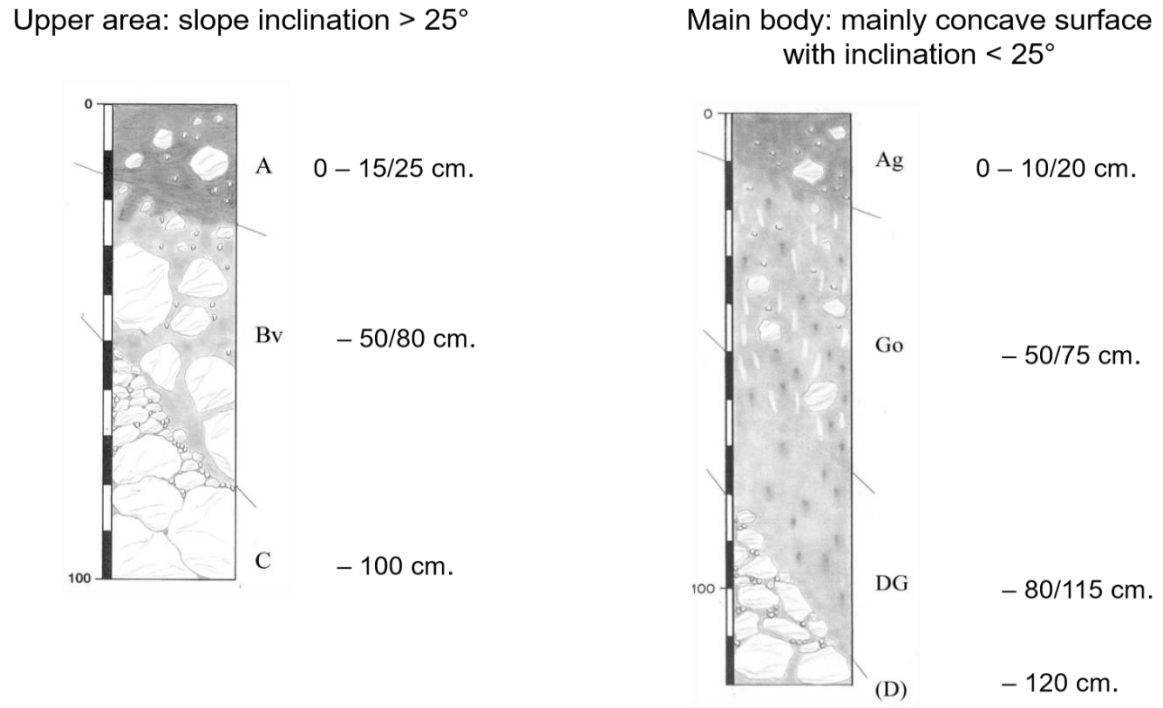

Figure 22: Soil profile I (ID 73 KB 196) upper slope (left) and soil profile II main body of the landslide (ID 58 KB 196) right (changed from BFW 2021)

Soil I (left) is characterised as being moderately dry with a high-water permeability and moderate water storage capacity. In case of rainfall events, the surface runoff is high and exacerbated by the slope gradient. Typically, the soil here has low lime content and consists of brown podzol from slope debris or weathered rocks.

Soil II (right) in contrast is more humid due to pressurized water and the flatter slope. The water storage capacity of this soil is high. Similar to Soil I, the lime content is low as well and the slope consists of predominantly fine colluvial material, which is partly situated over weathered rocks like marl and sandstone.

(BFW 2021)

Similar results were also obtained from subsurface investigations of the soil directly on the slope. Fig. 23 shows the cut open drill core as well as a classification of the different soil horizons according to their silt and clay content according to ÖNORM L1050.

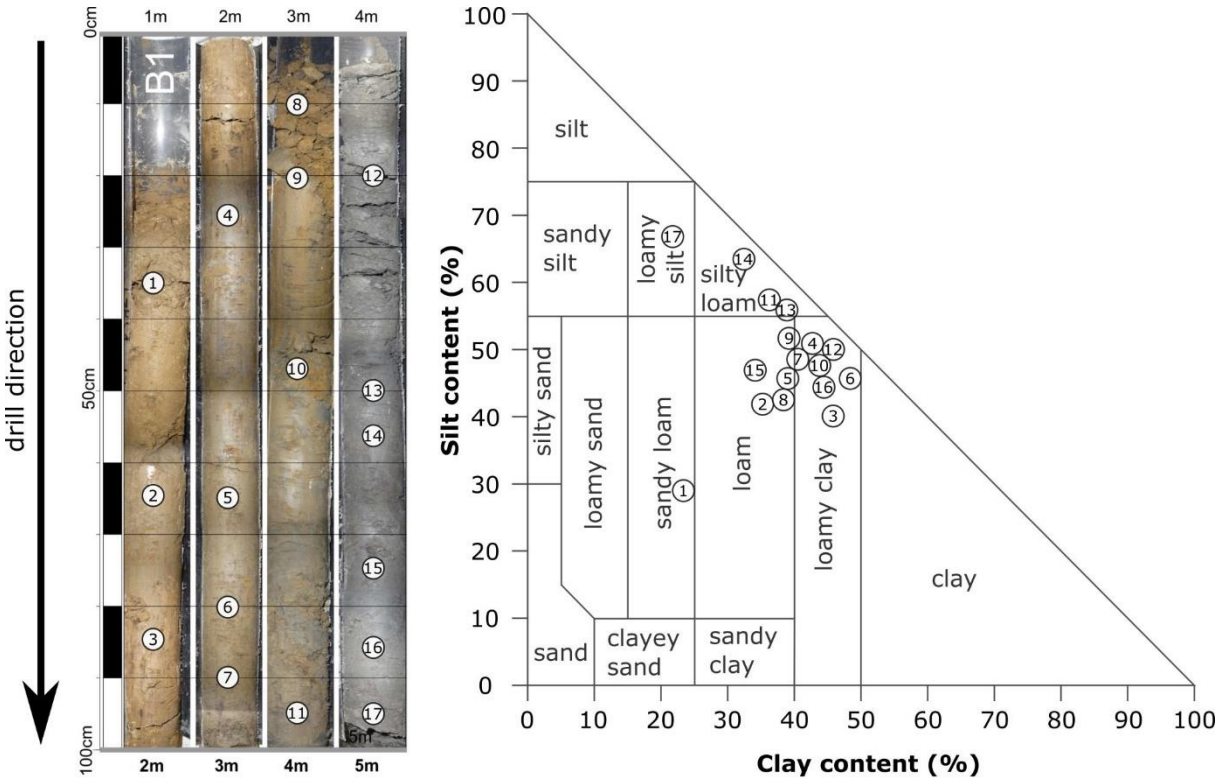

Figure 23: Drill core samples from Salcher landslide with classification (STUMVOLL et al. 2020: 1843)

Direct investigations with core samples, extracted on-site at the Salcher landslide and analyzed in a lab between 2014 and 2015, indicate that the ground consists mostly of loam, loamy clay, and silty loam (STUMVOLL et al. 2020). There is a tendency towards more silty loam than sandy loam, with exception of the top layer (1).

This composition of the soil, with mainly loamy content, along with the complex geology and weathered material, are predisposing factors for the frequent occurrence of landslides in Lower Austria.

5.5 Climate

According to the updated and revised *Köppen-Geiger* climate classification (KOTTEK et al. 2006; PEEL et al. 2007), the research area is situated in the temperate zone (*C*) without dry seasons (*f*) but with warm summers (*b*) – shortly classified *Cfb*. The region is characterised by mean temperatures of above -3°C during the winter and summers not exceeding +22°C, as well as relatively evenly distributed rainfall over the year with every month having at least 30 mm of precipitation on average (PEEL et al. 2007).

Official climate measurements over several decades revealed that the annual precipitation in Gresten is 1215 mm (average of period 1981-2017; see BMLRT 2021a) and the mean annual air temperature is 8,5°C (average of period 1981-2010; see ZAMG 2012). Precipitation data in Fig. 24 was taken from eHYD, a hydrological service provided by the Federal Ministry of Agriculture, Regions and Tourism (BMLRT 2021a) which hosts a measuring station in Gresten, approximately 1,2 km away from the Salcher landslide. The temperature data in Fig. 24 was taken from the ZAMG (2012), a meteorological service provided by the Federal Ministry of Education, Science and Research. Unfortunately, no meteorological station has been installed in Gresten for a long enough time to consider it a climate station, which is the reason why the data was taken from the meteorological station in Waidhofen a. d. Ybbs, being the closest one, approximately 18 km away from the research area.

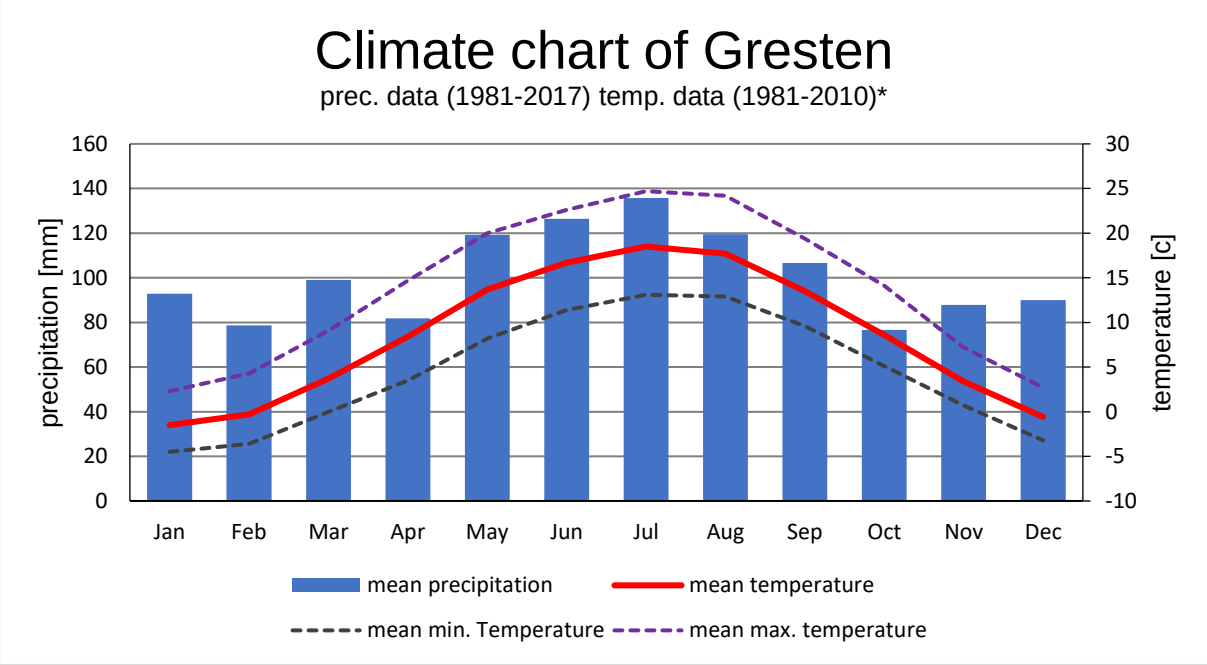

Figure 24: Climate Chart Gresten (BMLRT 2021a; ZAMG 2012)

Fig. 24 displays the mean monthly rainfall in Gresten over 37 years. On average, it rains 101 mm. every month, with the driest periods being February, April, and October, while July is the most humid month. Nevertheless, the distribution of rainfall does have extremes, like May 2010 with 378 mm. and June 2009 with 344 mm. and the dry November in 2011 with hardly any precipitation (1,2 mm.).

The mean monthly temperature over 30 years is also included in Fig. 24. The coldest month is January with an average of -1,5°C, while the hottest temperatures were measured during July with 18,5°C. The mean monthly maximum temperature measured between 1981 and 2010 reached 24,7°C in July. Besides, there is an increase of the mean annual air temperature of 0,3°C between 1971-2000 and 1981-2010 rising from 8,2°C (ZAMG n.d) to 8,5°C (ZAMG 2012).

The mean annual precipitation in Gresten is shown in Fig. 25. The data basis is the same as Fig. 24. It is provided by the BMLRT (2021a) and covers the period from 1981 until 2017. The rainiest year since the beginning of precipitation measurement was 2009 with 1577 mm. and the driest year was 2015 with only 922 mm. of precipitation.

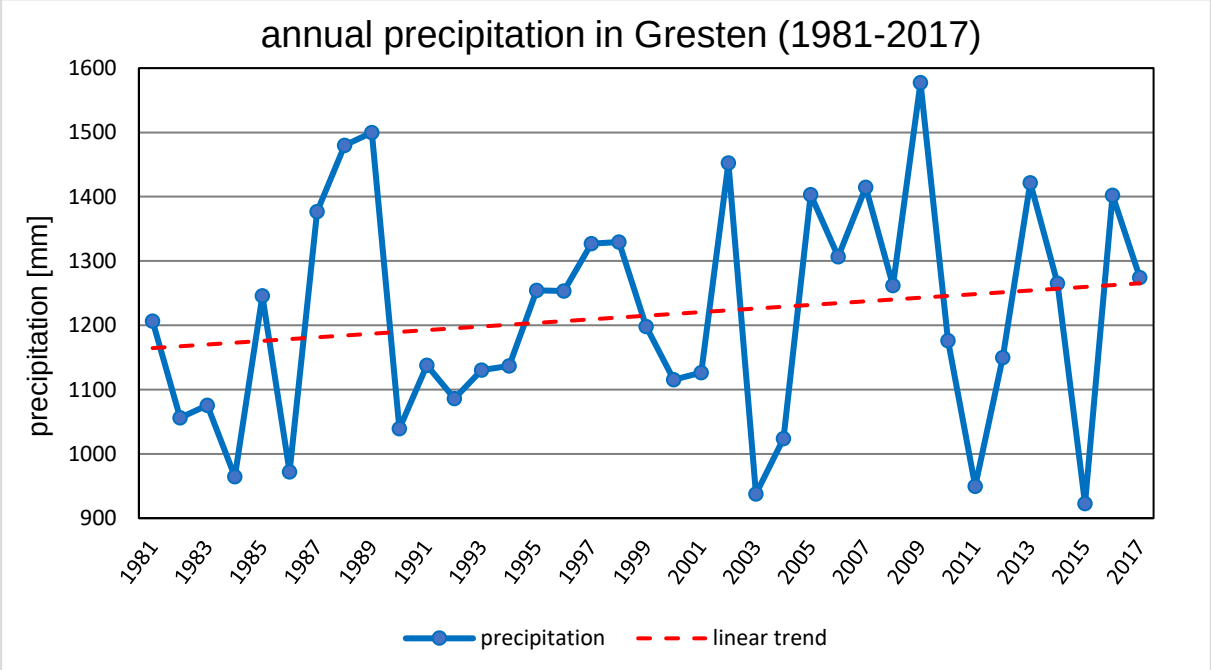

Figure 25: Annual precipitation Gresten (BMLRT 2021)

Noticeable is that the three driest years (2003, 2011 and 2015) occurred in the last 14 years of the 37 years of monitoring. Nevertheless, the linear trend line indicates an increase of annual precipitation. The amplitude between humid and dry years seems to enlarge, which can be seen in Fig. 25.

5.6 Hydrology

The runoff regime describes the water balance in its temporal changes related to the determining factors of precipitation, temperature, evapotranspiration, geology, and geomorphology, as well as soil and vegetation, with mean annual precipitation mainly determining the mean annual runoff. Hydrology of the Flysch zone is characterised by its impermeable hard rocks, clays, and clay marls (see Chapter 5.4). The bedrock has a water stagnant effect and thus also determines the groundwater formation, which is therefore limited to fissures and crevices of a few meters (GATTINGER 1980).

The research area is situated in a small catchment area that discharges into the small river “Kleine Erlauf”, located around 530 m westwards. The difference of elevation between the lowest point of the landslide and the stream is approximately 20 m The spring of the Kleine Erlauf is located approximately 9,4 km upstream of Gresten, having one right tributary, the “Brettlbach”. In Wieselburg, the Kleine Erlauf and the Große Erlauf confluence and form the Erlauf which flows into the Danube near Pöchlarn.

Fig. 26. displays the mean monthly discharge of the Kleine Erlauf near the municipality of Wang, approx. 12 km downstream of Gresten since the nearest available measuring station is situated here. The data was provided by eHYD (BMLRT 2021b).

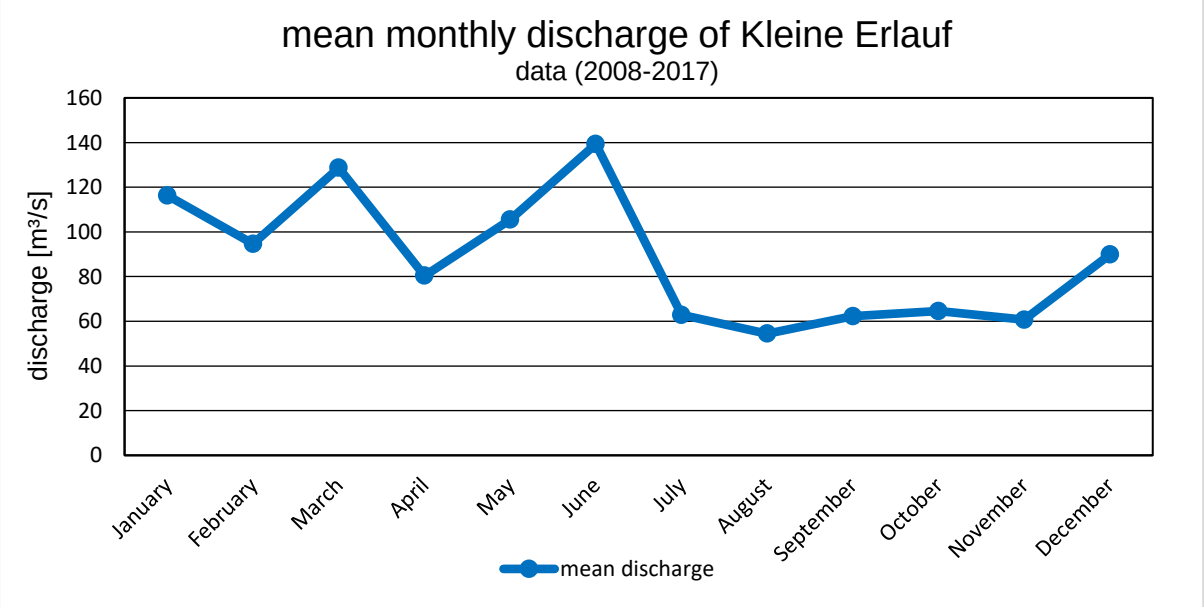

Figure 26: Mean monthly discharge of Kleine Erlauf 2008-2017 in Wang (BMLRT 2021b)

The graph (Fig. 28) shows that the Kleine Erlauf carries most water during the first half of the year, strongly influenced by the snowmelt during spring. The average daily discharge for the period 2008-2017 is 2,61 [m³/s] which in case of a flood can exceed up to 175 [m³/s] (24th June 2009). A 100-year flood is marked at 190 [m³/s] (Federal State of Lower Austria 2021). Nevertheless, little is known about the hydrology of the study area itself. It is expected that the data evaluation of the permanently installed ERT (see Chapter 6.3) will provide further insights (STUMVOLL et al. 2020).

6 Active monitoring at the research area

After the previous chapter provided information about the most important characteristics of the research area, this chapter describes the investigations that have already been carried out there. Most current results are taken from STUMVOLL et al. 2020 and other publications from the ENGAGE group. At first, a historical overview about the landslide and the monitoring aspects is given, followed by depicting recently used monitoring and investigation methods which are part of the interpretation for the collected UAV-data. The chapter closes with the status quo of the research activities and what dynamics are known by now [June 2021].

6.1 Historical Overview

Investigations by the Geological Service of the State of Lower Austria and Geological Survey of Austria (GBA) started in the 1970s due to reports of damage caused by slope activities (JOCHUM et al. 2008; SCHWENK 1976, 1979; SCHWEIGL 2013). The first documented sliding process occurred in July 1975, where a huge part of the slope, approx. 60 – 70 m long and more than 100 m wide, started to move between 30 and 60 cm downhill (SCHWENK 1976). The main scarp nearly reached 2 m and led to the skiing operation to be stopped. The triggering factor for this event was presumably heavy rainfall a few days before with precipitation about 200% above average values (SCHWENK 1976). Three years later in 1978, the landslide was reactivated, but this time slid nearly two meters downhill, blocking a pathway and a driveway (SCHWENK 1979). After several decades of only minor movements, new dynamics of the slope appeared in 2006, damaging several walls and cellars of two surrounding residential buildings. A smaller landslide occurred about 80 m northwest of the research area in September 2007. These events lead to investigations being resumed by the Geological Service of the State of Lower Austria (JOCHUM et al. 2008). The monitoring was discontinued in 2012 since the annual movement rate of the slope has only been a few centimeters over the years. After increasing reported dynamics in 2013, the project NoeSLIDE was brought to life in which the ENGAGE working group from the University of Vienna has since been involved for monitoring aspects in cooperation with the GBA and Provincial Government of Lower Austria.

6.2 Meteorological station

A meteorological station has been installed roughly in the centre of the main body of Salcher landslide to monitor weather in real-time. The data is transferred in five-minute intervals to a server of the University of Vienna and can be accessed via the NoeSLIDE webpage (noeslide.at) (Fig. 28). For the period of observation, this data is used for the discussion of surface changes in Chapter 9.3. Multiple sensors have been installed to measure air temperature, wind speed and direction, precipitation, relative air humidity and air pressure (Fig. 27). On the day of the second UAV-survey was carried out at the research area (22.02.2021), the precipitation measurement device was replaced by a new and enhanced one. Now a modern laser disdrometer records not only the amount of precipitation, but also the intensity, drop size and speed of falling particles (OTT HydroMet 2021). This upgraded sensor allows to distinguish between different types of precipitation and is expected to deliver more information about rain- and snowfall patterns.

Figure 27: Meteorological station Gresten (08.11.2020)

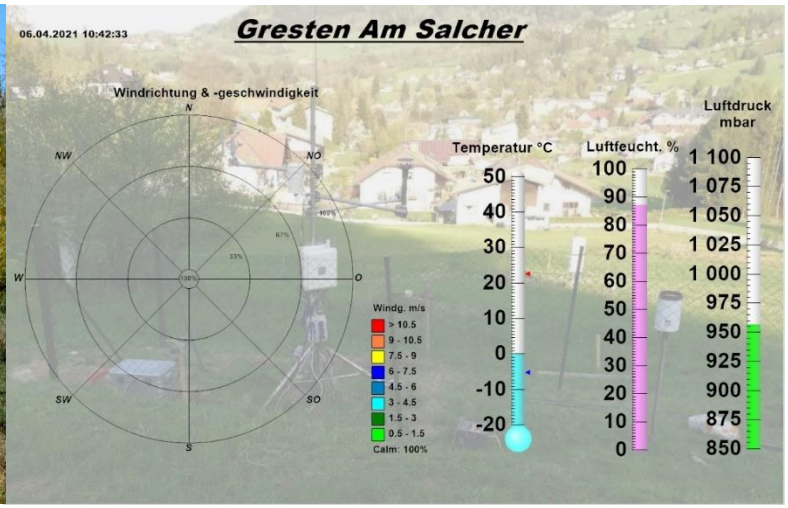

Figure 28: "Real-time" weather data (University Vienna 2021, accessed on the 6th of April 2021)

Generally, a combined analysis of different investigation methods and meteorological data is useful to indicate interrelations of measured parameters after specific rain- or snowfall events. Thereby information about precipitation and spatiotemporal infiltration patterns can be used, in combination with data on landslide dynamics, to determine interrelations and dependencies about slope movement trigger thresholds (HAUCK et al. 2018). By this, specific conclusions about hydro-meteorological conditions and landslide dynamics can be drawn.

6.3 Overview of subsurface and surface monitoring

As already stated, multiple subsurface and surface investigation methods as well as field installations have been applied at the Salcher landslide since the project NoeSLIDE started in 2014/15. Fig. 29 provides an overview of these methodologies and their spatial distribution at the Salcher landslide in Gresten.

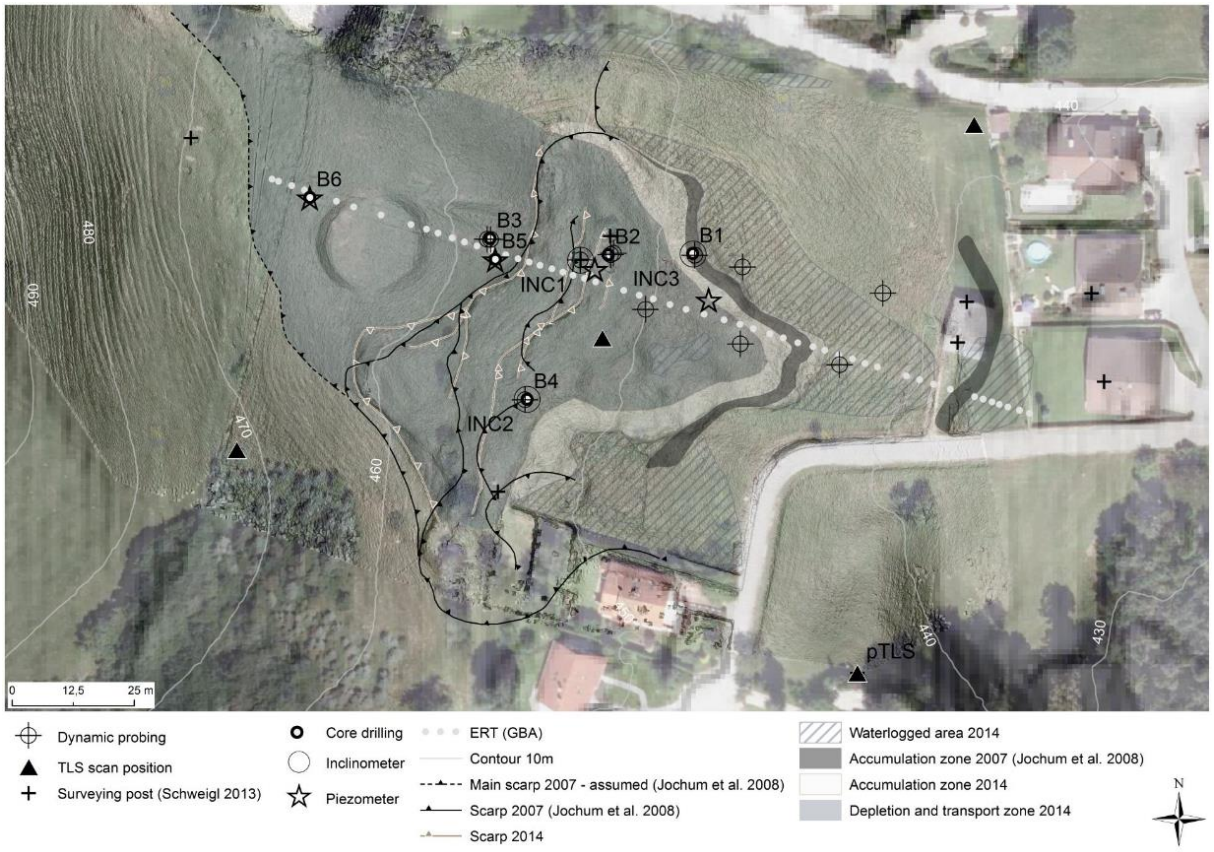

Figure 29: Overview of surface and subsurface investigation sites (STUMVOLL et al. 2020: 1837)

For subsurface investigation and monitoring permanently installed at the Salcher landslide are (see Fig. 29):

- Three TDR-devices directly next to the meteorological station (see Chapter 6.2) in 0.5, 1- and 2-meters depth. In 5-minute intervals, the TDR sensors analyze the volumetric soil moisture content. The data can be accessed via the monitoring webpage of NoeSLIDE.
- Five Piezometers, of which three are applied along the longitudinal profile of the landslide, one along the upper transverse profile and one near the meteorological station. Same as for the TDR-devices, the data can be accessed in real-time via the monitoring webpage.

- Four Inclinometers, of which one is operated automatically and the other three are measured manually about once per month. The tubes of the manual inclinometers are about 4 - 4.65 meters deep in the ground, while the tube of the automatic one is at a depth of nearly 13 meters. Two previously installed inclinometers became unusable due to the movements of the slope in 2018.

(STUMVOLL et al. 2020)

Additionally, to the monitoring devices hosted by the ENGAGE working group, the GBA used to operate a permanently installed ERT at the Salcher landslide. The electronic profile is approx. 170 meters long and buried in a depth of 30 cm (OTTOWITZ et al. 2018). The measurement was carried out in three-hour intervals, whereby changes of moisture conditions of the subsurface can be determined.

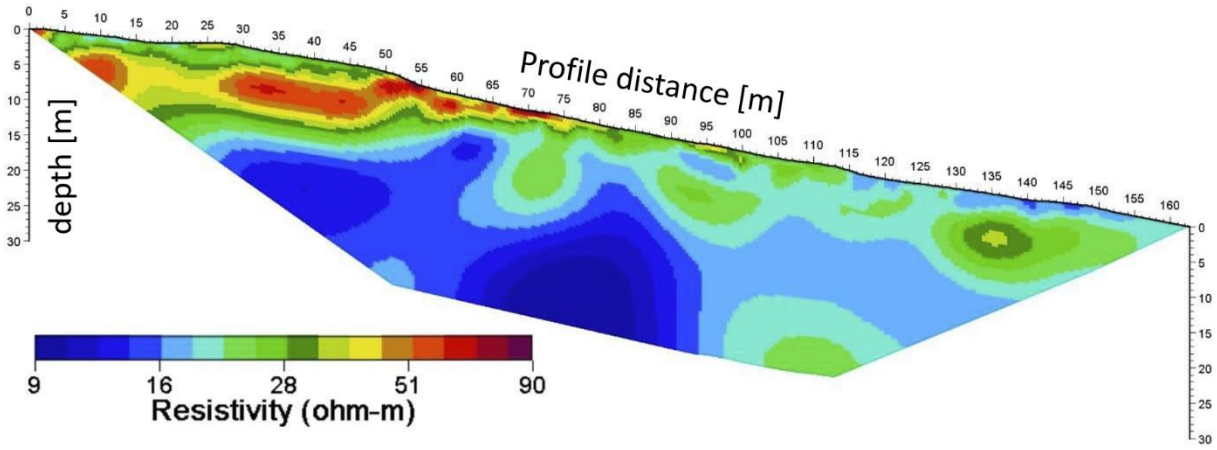

Figure 30: Representative model results of the ERT monitoring profile (translated; OTTOWITZ et al. 2018: 27)

The results of the ERT monitoring profile (Fig. 30) tends to show higher electrical resistivity values near the surface. Indeed, the upper slope part of the profile (0-75 meters) has significantly different characteristics than the remaining part down towards the end of the profile. As already known from previous investigations (see JOCHUM et al. 2008), this initial area is under the influence of a neighboring geological unit – hence the significantly higher values of the specific electrical resistance. Due to the clayey ground of the research area, the subsurface area from a depth of about 10 m generally shows a very low specific electrical resistance. Further downslope, from profile meter 75 and on, the values for ground resistivity are also comparatively low, but here was a certain subsurface heterogeneity identified, mainly due to the rearrangement processes in this active area of the slope (OTTOWITZ et al. 2018).

To monitor dynamics and changes of the surface, a permanent TLS (= pTLS) was installed about 70 meters south from the former ski lift hut (see Fig. 29). The pTLS scans the most active parts of the research area (Fig. 31) daily and transfers the data to the servers of the University of Vienna. Thereby spatial and temporal information about surface changes over time can be gathered. This permanent data acquisition enables further interpretation of landslide dynamics by using the resulting high-resolution point clouds with millimeter accuracy and precision (CANLI et al. 2015).

Figure 31: Area covered by the permanent TLS scanner at Salcher landslide POV (University Vienna 2021)

Having a pTLS installed has the advantage of (i) having measurements in fixed time intervals, (ii) having the exact same measuring position, which can affect the accuracy and (iii) saving time by not having to set up a regular TLS for every data acquisition.

GNSS measurements, which have been applied at the beginning of the monitoring program, are no longer used. They have been carried out monthly to detect punctual and linear changes of the surface.

6.4 Current knowledges of Salcher landslide dynamics

Combining monitoring investigations along with on-site measurements result in a broader overview of the general landslide dynamics. Before the UAV-survey was carried out for this master thesis, a lot of information about the structure, characteristics and movement rate had already been collected over the last years of investigation.

Further investigations in 2014 gave insight about the internal structure of the research area. Fig. 32 shows the results, displayed in a transverse profile of the landslide.

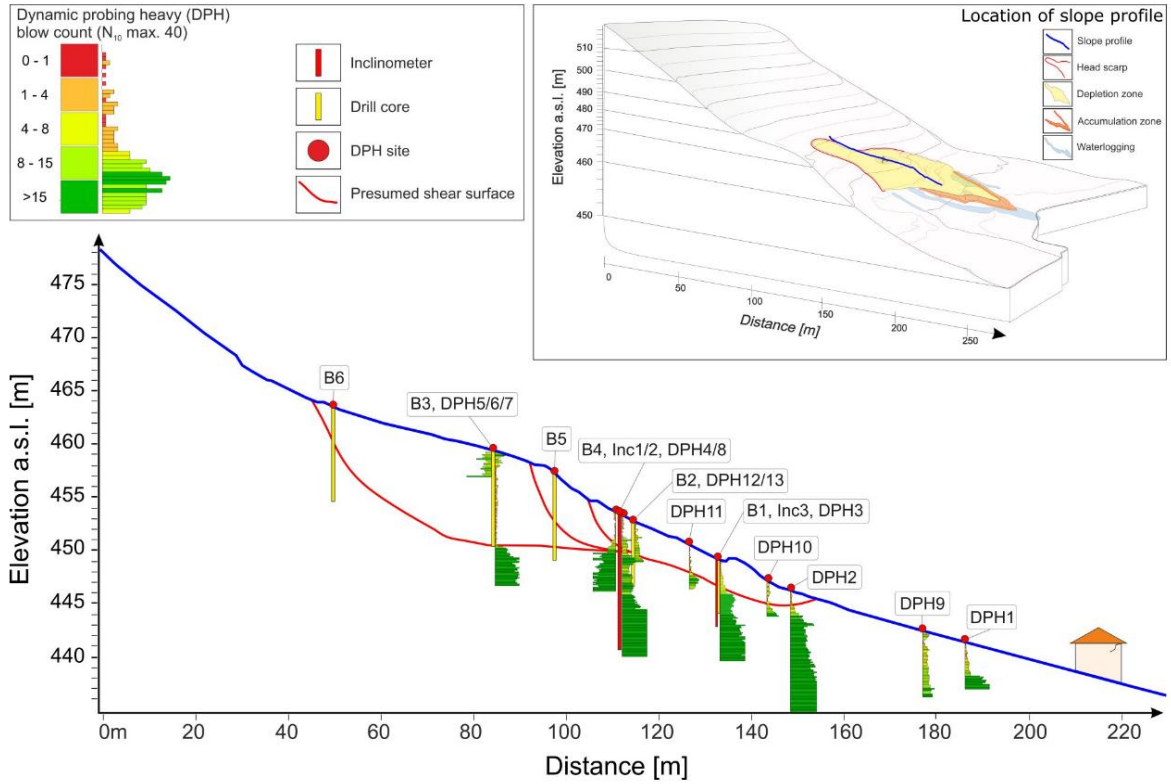

Figure 32: Underground model of internal structure of the Salcher landslide (STUMVOLL et al. 2020: 1845)

By counting the number of blows needed for every 10 cm of ground penetration and analyzing local displacement measurements with inclinometers, two presumed shear surfaces in approx. 3- and 9-meters depth below the surface could be identified. Especially in the depletion zone, the depleted mass is looser due to the movements and the resulting mixture of internal structures. Similar results about the subsurface have been shown by the first results of the ERT (see Chapter 6.3).

The underground model also presumes that the research area is a larger rotational landslide, consisting of multiple interconnected sliding bodies, but with translational

characteristics for the area between the visible scarps in the mid and the bulged foot of the landslide. Drill core samples lead to the conclusion that the first shear surface are clay-rich layers in 2 to 3 meters depth, which can trigger movements if saturated by rainfall. (STUMVOLL et al. 2020).

Analysis of surface dynamics prior to this master thesis were carried out in 2007 by the GBA (TLS), 2009 by the State of Lower Austria (ALS) and since 2014 by the ENGAGE working group (TLS and pTLS). Using this data and comparing digital point clouds of the surface can be the basis for DoD's (=DEM's of difference), which display the changes of the landslides' surface over time.

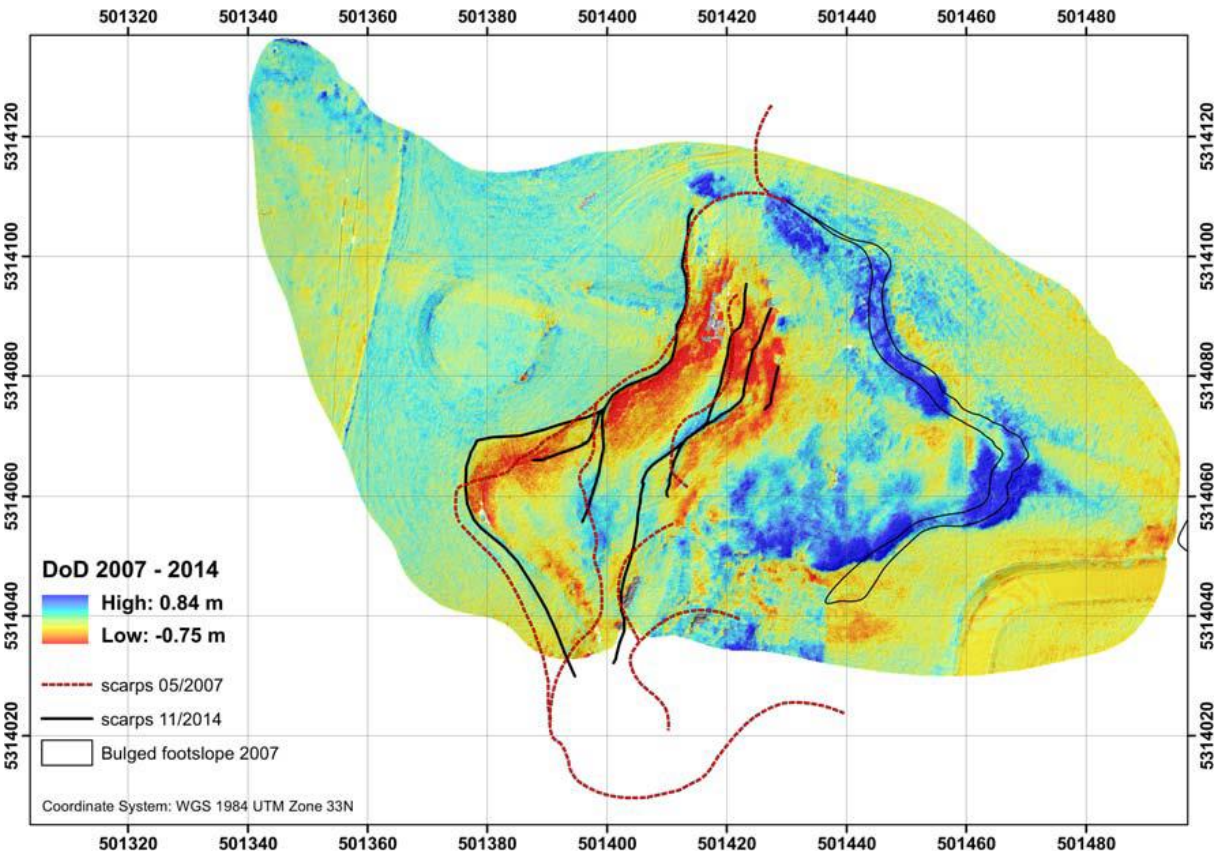

Figure 33: DoD based on TLS clouds 2007 and 2014 with 10 cm resolution (STUMVOLL et al. 2020: 1840)

Fig. 33 is a DoD based on TLS data from 2007 and 2014 and showing that the zone of depletion has sagged down, partly up to 75 cm over seven years while parts of the accumulation zone lifted nearly 84 cm due to the rotational movement of the material. The "lost" depleted mass from the upper part of the slope moved slowly over the toe of the surface of rupture to accumulate on the lower parts of the research area. Tension cracks are visible in the field. Mapping of main scarps is also included in Fig. 33 and shows how they have changed over seven years. While the rough course of the scarps

remained the same in 2014 compared to 2007, dynamics can still be seen that in some cases the scarps have shifted either up or down the slope.

Figure 34: Uneven surface of the Salcher landslide, camera facing west (22.02.2021)

Prior to 2014, the most active zone of the Salcher landslide had a movement rate of 11 to 17 cm per year (SCHWEIGL 2013). Figure 34 is an image taken on the date of the second UAV-survey. The uneven surface is clearly visible and is the result of material moving downslope on multiple presumed shear surfaces (see Fig. 32) leading to such an “hilly”, almost “wavy” slope.

Analysis of the data from the pTLS near the landslide until 2019 do not indicate major changes here – the average movement rate of the surface is approx. 15 cm per year, even though these values vary because certain parts, especially near the edge of the research area, show lower to no movement at all (STUMVOLL & GLADE 2019). The values calculation is based on six different surveys, in which all of these datasets have been calculated with each other to determine an average value for one year. The span between the maximum values in both directions was used for this (see STUMVOLL & GLADE 2019: 6).

Selected points were marked on the pTLS produced point clouds and monitored over 3 years. The resulting position differences due to ground movements can be measured and are presented in Fig. 35.

Figure 35: pTLS-data; distance measurements 2016-2019 (GLADE et al. 2019)

As seen in the image above, horizontal displacements for specific points ranged from 5,5 to 23,2 cm within three years, which already indicates different rates of movement of the surface. Similar measurements have been conducted with the antenna of the meteorological station. Here, the pTLS-data revealed a slight downslope tilt of 8,6 cm at the top of it, while the lower parts of the station only experienced smaller displacements (GLADE et al. 2019).

7 Methodology: UAV-based SfM

To analyze the surface dynamics of the Salcher landslide, an image processing method called "*Structure from Motion photogrammetry*" was applied for this study. RGB-images taken by a UAV device are used as the basis to create multidimensional point clouds and elevation models for further investigations. To explain the whole process, this chapter will start with a detailed description of different steps required for data acquisition and then continue by explaining the principles of photogrammetry and the subtype structure from motion as well as data post-processing.

UAV-based SfM analysis for landslides have already been carried out worldwide and a lot of literature is available. The whole workflow for this thesis is based on LINDER et al. (2015) who monitored and documented a larger landslide in Upper Austria with multiple UAV flights, EKER et al. (2017) who used the software CloudCompare for post-processing analysis of elevation changes and investigated the Gallenzerkogel-landslide which is about 30 km southwest of the Salcher landslide as well as WARRICK et al. (2019) and LUCIEER et al. (2014) with their papers focus being on accuracy assessments and repeated aerial survey analysis of landslides.

Since UAVs are a newer methodology in geosciences for monitoring and investigation, LINDER et al. (2016) has been one of the first to describe the whole workflow of UAV-based SfM (Fig. 36).

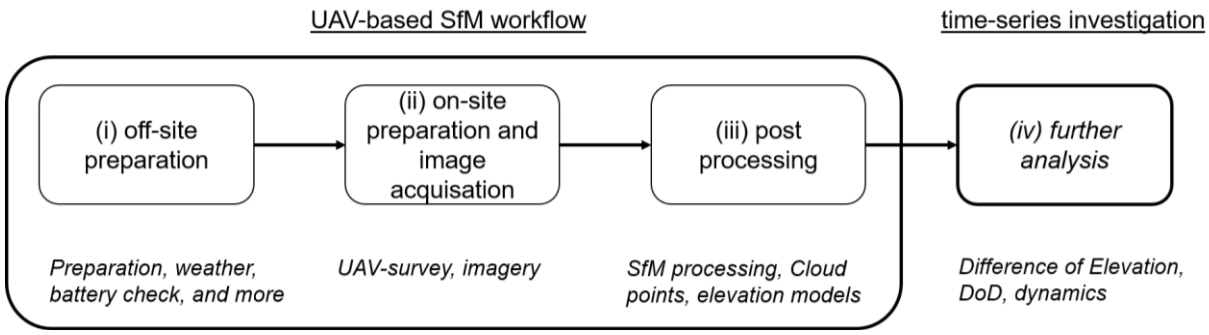

Figure 36: SfM-Photogrammetry workflow (adapted from LINDER et al. 2015: 3)

The main steps can be categorised as the following, (i) off-site preparation, (ii) on-site preparation and image acquisition (iii) post-processing. Nevertheless, this master thesis adds a fourth step by doing further analysis (iv) of the results produced during step (iii).

7.1 Structure from Motion: Photogrammetry

The basis of photogrammetric measurements is to reconstruct the paths of rays from an area of interest to the sensor of the used camera (ABER et al. 2010). The principles date back over 150 years, just like photography itself. It was originally used for mapmaking and surveying territories of enemies during times of war and was expanded regarding applications after World War II (SMITH 1979). Since then, it has become a widely used approach for 3D modelling of surfaces or features of interest in various disciplines (NYIMBILI 2016). Depending on the chosen platform, photogrammetry can either be a terrestrial or aerial methodology, like laser scaninng (see chapter 4.2.3). Photogrammetry and SfM are both image processing methods and share the same principles.

SfM is an image processing method to create 3D models on the basis of 2D images. These images are usually a series of overlapping, offset images, covering a "*feature of interest*", which in this case is the Salcher landslide. The term SfM refers to the images derived from a moving sensor, so the pictures are all taken from a slightly different position (WESTOBY et al. 2012).

However, SfM-photogrammetry differs fundamentally from the traditional photogrammetry since the field of computer vision has improved over the last decades and issues like camera orientation and position as well as geometry of the scene are now solved automatically by software and algorithms (WESTOBY et al. 2012).

Traditional photogrammetry	SfM-photogrammetry
Stereo-image reconstruction	Multiview-stereo reconstructions
Parallel optical axes	Variable directions of optical axes
Fix scales and resolutions	Various scales and resolutions
Pre-calibrated cameras	Any camera
Exterior orientation indispensable	Exterior orientation not necessary

Table 4: Traditional photogrammetry vs. SfM-Photogrammetry (after ABER et al. 2010)

As seen in Tab. 4, the main differences between traditional – and SfM-photogrammetry is that SfM-photogrammetry; (i) requires less calculation by the user due to the technical improvements, (ii) has a broader field of applications since it is no longer based on stereoscopic view and (iii) is capable of reconstructing complex three-

dimensional objects and forms (ABER et al. 2010; WESTOBY et al. 2012). SfM can therefore be seen as an automation and extension of the traditional photogrammetry (SHALABY et al. 2017).

7.2 UAV-Surveys

To acquire the data of the surface, three UAV-surveys have been carried out between autumn 2020 and spring 2021. By having more than one survey, time-series analysis is possible, and changes and dynamics of the landslide's surface can be detected (LINDER et al. 2016). For a better understanding and clarity, the three surveys will be named as the following:

- **UAV-I** carried out on 18th November 2020
- **UAV-II** carried out on the 22nd of February 2021 (96 days since UAV I)
- **UAV-III** carried out on the 23rd of April 2021 (156 days since UAV I)

By covering a period of slightly more than five months over the winter and spring season, it is assumed that precipitation and snowmelt have direct impacts on surface dynamics, which can be visibly displayed and calculated. Besides, during winter and spring, vegetation and grass are comparatively lower than during summer. This is one of the main reasons for picking this period, since grown vegetation can distort surface measurements (ABER et al. 2010).

7.2.1 Platform

The UAV used for capturing images of the research area is the DJI Mavic 2 Pro (Fig. 37). It weighs about 900 gram and can reach a velocity of 72 km/h and a flight height of 6000 meters. Maximum operating time for one battery is approximately 30 minutes and its internal storage allows to save up to 8 GB of images and videos (DJI 2021).

Figure 37: DJI Mavic 2 Pro with Hasselblad L1D-20c camera at the Salcher landslide (18.11.2020)

The camera attached to the UAV is a Hasselblad L1D-20c with a CMOS sensor. Images are captured RBG 5472 x 3648 pixels with a focal length of 10mm (fixed). To avoid blurred and overexposed images, the camera was set on automatic mode for the UAV-surveys so ISO- and shutter speed settings vary.

The UAV is controlled by the DJI Smart Controller and carries out the flights automatically with the Pix4Dcapture application. This app allows users to mark the research area as polygons or grids as well as adjusting camera tilt, flight height and velocity. During flight, it proceeds to take pictures in pre-fixed intervals to have accurate overlapping imagery. In the field, it was also tested, to manually gather the aerial data, however the results have not been satisfactory.

7.2.2 Off-site preparation

Before going into the field to gather data, it is important to be well prepared since several prerequisites need to be met for a successful UAV-survey. First of all, batteries of the UAV and the remote controller need to be checked, as well as the function of a GNSS-device which is later needed to measure GCPs in the field. Secondly, the weather forecast needs to be checked. Optimal weather conditions for UAV-surveys are windless, cloudy and no rain (EKER et al. 2017). Rain- or snowfall can not only destroy the electronics and devices used but also have negative impacts on the image quality and wind can result in blurred images due to the mid-air movements of the UAV if strong enough (ABER et al. 2012; LINDER et al. 2016). The reason why cloudy weather conditions should be preferred to direct sunlight is because shadows can eventually lead to misinterpretation of the surface during the post-processing step (ABER et al. 2012). The weather forecast was checked carefully before driving two hours to Gresten from Vienna, however it wasn't possible to avoid sunny days, nevertheless the shadows didn't play a major role since the vegetation was not fully grown due to the season.

Prior to the on-site data acquisition, two visits to the landslide have been made to determine the exact area of investigation and to get a general overview. Additionally, the area was assessed roughly by using NöAtlas and Google Earth, to gather information about the size and elevation differences of the research area.

Even though LINDER et al. (2016) names flight planning as an off-site preparation, the actual flight plans for the three UAV-surveys have been made on-site due to a relatively user-unfriendly operation of the flight planning app Pix4Dcapture. The application struggled to fix the research area if tried from a different location other than the research area itself. However multiple theoretical flight plans have been tried out before to get comfortable with the user interface.

7.2.3 On-site data acquisition

The on-site data acquisition started by distributing multiple Ground Control Points (GCP) which are needed during post-processing to reference the results. Generally, the more GCPs used, the more accurate are the results, however GINDRAUX et al. (2019) found out that after a certain "*optimal GCP density*" related to the Ground Sampling Distance (GSD) is reached, accuracy will not increase for produced cloud points and elevation models. Based on this, 13 GCPs were manually distributed over the research area. Even though this is more than enough, it is safer to have more than the minimum requirement in case errors occur during the GCP survey or other unpredictable events happen, for instance a horse, which flipped two GCPs shortly after they have been surveyed. These GCPs were excluded from further processing.

Figure 38: GCP with metal plate (left), Leica GNSS system (right) (05.11.2020)

The used GCPs as seen in Fig. 38. are printed DinA2 papers glued to a heavier metal plate to avoid any movements by the wind. During the distribution, care was taken to not distribute the GCPs in patterns, since this can result in distortion of the x/y/z axis (ABER et al. 2012) and, in particular, to cover the peripheral areas of the landslide. After every GCP has been placed over the research area, each of them was surveyed by a Leica GNSS-system with enabled real-time kinematic measurement (Fig. 38). Even though the DJI-drone has a built-in GNSS receiver and geotags all captured images, the real-time kinetic measurements are more accurate (LUCIEER et al. 2014), which was also confirmed during the post-processing of the data.

After the exact positions of the GCPs have been determined, the UAV-survey begins. For each of the three surveys, the flight attributes were the same. Flight height was 65 meters above the starting point, which was in the southeast corner of the research area. The starting point was 484 m (WGS84 UTM33N), meaning the UAV carried out the survey at approx. 550 m above sea level and had a flight height of approx. 34 meter above the highest point of the landslide. With these settings and the used camera, the UAV-survey results in a GSD of approx. 1.52 cm/px.

For each of the three surveys, two flights have been carried out, one with the camera tilted 90° vertically and one with a tilt of 75% to capture structures of the surface. Image overlapping for x and y axis was set to 80% (Fig. 39) to make sure that there are enough keypoint matches. Flight paths and number of captured images vary (see Fig. 40.). This was done on purpose to avoid errors arising for certain flight patterns. ABER et al. (2012) suggest that slightly different flight paths for each survey result in more accurate point clouds and elevation models.

Figure 39: representative settings for a UAV-survey (taken from Pix4Dcapture 22.02.2021)

Flight speed was set on “slow”, to avoid blurred imagery, however the exact velocity can’t be determined due to the “blackbox”-like user interface of Pix4Dcapture (Fig. 39). However, during post-processing, the median velocity on the basis of time-tags for every image could be calculated back to approx. 1.6 - 2.4 m/s (= 5.8 – 8.6 km/h).

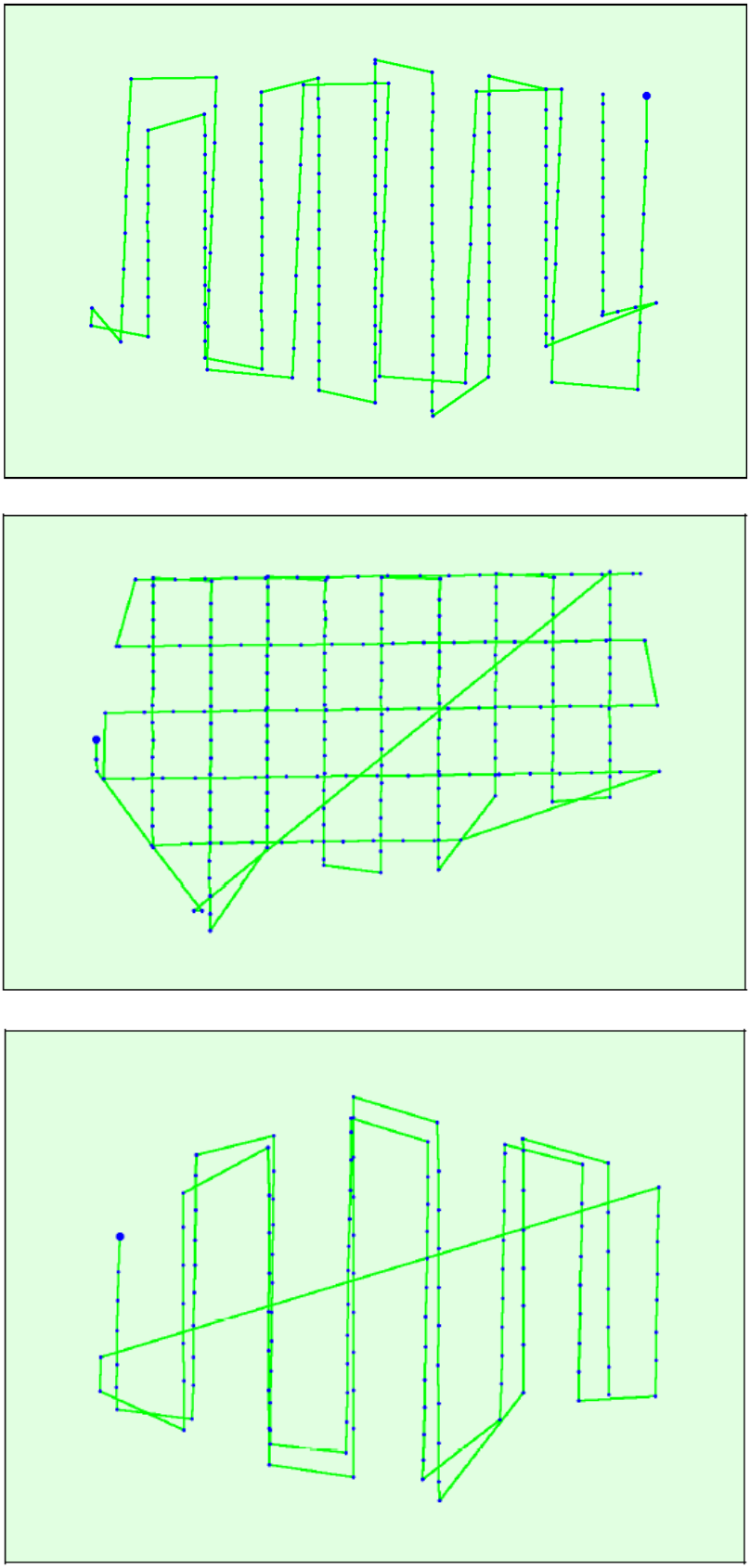

Figure 40: UAV I flight path with n=213 images (top), UAV II flight path with n=242 images (middle), UAV III flight path with n=138 images (bottom), (created with Pix4Dmapper, Pix4D SA 2021a)

Each flight took about 12 mins, take off and landing was performed automatically with the flight planning app and imagery was saved on the onboard SD-card of the UAV. Some initial problems with the UAV and the remote controller occurred during the first surveys leading to several images to be deleted due to their low quality. However after adjusting a few settings within Pix4Dcapture and DJIGo, the UAV-surveys proceeded without problems. To summarise, six surveys on three different days have been performed resulting in 213 images for UAV I, 242 images for UAV II and 138 images for UAV III.

7.3 Post-processing: Structure from Motion Photogrammetry

After the field work was finished, step iii (see Chapter 7) of the SfM-processing was started. For the whole post-processing step, WGS 84 UTM33N EGM96 Geoid coordinate system was used. This subchapter describes the workflow from 2D imagery to 3D elevation models.

7.3.1 Image processing

The images are loaded into the commercial software Pix4Dmapper which identifies features and points of interest for every image and extracts these. This is called keypoint extraction. After these points are identified, an algorithm proceeds to “scan” all remaining images to find which pictures have the same keypoints to match. These points are called “tie points”. How many keypoints are identified depends on the image texture and quality and not on the scale (WESTOBY et al. 2012). Based on matched keypoints, the internal and external parameters of the camera for every captured image during the survey can be determined. The software uses Automatic Aerial Triangulation (AAT) and Bundle Block Adjustment (BBA) algorithms for these steps and calculates a mean reprojection error of the image processing (see Tab. 5). Multiple 2D matching keypoints are triangulated together by using the camera parameters to generate a 3D point (Pix4D SA 2021a).

	UAV I	**UAV II**	**UAV III**
Number of 2D keypoint observation for BBA	7.877.419	11.152.304	5.149.541
Number of 3D Points for BBA	2.112.731	2.116176	1.610.314
Mean Reprojection Error [pixel]	0.164	0.171	0.156

Table 5: Bundle Block Adjustment Details for UAV-Surveys

In total, a median of 76.816 (UAV I), 73.547 (UAV II) and 74.936 (UAV III) keypoints have been extracted. All used images were calibrated with a median of 37.657 (UAV I), 46.865 (UAV II) and 39.313 (UAV III) matches per image. The processing options were set to “full” and “original image size”. The newly calculated GSD decreased from the original 1.52 to 1.31 (UAV I), 1.22 (UAV II) and 1.26 pix/cm (UAV III) due to the

lower absolute flight altitude over the elevated areas of the landslide. The calculations for the three surveys required about four hours each with the following components: AMD Ryzen 7 5800x 8-Core Processor, 32GB of RAM and a NVIDIA GeForce RTX3070 GPU.

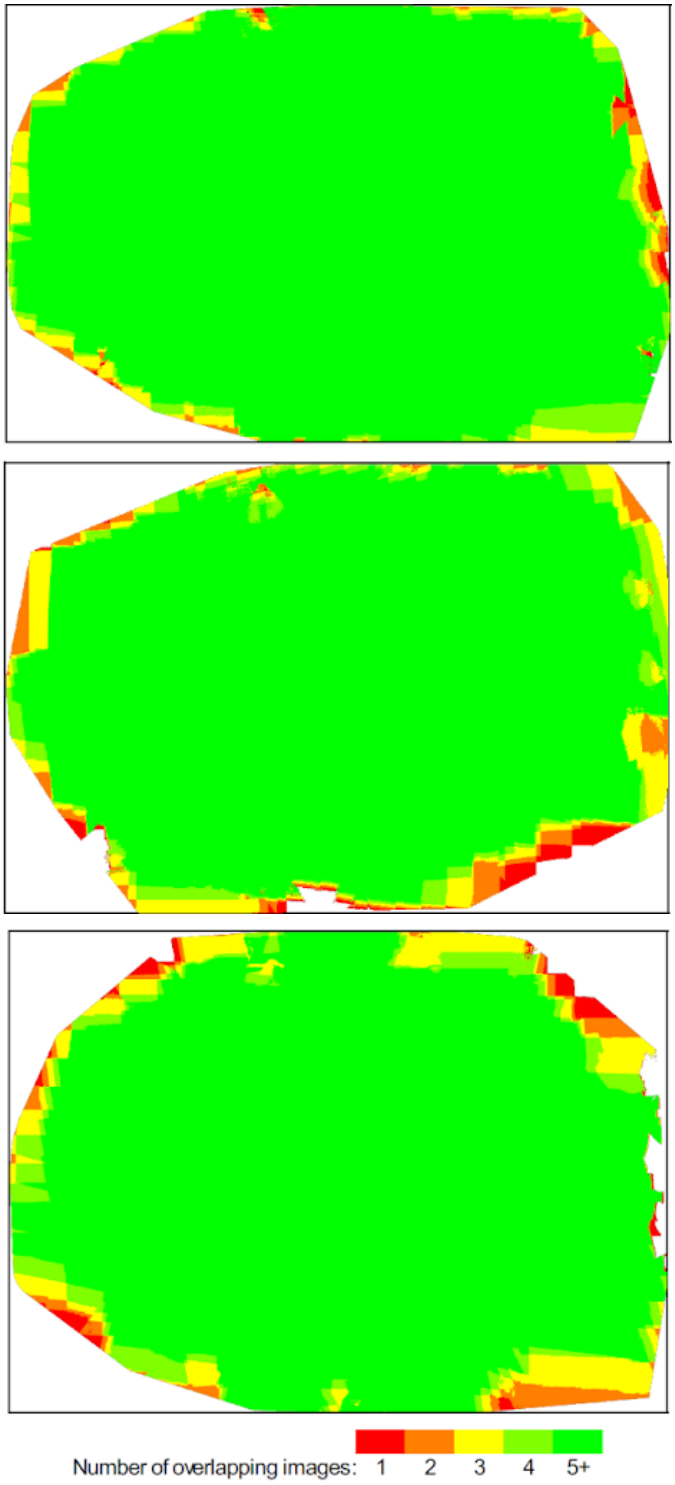

Figure 41: Number of overlapping images for UAV I (top), UAV II (middle), UAV III (bottom)

The number of overlapping images computed for each pixel can be seen in Fig. 41. The green areas indicate an overlap of five or more images for every pixel which is sufficient to generate high-resolution results.

Since the used drone geotags the photographs, a rough estimation about the absolute camera position was already made during this step. However, the onboard GNSS of the UAV is not as accurate as real-time kinematic GNSS measurements (see Chapter 7.2.3) so the GCPs need to be identified manually (see Fig 42).

Figure 42: representative example of manual GCP marking on eight different images.

Each GCP was marked on at least six different images before reoptimising the geo-location of the tie points and calculating initial divergence errors. The results are displayed in Tab. 6.

	UAV I	**UAV II**	**UAV III**
used GCPs	12	11	12
RMS Error X [cm]	0.74	1.15	0.97
RMS Error Y [cm]	1.11	1.43	0.81
RMS Error Z [cm]	1.01	1.85	1.15

Table 6: Mean errors in the three coordinate directions for UAV-Surveys

7.3.2 Creating dense point clouds

The generated tie points from the image processing are the basis for point cloud densification and a 3D textured mesh of the research area. For processing, the original image size was used to compute additional 3D points with optimal point density and a minimum number of at least three matches, meaning that each 3D point must be correctly re-projected in at least three images. The result is a high-resolution dense point cloud (Fig. 43). A 3D textured mesh is generated by triangulating this dense point cloud which creates a 2.5D model of the topography with a surfacing algorithm (COMERT et al. 2019). Dense point clouds, just like DEMs, can be used for further analysis and investigations (see EKER et al. 2017).

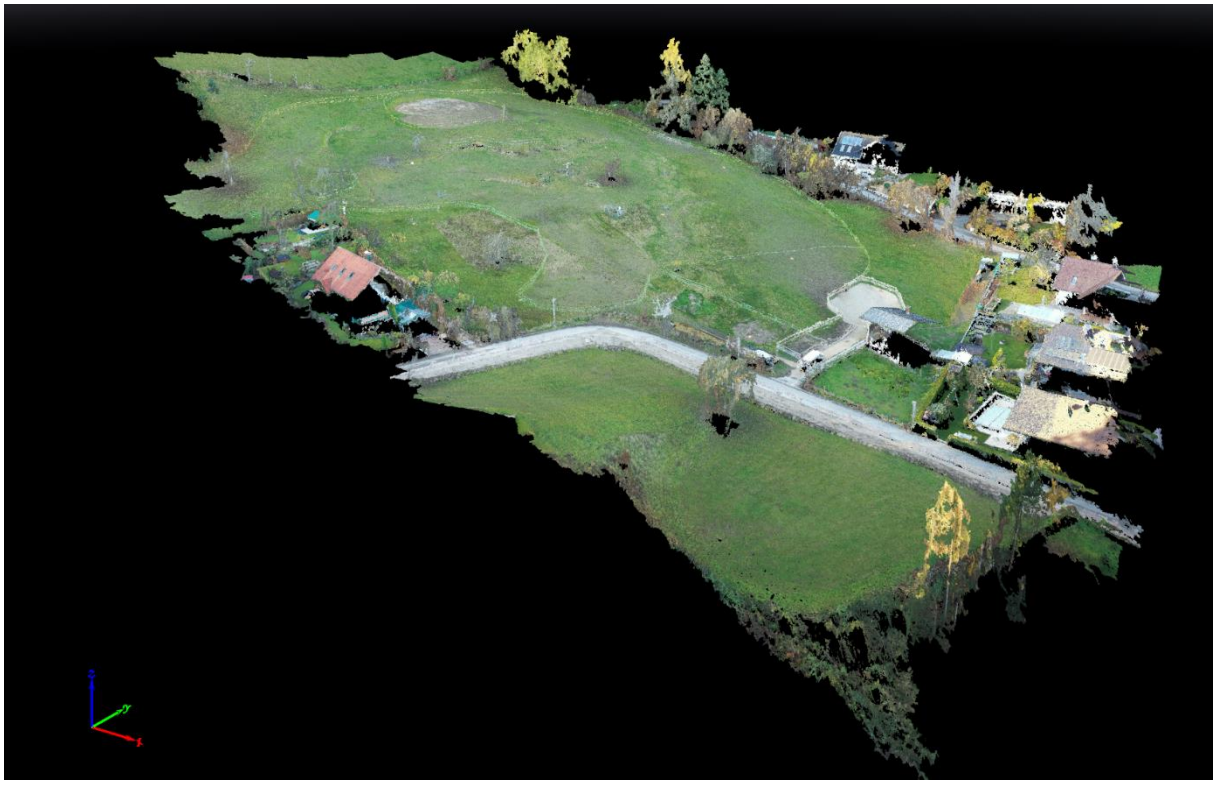

Figure 43: High resolution dense point cloud (UAV I)

Additionally, a point cloud classification algorithm was used to divide every point into the categories “Building” and “Human Made Object”. This pixel-based image analysis (PBIA) allows to remove features of the research area, which then will not be taken into further processing steps (COMERT et al. 2019; see previous Chapter).

Average number of 3D densified points per m3 was 6193,41 (UAV I), 8420,89 (UAV II) and 5324,7 (UAV III).

7.3.3 Creating elevation models

For the purpose of this master thesis, DTMs seem to be the most suitable models to analyze surface changes. By excluding trees and higher vegetation, errors related to moving tree branches are prevented and the pure ground surface can be investigated. The used software Pix4Dmapper already did an automatic classification for the dense point cloud, which allows to disable categories like human made object and higher vegetation in order to produce elevation models. However, the classification was incorrect for some areas of the landslide, which required manual adjusting and reclassification for certain misinterpreted spots, especially ground surface beneath and near higher objects like fences and trees (Fig. 44).

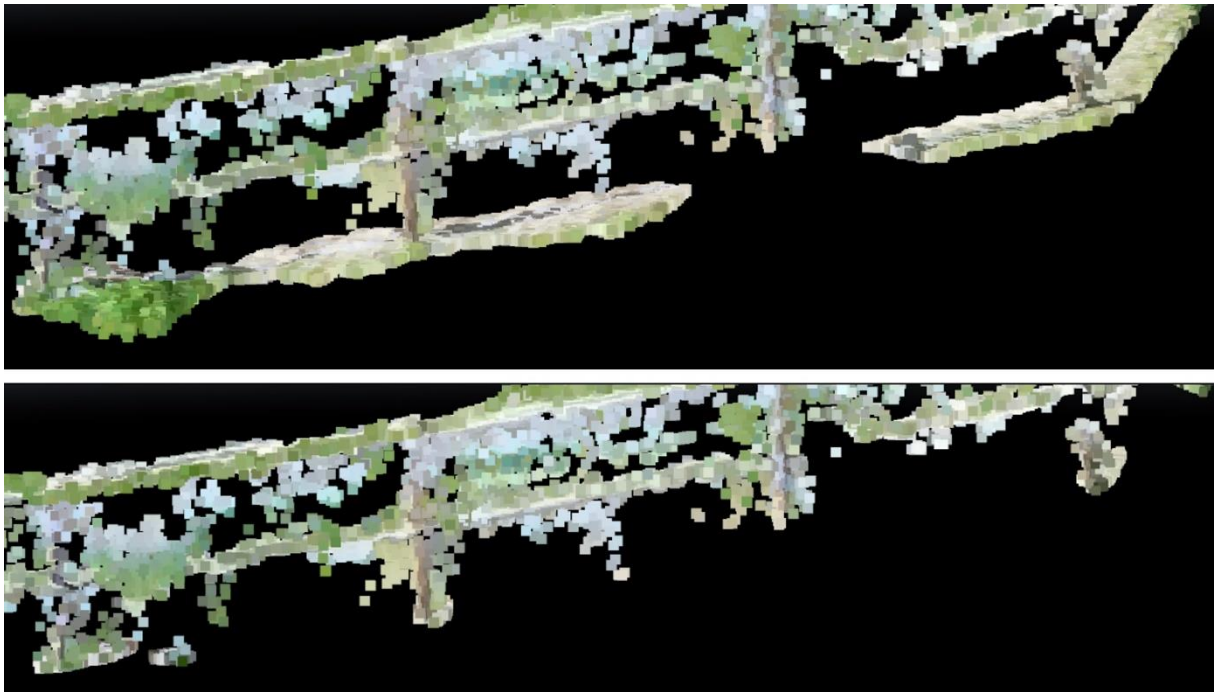

Figure 44: Pre manual classification (top) after manual classification adjustments (bottom)

The software generates DSMs in original resolution, but unfortunately upscales DTMs by factor five which results in lower quality and higher GSD. This issue was solved by manually aligning all categories except “ground” and disabling them and then generating a DSM, which technically is a DTM in this case.

Based on the dense point cloud, a DTM was produced using an algorithm based on the Delaunay triangulation, which is recommended for flatter areas (COMERT et al. 2019), like the Salcher landslide. Alternatively, the IDW (Inverse Distance Weighting) algorithm could have been used, which is mainly applied for steeper slopes and sharp

scarps (see SAMODRA et al. 2020). The DTMs were created using noise filtering to clean noisy and erroneous points and surface smoothing type “*sharp*”, which flattens the area but keeps sharp features like corners and scarps. DTMs are later used to produce DoDs for time-series analysis (chapter 7.4.3). Additionally, orthophotos of the research area are produced during this step, which are useful for visual interpretations of landslide surface features.

7.4 Time series investigations

The SfM-workflow ends with the generation of DTMs (see Chapter 7) however an additional processing step is added for this master thesis to analyze surface changes of a landslide over time between November 2020 and Spring 2021. By now, three dense point clouds and three DTMs have been generated.

In total, three different approaches, cloud to cloud (C2C), multiscale model-to-model cloud comparison (M3C2) and DEM of Difference (DoD) to investigate changes over the observation period of 156 days were used. The first two methods are based on dense point clouds while the DTMs were used to calculate DoDs.

7.4.1 Cloud-to-Cloud Comparison

Direct cloud-to-cloud (C2C) distance estimations were calculated with the opensource software CloudCompare 2.11.3. The C2C distance tool is a plugin for point cloud software which is based on a nearest neighbour distance. C2C allows only to compare two clouds at one time. Before measuring the distance between two different point clouds, a "*reference*" and a "*compared*" cloud need to be defined (Fig. 45), whereas the reference cloud is usually the "older" one.

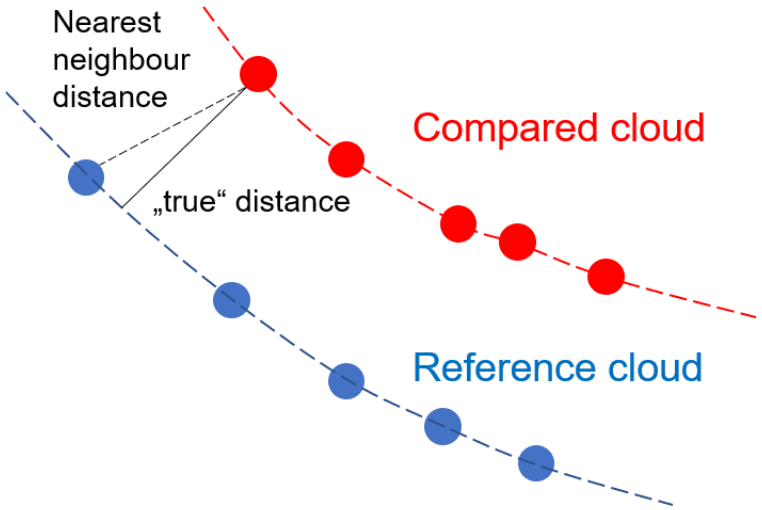

Figure 45: Basic concept of C2C distance calculation (after FUAD et al. 2018: 12)

As seen in Fig. 45 the nearest neighbour point does not automatically refer to the "true" distance of the two clouds. The C2C distance computation algorithm implements the

Hausdorff distance function to measure distances between corresponding points (JAFARI et al. 2017). The equation of Hausdorff distance function defines as the following from set A to set B:

$$H(A, B) = \max_{a \in A} \{\min_{b \in B} \{d(a, b)\}\}$$

where a = points of set A

b = points of set B

d (a, b) = any metric between the points

(FUAD et al. 2018: 13)

One of the advantages of C2C comparison is that the results can be displayed for each axis independently. So not only height differences (z) but also displacements in x-, and y-directions can be determined independently.

Local surface modelling of the point cloud can also be performed during the C2C computation. Users have three options to choose which affects the distance calculation (i) "*Least squares plane*" where distances are computed directly from points, (ii) "*2D ½ Triangulation*" in which corresponding 2D points are triangulated and the mesh is applied to the 3D points and (iii) "*Quadric*" for which a quadric function is used for the corresponding model to measure only z-axis deviations (CloudCompare 2015). These local surface models vary from the also known Cloud-to-Mesh (C2M) methodology. The C2M algorithm however, uses a generated mesh surface based on all points, while C2C computed each local surface by using a selection of points.

Based on FUAD et al. (2018) findings about change detection of landslides, "Least square planes" was chosen for this master thesis, since this approach produced the most accurate results for surface investigations.

Before processing, dense point clouds were cropped, so that surrounding vegetation and buildings are not accounted into calculations. To speed up computations, the clouds were subsampled randomly by 50%. The built-in noise filter of CloudCompare was applied to remove isolated points, which are not connected with the slopes surface.

Figure 46: CSF off-ground points - removed for further analysis (representative example)

Outliers created by higher vegetation, and trees have been removed by applying Cloth Simulation Filter (CSF) to extract ground points. A value of 0.2 in cloth resolution has proven to be the best option after several computations. For more information see ZHANG et al. (2016). CSF removed trees, fences, and any points situated significantly above the slopes surface (e.g., meteorological station) (see Fig. 46).

7.4.2 Multiscale model-to-model cloud comparison

The multiscale model-to-model cloud comparison, or shortly M3C2, was introduced by LAGUE et al. (2013). A similar approach to detect surface changes is Cloud to Mesh (C2M), whereas M3C2 method provides better results in landslide activity investigation than C2M method (FUAD et al. 2018), especially for slopes with heterogeneous characteristics since C2M makes use of 3D mesh which only corresponds to average reference points (LAGUE et al. 2013), so certain scarps might be flattened.

The M3C2 method for landslide surface investigation was inter alia applied by EKER et al. (2017) in Lower Austria and WARRICK et al. (2019) in California.

Before running the M3C2 algorithm, same as for the C2C comparison, a noise filter was applied for the point clouds to remove unconnected points and to reduce surface noise of vegetation. CSF was applied afterwards to remove leftovers, fences and points not associated with the slopes surface.

Three main characteristics of M3C2 are that it (i) operates directly on point clouds without meshing, (ii) computes local distance between two point clouds along the surface direction and (iii) estimates a confidence interval for each distance measurement (LAGUE et al. 2013: 11). (ii) is especially useful for displacement investigations of landslides since the M3C2 algorithm tracks 3D variations and features of the slope in surface orientation.

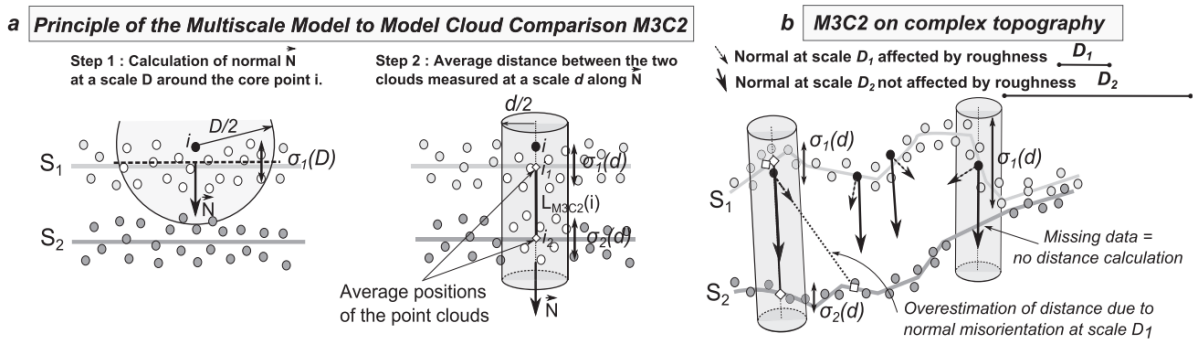

Figure 47: Principles of M3C2 methods including workflow (LAGUE et al. 2013: 14)

M3C2 makes use of “core points”, which are just regular selected points of the cloud to speed up computations, so a sub-sampled version of the dense point cloud is used (CloudCompare 2019). LAGUE et al. (2013: 13) justifies this down-sampling of a point cloud because “calculation results are generally needed at a lower, more uniform spatial resolution”. Fig. 47 displays the workflow for M3C2 by first calculating surface

“normals” in 3D (step 1) and then distance calculation between the two clouds (step 2) without meshing or gridding. For further explanation see LAGUE et al. (2013).

The point cloud comparison was carried out using the M3C2-plugin in CloudCompare. Users can set four parameters for the M3C2 algorithm which include (i) the definition of reference and compared cloud (similar to C2C), (ii) defining the amount of “core points”, (iii) defining the scale and (iv) defining the registration error (EKER et al. 2017; CloudCompare 2019). Core points were selected randomly from a subsampled version of the cloud (by factor 5). The scale parameters were set at 0.3 m for the average spacing between the core points, 0.15 m for the diameters and 0.09 m registration error. The outputs are distance uncertainty, absolute distance, and (non) -significant change between two-point clouds (see also COOK 2017; EKER et al. 2017). The M3C2 algorithm identifies areas of significant change based on the set scales. As in WARRICK et al. (2015) this approach can be used to identify zones of accumulation and depletion of active landslides.

7.4.3 DEM of Difference

DoDs have been applied in various fields of geomorphology to quantify volumetric changes and measure elevation differences between topographic surveys of the same research area (WILLIAMS 2012). In this master thesis, DoDs were applied to indicate elevation changes of the Salcher landslide, in addition to the time-series analysis done with dense point clouds. DoD analysis allows detection of zones of depletion and accumulation. The DTMs (see chapter 6.3.3) were used to produce three different DoDs so that elevation changes between the …

18th November and the 22nd February,

22nd February and the 23rd April and

18th November and the 23rd April

… can be determined.

The DTMs have been clipped to represent the same extent and a noise filter was applied to reduce outliners. Since the DTMs are stored as raster-layers, a simple subtraction of two layers (with Rastercalculator-Tool) in ArcGIS Pro displays changes in z-axis direction. The “newer” DTM is the minuend and the “older” DTM the subtrahend.

DoD changes from 18.11 to 23.04 **= DTM_23.04 – DTM_18.11**

While DTMs have height information stored, the produced DoDs only display the range of elevation change.

7.5 Expanded investigations

The time series analysis was extended back to 2007 in order to cover a longer time span than just the few months over the winter of 2020/2021. Thereby the following surface data of the Salcher landslide, provided by the University of Vienna was used:

2007: TLS data - by the Geological Survey of Austria (~0.25 m)

2009: ALS data - by the Federal State of Lower Austria (~1 m)

2014: TLS data - by the University of Vienna (~0.25 m)

2020/**2021**: UAV data – acquired for this thesis (three surveys)

At first, a DoD, displaying elevation changes between 2009 and 2021 was created. This analysis was then used to produce cross-section profiles of the landslide. In total four different profiles were created to determine changes of surface characteristics. In conclusion, surface data from 2007, 2009, 2014 and 2021 was used for a visual morphological mapping of the main scarps and the accumulation zone. This expanded surface investigation aims to (i) put the results of the UAV-survey into context, (ii) enables the answering of research questions related to the third hypothesis and (iii) hopefully provides further insights in the development and movement of the slope. In total the expanded investigation covers nearly 14 years.

7.5.1 DoD analysis 09-21

The DoD was produced to display elevation differences between 2009 and 2021. A DEM, by the Federal State of Lower Austria with a resolution of 1 m, acquired by an ALS was used to expand the time series investigation. For the final DoD of a time span of nearly twelve years, this elevation model and the most recent DTM from 23.04.2021 were subtracted. However, a geographic projection was needed for the DEM of 2009 since it was stored in the local coordinate system of MGI Austria GK East (EPSG 31256) and the DTMs are in WGS 84 UTM Zone 33N (ESPG 32633). The transformation was done in ArcGIS Pro, however elevation values (z-axis) needed

manual adjustments, so the height difference of 46.3 m was simply added to the DEM with the raster-calculator. For more information about the coordinate system projection see BEV (n.d.) During the coordinate system transformation, a dataset is projected into a new spatial reference using an interpolation method to project each pixel on a new mesh grid. By default, the "*nearest neighbour assignment*" is used for the interpolation, however the results were not satisfying due to a lot of pixel-related noise and blur. Instead, the bilinear option with "*cubic convolution*" was chosen. The new cell value is determined by fitting a smooth curve through the surrounding points (ArcGIS Pro n.d.).

7.5.2 Topographical profiles

An elevation-, transverse or topographical profile displays the relief of a terrain in a cross-sectional view. These profiles can be longitudinal or transverse depending on the wanted information.

Regarding landslide surface investigations, topographic profiles are often used to measure and display relief changes along a predetermined profile line (ROSSI et al. 2018; KOWALSKI et al. 2018). In many cases, more than two surface datasets are used to present the development of the relief over time. WARRICK et al. (2019) for example, used up to twelve different surface datasets in elevation profiles to present a chronological development of a landslides slope.

The cross-section profiles were created with the commercial software ESRI ArcGIS Pro and three different elevation models were used as a basis. Resulting profile graphs include reliefs based on the ALS 2009, UAV I (2020) and UAV II (2021) data and enable a discussion about the surface development. In order to collect as much information as possible about the evolution of the slopes' topography since 2009, four spatially distributed elevation profiles were created (see Fig. 48). When placing the profiles, deliberate care was taken to ensure that all of them run through an active part of the landslide.

As seen in Fig. 48:

Profile 1: running 128 m covering 26 m height difference from the adjacent (southwestern) slope towards the former ski lift hut through two scarps, the bulged footslope and horse pasture.

Profile 2: running 122 m covering 23 m height difference from the adjacent (western) slope towards the driveway of the former ski lift hut, through the circular plane and two of the major scarps with 23m height difference.

Profile 3: 98 meters and *Profile 4*: 81 meters, both running parallel from northwest to southeast, one above and one beneath the bulged footslope. *Profile 3* has a height difference of 15 m and *Profile 4* of 11 m

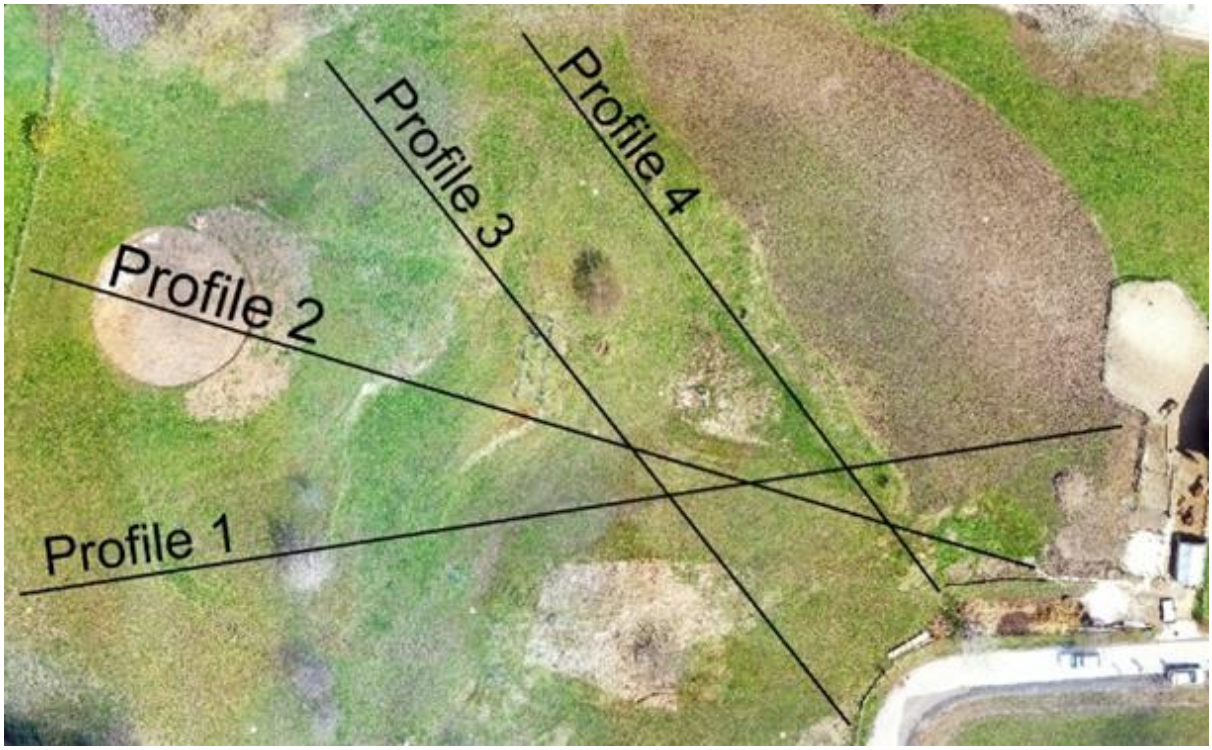

Figure 48: Spatial distribution of cross-section profiles at the Salcher landslide based on 2009 and 2020/2021 data

By placing the profiles distributed, more relief information can be gathered and surface features like scarps, bulges, sinks and tops are visible in the cross-section.

Similar landslide investigations using topographical profiles to detect surface changes have been published by CIGNETTI et al. (2019); GODONE et al. (2020); ROSSI et al. (2018) and PETERNEL et al. (2017).

7.5.3 Mapping of scarps

Due to technical problems and lack of processing time, the 2007 and 2014 datasets could not be examined as elevation models. Nevertheless, a mapping of the morphological characteristics was performed on a visual basis. The commercial software ArcGIS Pro, Adobe Illustrator 2020 and Adobe Photoshop 2020 were used for this purpose. The aim of this mapping is to present a position map of the main scarps from 2007, over 2009 and 2014 until 2021. Aside from the main scarps, the location of the bulged footslope in 2014 and 2021 was added to detect displacements of the accumulation zone. Fig. 29 served as a basis and the surface features from 2009 and 2021 were added based on their elevation models. Here, the landslide surface mappings of DEMOULIN & GLADE (2004) and CIGNETTI et al. (2019) were used as a guideline and implemented in a simplified way for the Salcher landslide.

Since this is a visual mapping, it might not be as accurate as a surveyed map. However, the result displays the location and therefore the development of the main scarps and shows surface dynamics over nearly 14 years. It will be further used to answer research questions and to verify/falsify the third hypothesis about the movement rates of the surface.

8 Results

This chapter presents the results of the SfM-workflow, as well as the time-series analysis to detect changes of the surface of the Salcher landslide. First, the produced DTMs are presented for each of the three UAV-surveys, before going into detail about the results of the time series investigation. Here the three different approaches C2C, M3C2 and DoD analysis are presented and an additional subchapter about the results of the expanded investigation in which data from previous surveys is included.

8.1 Digital Terrain Models

Three DTMs have been produced to visually display surface features and characteristics for each of the carried-out UAV-surveys. All DTMs are provided in higher resolution in the Annex.

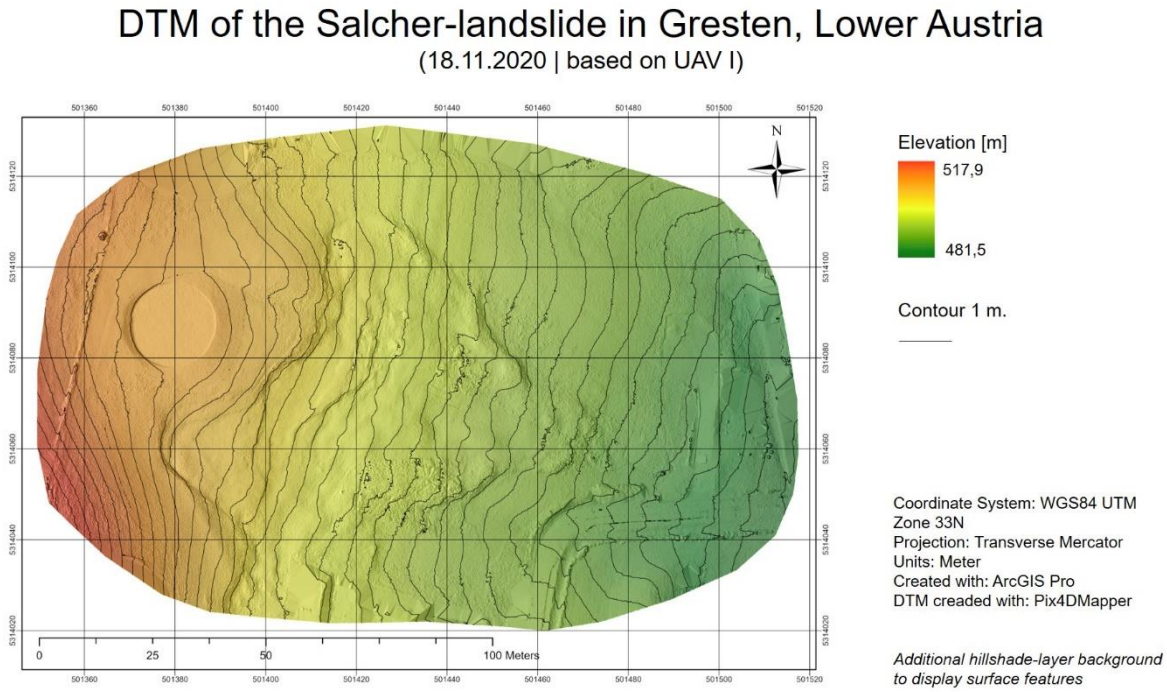

Figure 49: Result I of SfM-workflow: DTM from 18.11.2020

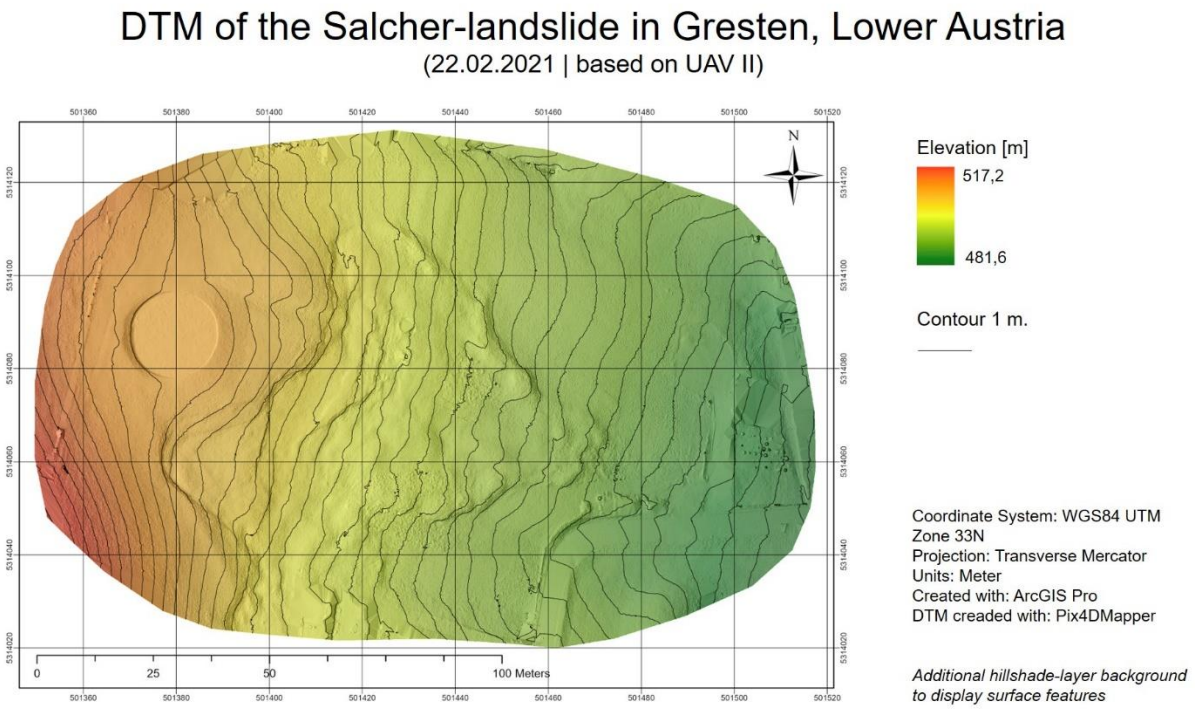

Figure 50: Result II of SfM-workflow: DTM from 22.02.2020

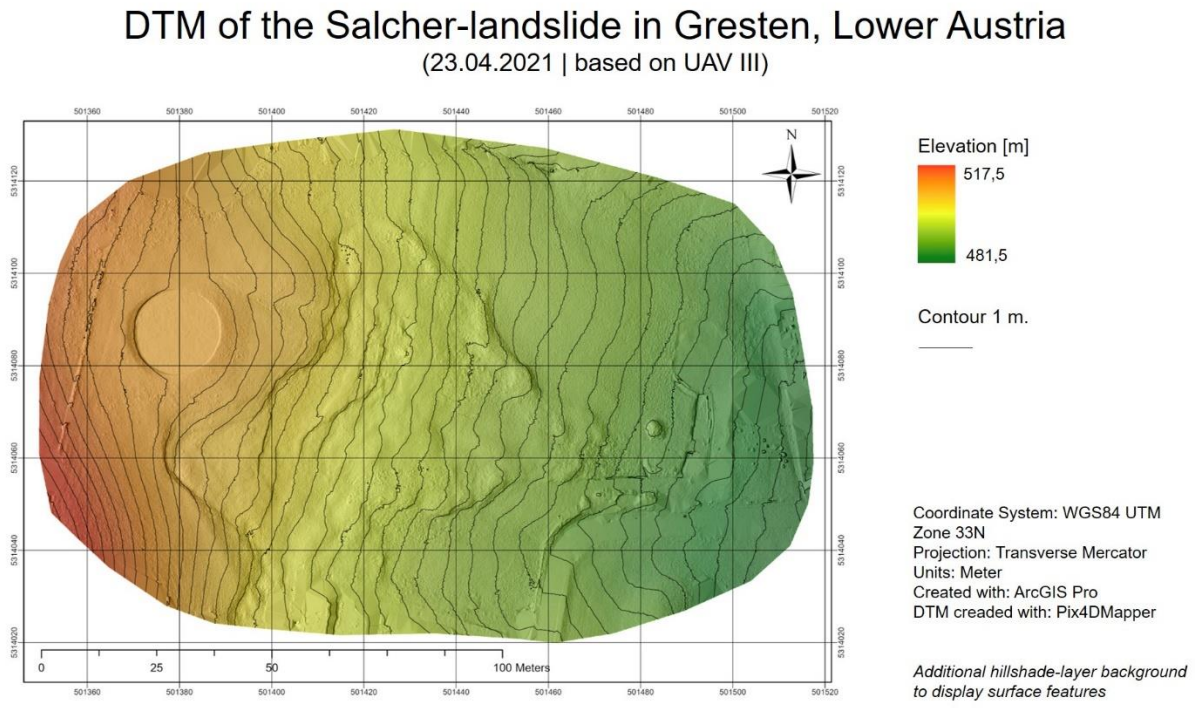

Figure 51: Result III of SfM-workflow: DTM from 23.04.2020

Contour lines in one-meter intervals were added for a better visual interpretation of the surface (see Fig 49-51). Since the original DTM files use red-yellow-green scalar fields, a hillshade-layer for the background was processed for each of the three DTMs. The hillshade-layers were produced in ArcGIS Pro by simulating a light source (45° angle, facing east) to visually display scarps, flanks, and bulges.

The visual interpretation of the DTMs results in, as expected, only minor changes over the observation period. However, it already provides information about the surface and the spatial distribution of scarps, which is helpful for the interpretation of the time series analysis and to detect the active zones of the slope in order to further investigate them in detail.

Nevertheless, human influences like the circular plane (horse vaulting) near the crown of the landslide are perfectly visible in all three DTMs. Other anthropogenic influences can also be determined in the DTM from the 18th. November and 23rd April 2021. In Fig. 49, in the central part slightly south of the middle, uncut grasses and bushes result in irregular, nearly noisy contour lines. This part of the landslide was mowed during the other UAV-surveys. In Fig. 51, close to the former ski lift hut in western direction, a pile of soil can be seen, which is framed by a contour line since it is slightly higher than one meter.

These two examples show that influences caused by humans can heavily disturb DTMs and need to be considered when interpreting data and for further processing steps.

The absolute (maximum) elevation data must also be interpreted with care. Ranging from the lowest 517.2 (DTM II) to the highest 517.9 (DTM I), does not automatically mean an increase of elevation. This small deviation could also be the result of slightly inaccurate Delaunay triangulation calculations for the periphery areas of the landslide due to lower point density there.

8.2 Change detection

While previously the DTMs displayed a snapshot of the landslide's surface, the results of the time-series investigation of the three applied methods are presented in the following. Full size imagery of all DoDs can be found in the Annex.

8.2.1 Cloud-to-cloud results

The results of the C2C absolute distances approach with least square plane modelling surface can be seen in Fig. 52 and 53. It shows changes of elevation (z-axis) between the first UAV-survey 18th. November 2020 and the last survey on the 23rd. April 2021.

Areas marked in orange/red have lifted, while dark green/blue areas have lowered over the time period. The C2C analysis was carried out for the "main" part of the landslide, periphery areas with trees, streets and the former ski lift hut have been removed since they affect elevation calculations on a greater scale.

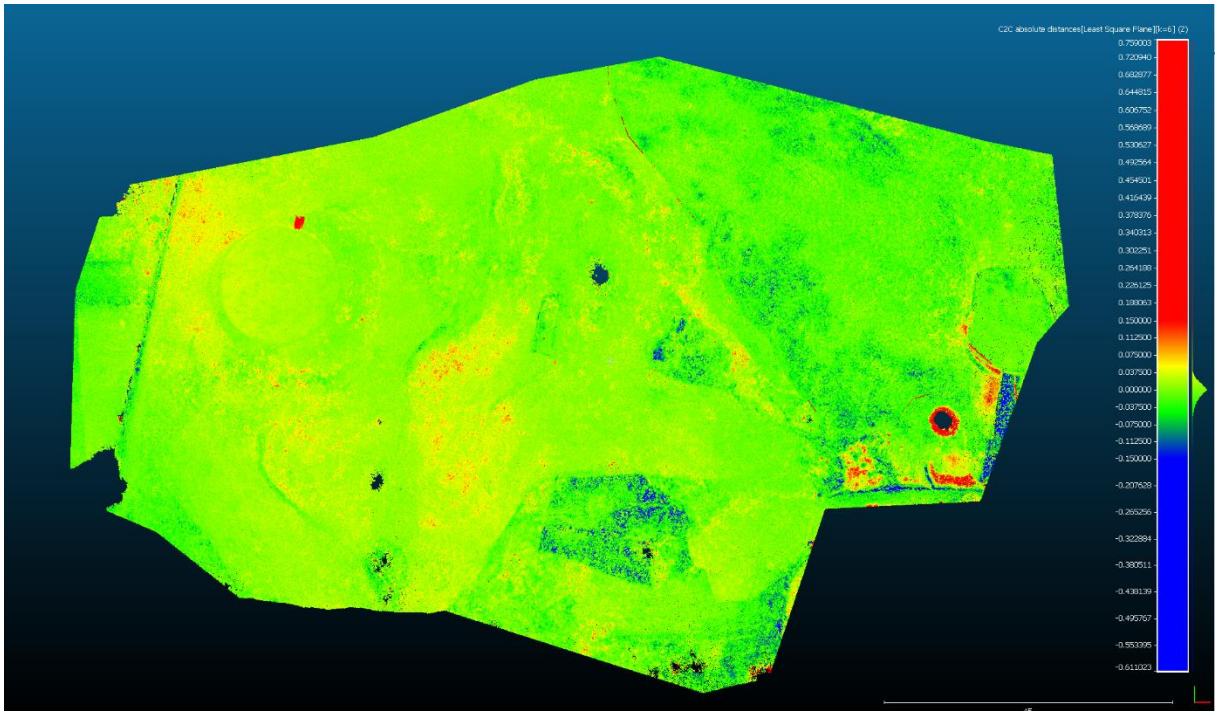

Figure 52: Vertical view of C2C computation results between 18th November and 23. April

As seen in Fig. 52 a large part of the research area has not changed significantly over the Winter 2020/2021. However, elevation differences are visible along existing scarps which indicates that some sort of movement happened. In the central part of the slope, an uplift can be detected, right below one of the main scarps, as well as slightly south

and north west of the anthropogenic circular plane at the crown of the landslide. Areas of subsidence can be identified in the lower middle half (Fig. 52 & 53) and generally in the north-eastern area. However the decreasing elevation in the lower middle half is due to the area being mowed after the first UAV-survey. So interpretations for surface dynamics can not be made for this particular area.

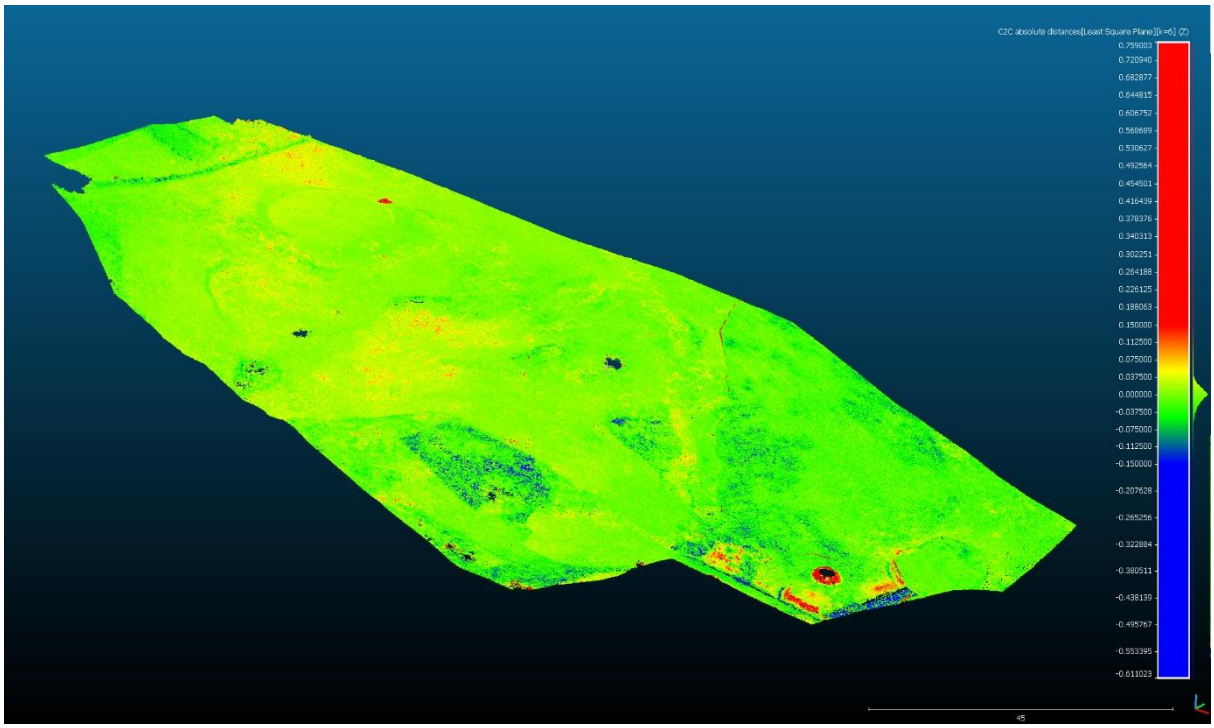

Figure 53: Tilted view (from south east) of C2C computation results between 18th November and 23. April

Saturated red areas like the little spot near the circular plane at the crown as well as the toe of the landslide (Fig. 53) are due to human disturbances between the two UAV-surveys. The red spot at the crown is a pile of logs and the red spot at the toe is a pile containing a mix of earth and gravel.

Due to these more “extreme” elevation change values, absolute numbers of height differences need to be interpreted with care. Even though the scale legend in Fig. 52 and 53 shows that the area experienced elevation changes between -0,61 meter to nearly 0,76, the maximum values are not meaningful since they are affected by (i) human impacts and (ii) the CSF algorithm (see Chapter 7.4.1) where higher vegetation and other points not associated with the slope’s surface have been removed. This effect can be seen at the pile of soil near the landslide toe, where the top of it has been cut off during the CSF computation.

8.2.2 Multiscale model-to-model cloud results

A similar spatial extent used for the C2C computations was applied for the M3C2 algorithm. The results of the computation can be seen in Fig. 54 – 56 and are attached in the Annex in full-size.

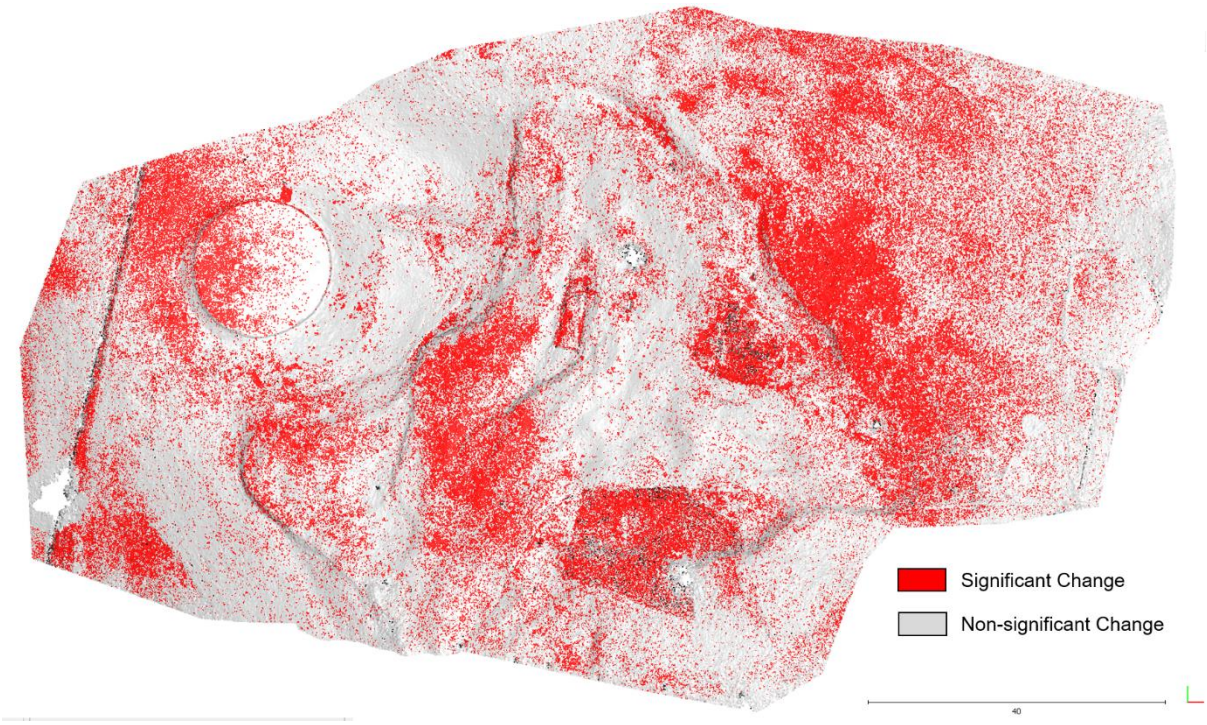

Figure 54: Results of the M3C2 computation, significant changes of the surface 18.11-23.04, vertical view

Fig. 54 shows the results of the M3C2 computations. Significant (red) and non-significant (grey) changes of the slopes surface between 18th of November 2020 and 23rd of April 2021 are spatially displayed. Areas marked red have changed significantly over the observation period in x-, y-, and/or z-axis. Grey areas have not significantly changed or are points for which no corresponding points have been found during the computation (CloudCompare 2019). Since there is a lot of noise, due to vegetation, only areas with a high density of red points should be considered to have changed significantly. The same result is shown in Fig. 55, however not vertically from above but from a tilted point of view from southeast to depict the surface characteristics.

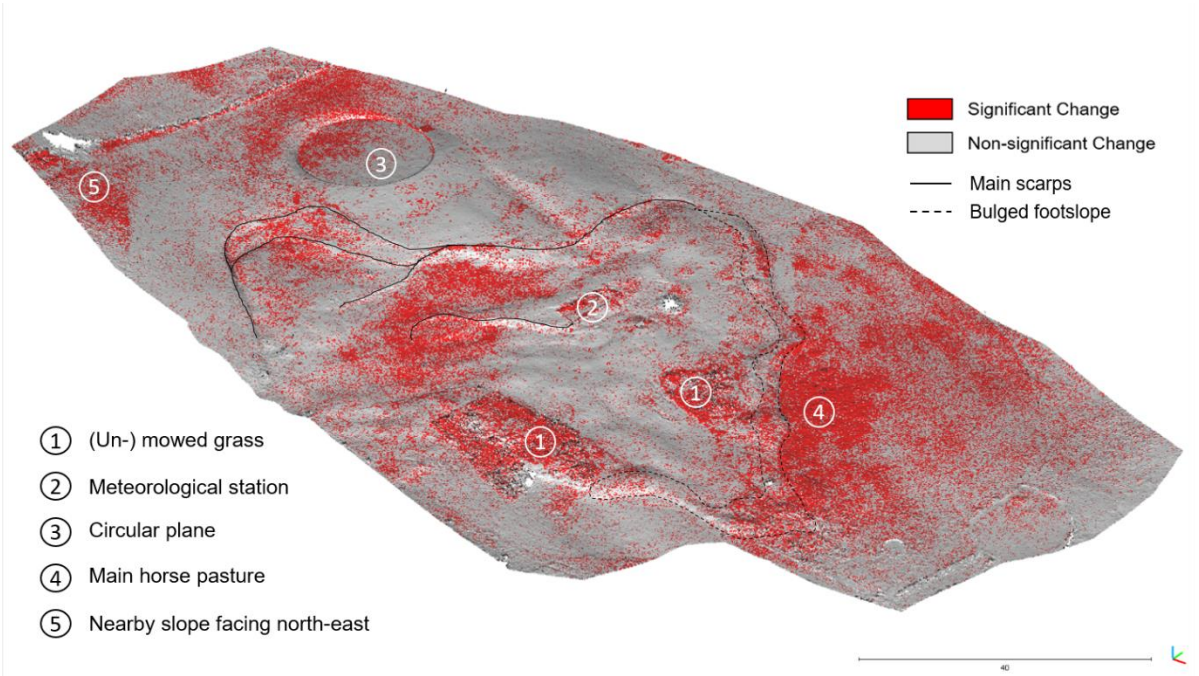

Figure 55: Results of the M3C2 computation, significant changes of the surface 18.11-23.04, tilted view

Significant changes can be seen spatially distributed over the entire slope. However, as already described for the results of the C2C-Method, some changes are due to human activity on the landslide like the areas 1 (Fig. 55) which were covered by grass on the 18th of November but have been mowed before the second UAV-survey in spring 2021 and area 2 where the meteorological station is situated (see Chapter 6.2 for details). Detected surface movement in this area needs to be interpreted with care since the level of human interference is very high here and a surrounding wired fence, which tends to tilt by the slightest movement of the ground, may distort the results.

Nevertheless, areas of significant change can be identified for the main horse pasture (4), the northwestern part of the circular plane (3), along the main scarps as well as along the bulged footslope at the toe of the Salcher landslide and at the toe of the nearby slope situated southwest of the main landslide area.

To determine whether these changes are uplifts or subsidence the results of the M3C2 computation can also be displayed for “absolute” distances instead of “significant change” (see Fig. 56).

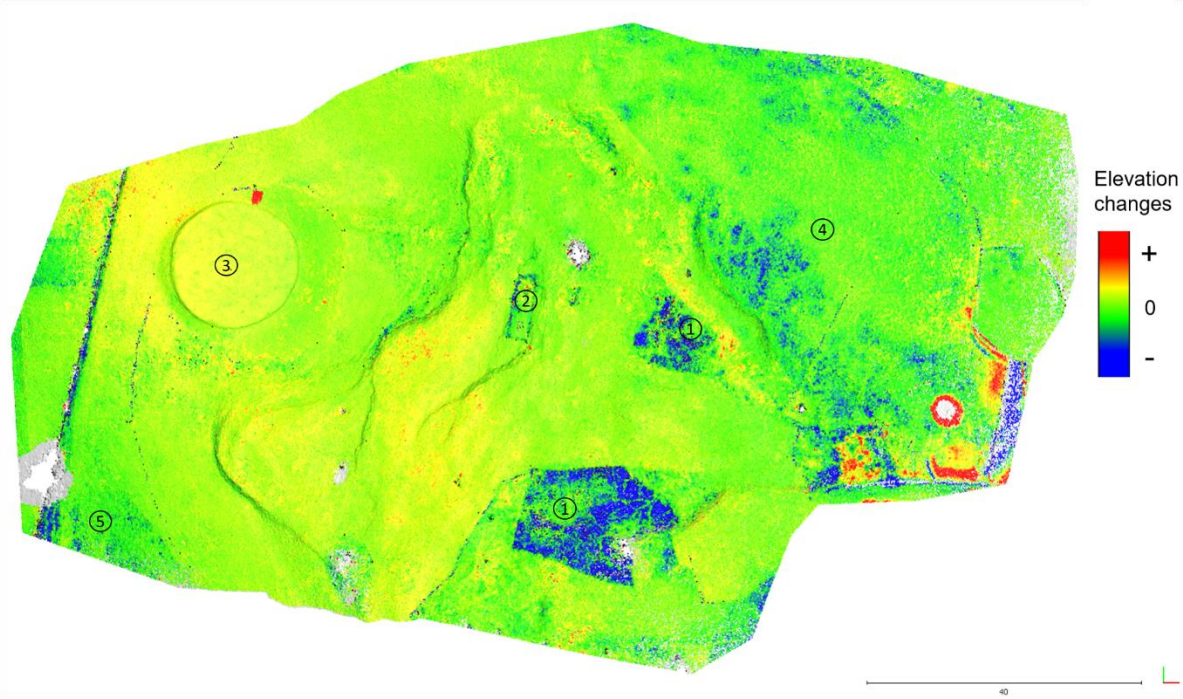

Figure 56: Results of the M3C2 computation, absolute distances of the surface 18.11-23.04 (for 1-5 see Fig. 55)

Considering the identified zones which had significantly changed between the first and third UAV-survey, Fig. 55 provides information about the direction of the movement for these. Self-explanatory, the elevation of the areas on which the grass was cut (1) after the first survey has decreased. The circular plane (3), in particular the area adjoining north-west of it seems to have lifted slightly. The main horse pasture (4) however has subsided. Whether this movement was triggered within the slope or due to the weight of the horses needs to be further analyzed (see Chapter. 9). Also subsided is the area of the nearby slope (5) near the southwest edge of the main landslide.

It is interesting to see, that nearly every area beneath a main scarp seems to have lifted slightly over the observation period, while the scarps itself remained their elevation and have not changed significantly (see Fig. 55 & 56). The bulged footslope, on the other hand, has gained height, which indicates a downhill movement and a resulting accumulation of material.

8.2.3 DoD analysis

The results of the DoD analysis are presented in the following, starting with the two periods from 18th of November to the 22nd of February and the 22nd of February to the 23rd of April and concluding with a DoD covering the entire period. The elevation difference was initially displayed in a stretched scale but was divided into manual intervals. Minor height differences from -0.03 m to 0.03 m have been disabled, since they may include errors due to smaller vegetation. The same scale was applied for all DoDs.

Values near the edge of the DoDs need to be interpreted with care since there are tendencies for distortion there.

Minimum and maximum elevation differences as well as mean values and standard deviation for all three DoDs can be seen in the table 7 below.

DoD	Max. negative elevation change	Max. positive elevation change	Mean value	Std. Deviation
18.11.2020 – 22.02.2021	-1,2221	0,66455	-0,04588	0,04063
22.02.2021 – 23.04.2021	-0,82367	1,25003	0,03164	0,04401
18.11.2020 – 23.04.2021	-1,05862	1,18451	-0,01421	0,05145

Table 7: DoD analysis results for min.- and max.-, mean-, and std. deviation [m]

For the first period, between the 18th of November and 22nd of February, only minor elevation differences of the slope were determined (Fig. 57). Most of the changes are within a range of -0.1 m to 0.1 m. Considering the whole area, a slight subsidence occurred due to a mean value of -4 cm (Tab. 7).

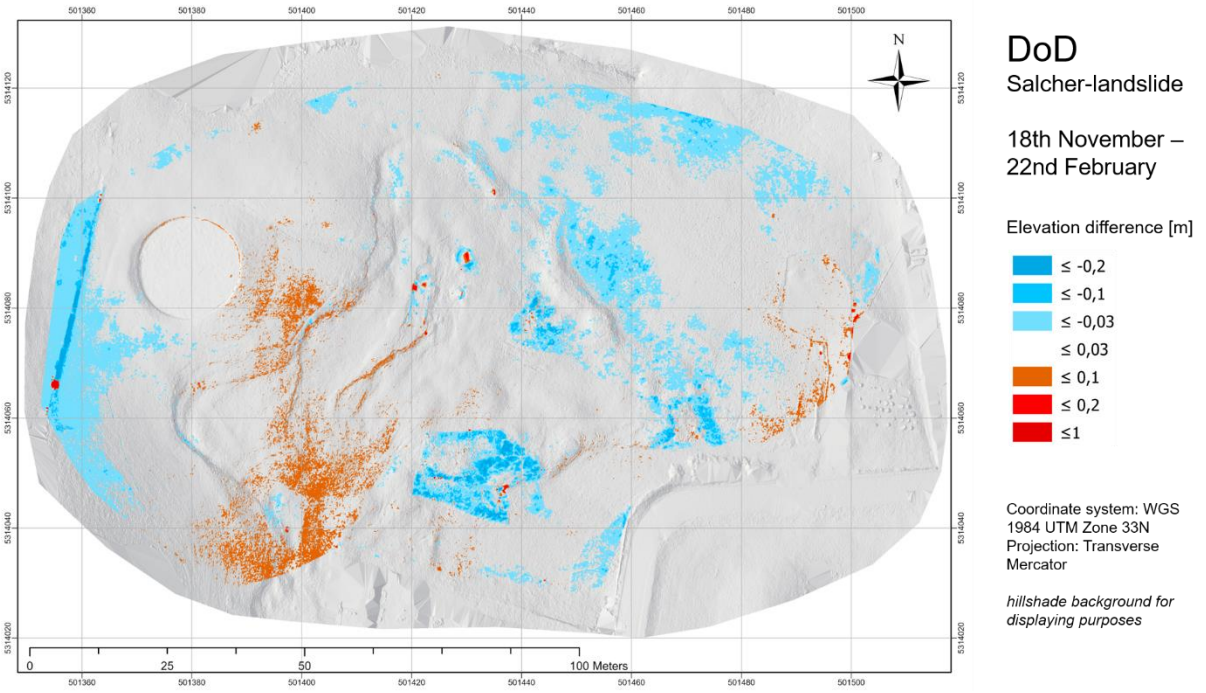

Figure 57: Results of DoD analysis Salcher landslide 18.11-22.02

Especially areas along the main scarps and in the upper zone of the landslide have gained elevation between 4 to 10 cm over the winter months. Red spots indicating major upward movements can only be found for spots where trees and higher bushes are situated so these can be ignored for the surface analysis. Subsidence is visible for the mowed grass spots, the main horse pasture and along the (south-) western edge of the DoD. The dark blue “line” along the western edge of the DoD is a misinterpreted wired fence and can be ignored for further surface investigations.

The second period in spring 2021 from the 22nd of February to the 23rd of April (Fig. 58) shows a different elevation development than the DoD covering the winter period (Fig. 57). The mean value of 3 cm already indicates more uplift movements than before.

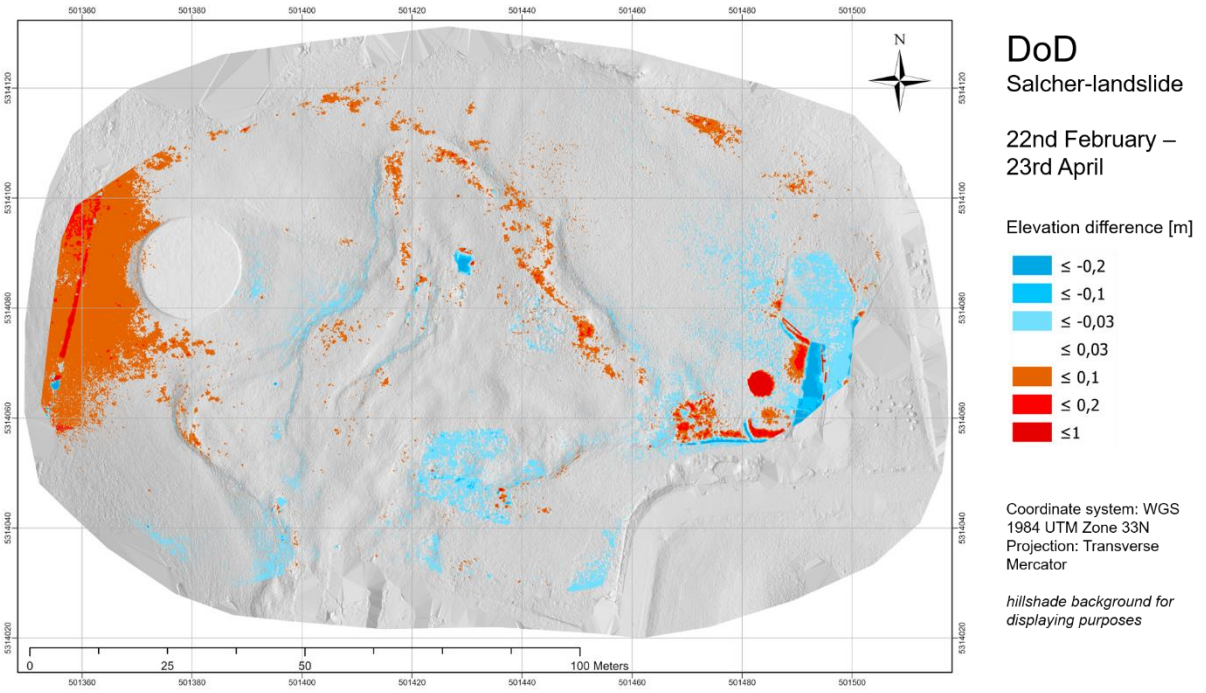

Figure 58: Results of DoD analysis Salcher landslide 22.02-23.04

The area at the crown of the landslide in the west is the most striking here. An elevation increase of up to 20 cm can be identified, whereas this zone has subsided over the winter. The area just above the bulged footslope also seems to have gained height. This development could be due to sliding movements of the slope resulting in an increase of the entire zone of accumulation. In line with this, heads of the main scarps have subsided slightly. Also, the small part at the southern end of the horse pasture and north of the street which can be identified as the toe of the landslide has experienced uplifts.

Other already identified areas of subsidence such as the places of mowed grass and the horse pasture have experienced little to no elevation differences over the spring. The slim dark blue line, parallel to the street near the toe of the landslide can be ignored, since a trench for a drainage was dug here.

To get an overview of the total elevation development, the third DoD displays surface changes from the 18th of November until the 23rd of April (Fig. 59), covering the whole observation period. Thus, results from the two previous DoDs are summarised here, but no surface information can be shown for spots here which sort of balanced out elevation differences between the first two DoDs. The mean value of -1 cm confirms this balance.

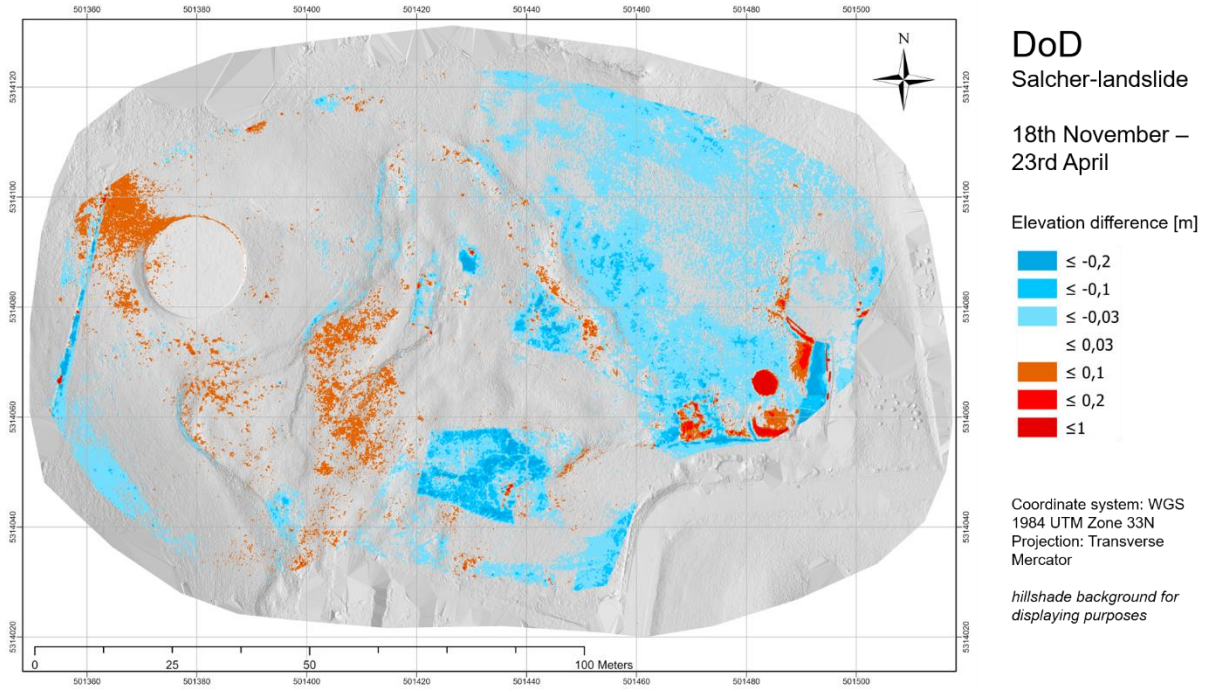

Figure 59: Results of DoD analysis Salcher landslide 18.11-23.04

An increased elevation is identified for the area north-west of the circular plane at the crown, slightly below the main scarps in the most active part, along the bulged footslope and at the toe of the landslide. Subsidence, related to non-human activity has occurred for nearly for the entire horse pasture, at the head of a few main scarps and at the nearby slope southwest of the landslide.

This DoD analysis reveals that most movements in either positive or negative direction are within the range of up to 10 cm. Major sliding or larger rapid movement did not happen over the observation period, even if the maximum and minimum values of the DoDs (Tab. 7) reveal that changes of more than 1 meter occurred. These high results are the result of misinterpretation of remaining pixels related to trees and branches.

8.3 Expanded investigations

The second part of the results, in which other surface data from previous investigations were used for a long-term analysis are presented in the following. Full size imagery is attached in the Annex.

8.3.1 DoD analysis 09-21

To expand the time series investigation, the DEM acquired with an ALS from 2009 (see Chapter 7.5) was included for the surface analysis and compared with the most recent DTM from the 23rd of April 2021. Covering nearly 11 years, surface dynamics on a greater scale are visible, and the results are presented in Fig. 60.

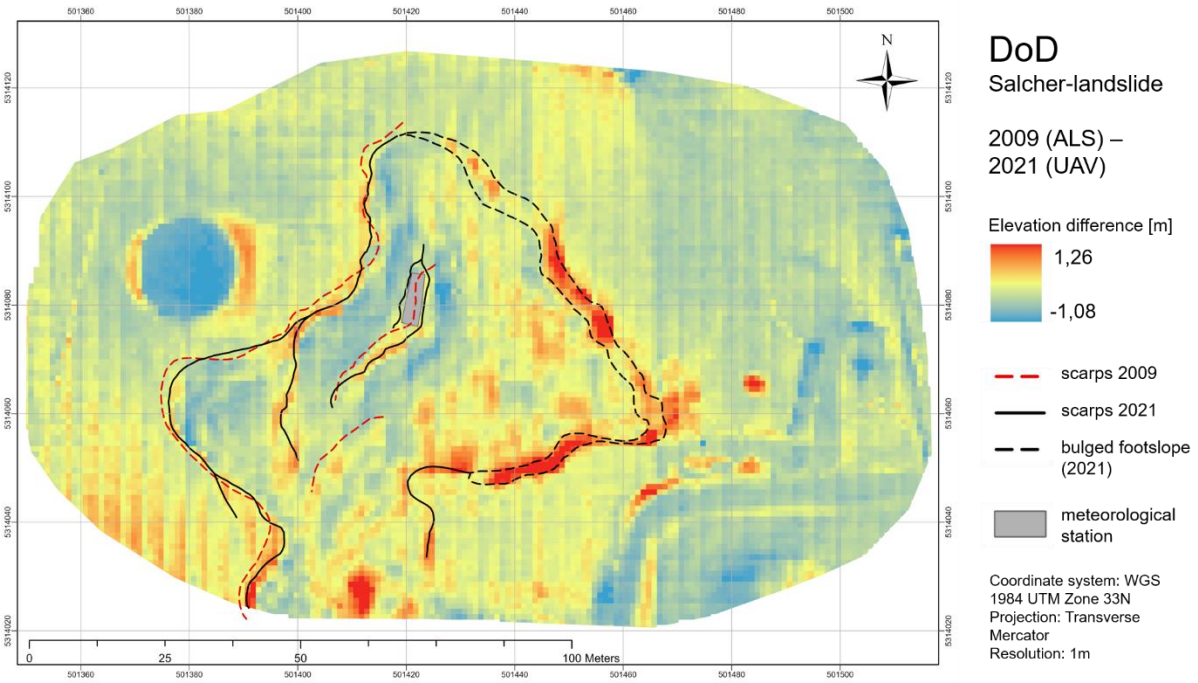

Figure 60: Results of DoD analysis Salcher landslide 2009-2021

Ranging from -1.08 to 1,27 m, the surface has experienced major structural changes since 2009. Main scarps from 2009 and 2021 are included to visually display how they have spatially changed. One of it was running right through where the meteorological station was later installed, so anthropogenic impact influenced this partial change.

Similar to previous results but on a greater scale, the bulged footslope and the main scarps gained elevation. Especially the zone of accumulation has gained elevation up

to nearly 1 m. Same for the main scarps but with lower height increasement, they seem to have uplifted over the eleven years of monitoring. Characteristic for a slow-moving rotational landslide (see CRUDEN & VARNES 1996) the areas right beneath the scarps have consequently lost elevation and the depleted mass was transferred downslope. The circular plane, now used as a horse vaulting area, has subsided by nearly one meter. However, this development is due to anthropogenic impacts again since material was purposefully removed from here.

8.3.2 Topographical profiles

The four generated topographical profiles are presented in the following. Using elevation models from 2009, 2020 and 2021, changes and the development of the relief can be displayed. However, in many cases, the graph presenting the surface 2020 (blue) is barely visible as it is mostly covered by the 2021 graph (red). The topographical line from 2009 is generally smoother than the other two, since the resolution of the data is 1 m. Nevertheless, various surface dynamics can be detected since 2009 in the following cross-sections (Fig. 61-64).

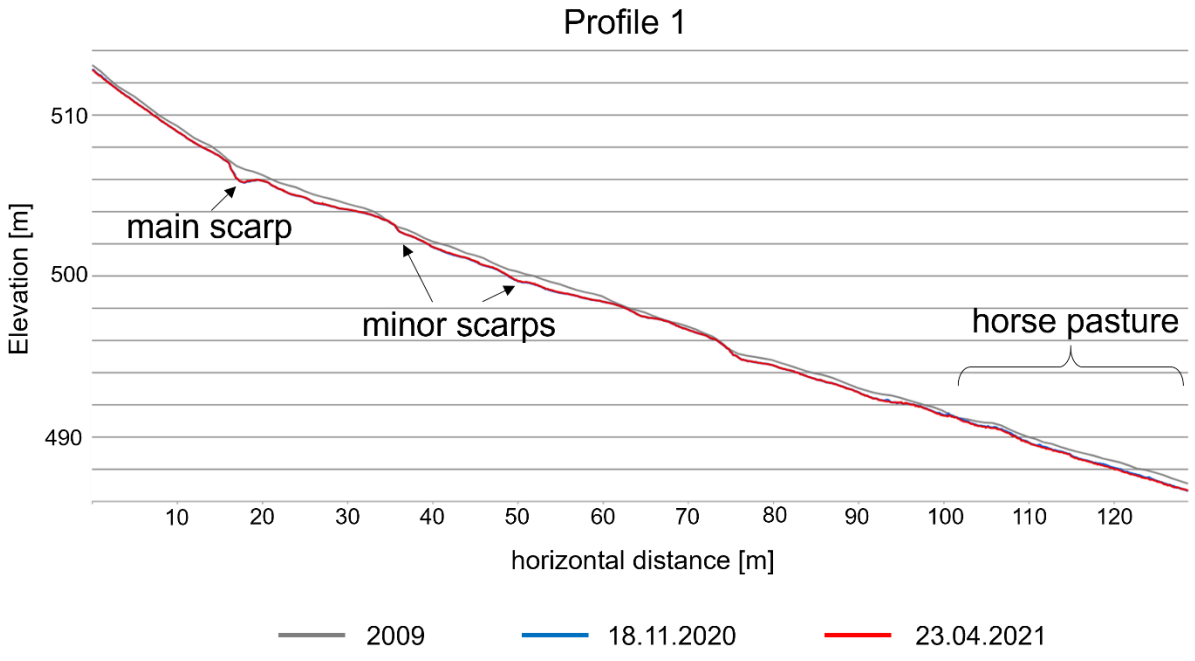

Figure 61: Cross-section profile 1 Salcher landslide 2009-2021

At about 18 m horizontal difference and 506 m height, the profile runs through the main scarp of the landslide which is perfectly visible in Fig. 61. Other than that, the three graphs of the cross-sections, representing the slope's surface, have not experienced greater differences, except for the lowest part. Here, the profiles run through the horse pasture (Fig. 61), which presumably lost height due to compression caused by the horses' weight.

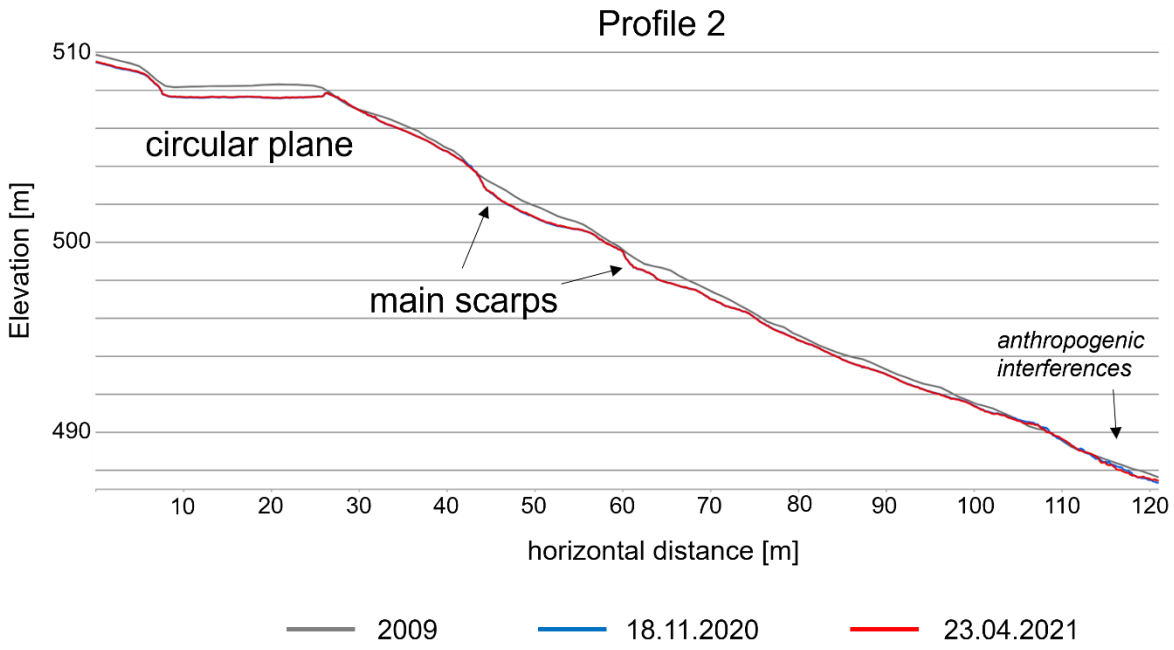

Figure 62: Cross-section profile 2 Salcher landslide 2009-2021

Profile 2 (Fig. 62) is slightly offset compared to Profile 1 (Fig. 61) but overlaps at about 90 m horizontal distance. Here the relief profiles run through the circular plane, situated at the crown of the main landslide body. A loss of nearly 70-90 cm in elevation since 2009 is detected here. However, this dynamic is not directly related to sliding processes, since the tenant of the land here has worked on the area to create a vaulting place for horses.

Two main scarps are visible in Fig. 62, showing that they have deepened since 2009. As mentioned, the dataset from 2009 has a spatial resolution of 1 m, meaning minor scarps are probably not visible if they existed - however, it can be assured, that the two main scarps in 2009 have not been present in this extent. These two kinks in the profiles reinforce the theories about the Salcher landslide being situated on multiple shear surfaces (see STUMVOLL et al. 2020). The graphs, from approx. 100 m horizontal

distance on to the end of the profile, are influenced by human activities on the field and are therefore not further considered in this surface analysis.

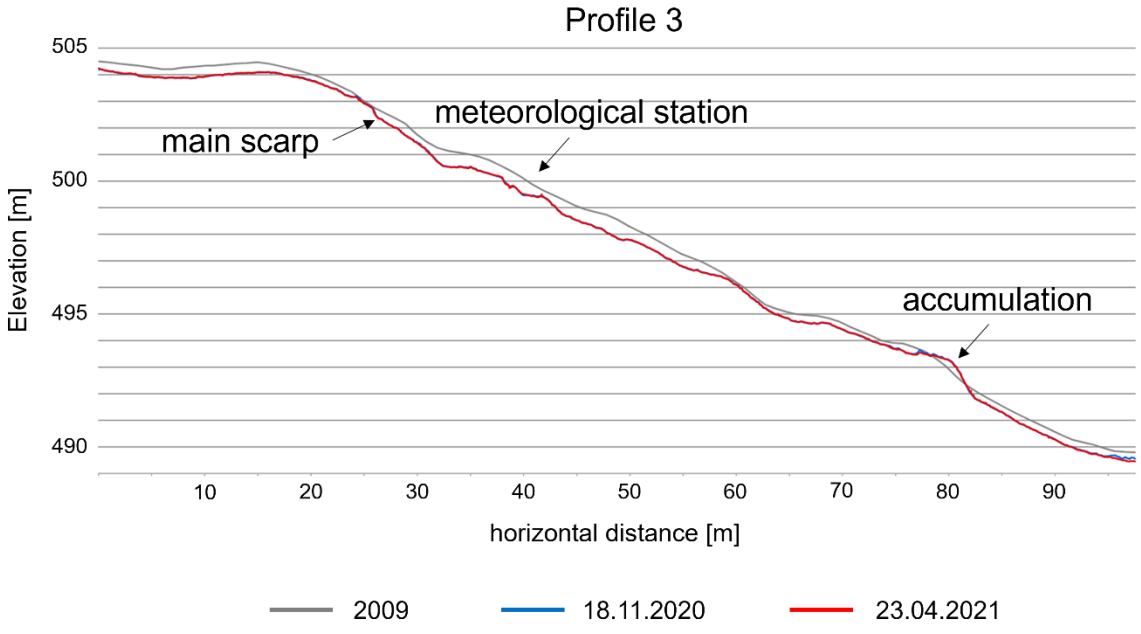

Figure 63: Cross-section profile 3 Salcher landslide 2009-2021

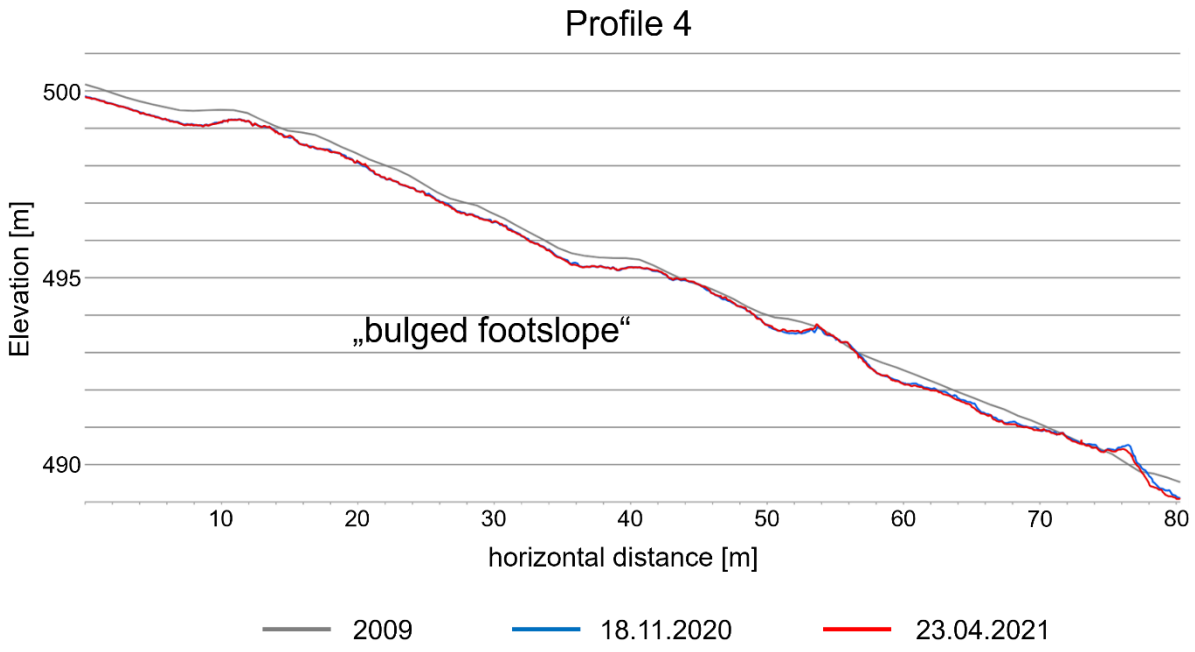

Figure 64: Cross-section profile 4 Salcher landslide 2009-2021

The topographical profiles 3 (Fig. 63) and 4 (Fig. 64) both run in parallel from northwest to southeast along the bulged accumulation zone. In Profile 3, the impacts of the installation of the meteorological station can be seen. Here, a human-made plane was created to place various measurement devices, which influences the shape of the

relief. Between 30-60 m horizontal distance (Fig. 63) the elevation differences between the surface in 2009 and 2020/21 are perfectly visible and range up to nearly 60-70 cm. As seen in both profiles, the lines representing the surface 2020/21 get more uneven and bumpier the further downslope they go. In some places there, the surface today is situated above the level from 2009, which probably indicates an accumulation of material. Profile 4 is the “most extreme” one since it was deliberately placed along the bulged footslope to investigate the roughness of the surface.

There is a general tendency, that the topographical line from 2009 slightly lies above the lines representing the 2020/2021 surface. This indicates that subsidence and compression processes have probably occurred since at least 2009. The DoD analysis 09-21 in the previous chapter basically presents the same results, just displayed in a different form. Observations like the loss of elevation, especially in Profile 2 and 3 (Fig. 62 & 63) can be seen from a different position in Fig. 60 as well.

8.3.3 Mapping of scarps

To conclude the expanded surface investigation, the main scarps as well as the position of the bulged footslope have been mapped. As mentioned in Chapter 7.5.3. four different elevation datasets were used for a visual morphological mapping to display their positioning since 2007.

As seen in Fig. 65, the main scarps of the landslide experienced dynamic changes since the first complete surface survey in 2007. The horizontal position of the main scarps has changed by up to 7-8 m over the last decade, with the greatest change being observed south of the circular plane at the crown of the landslide. Interesting to see here is that some parts of the main scarps have shifted upslope and some downslope due to movement processes of the (sub-) surface. Irregular surface movements can already be guessed by looking at the different positions of the scarps over the years.

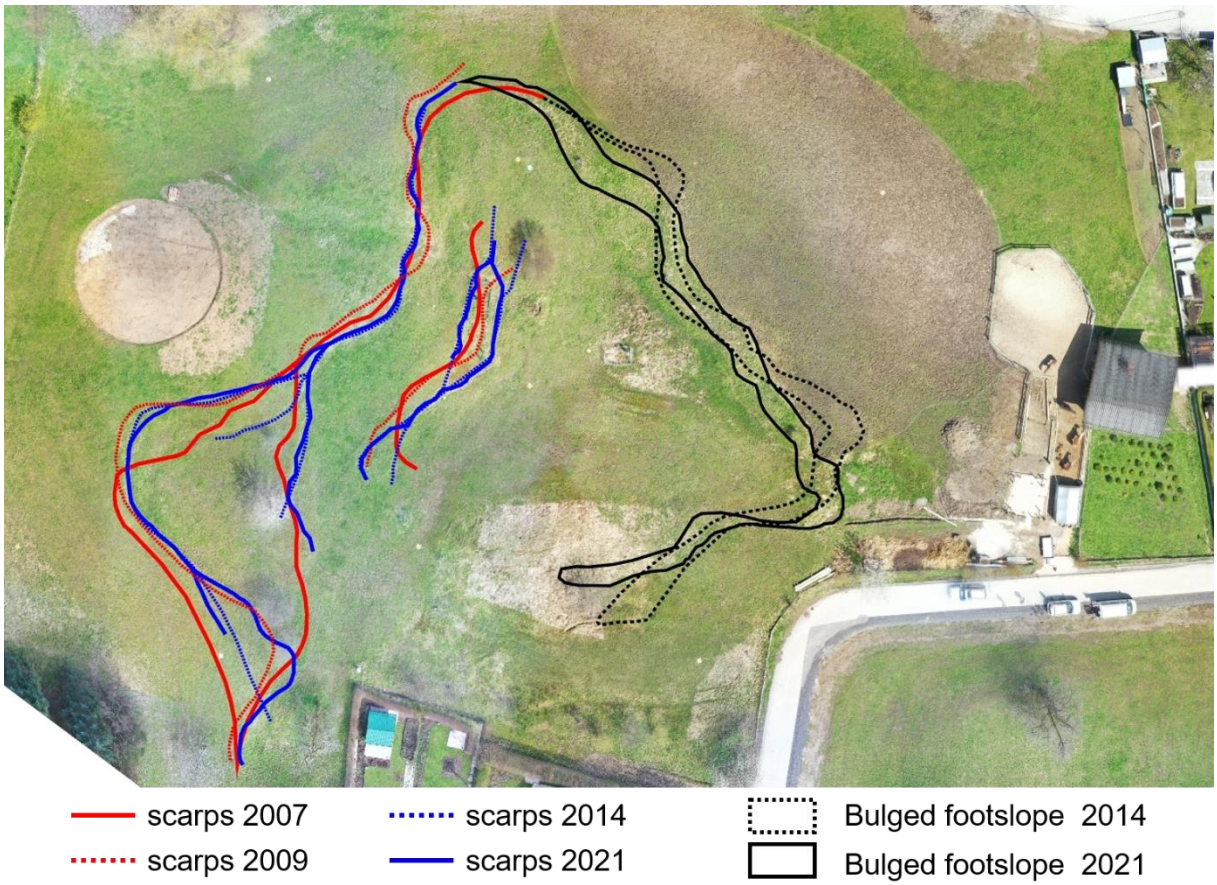

Figure 65: dynamics of main scarps and bulged footslope from 2007-2021

The installation of the meteorological station (see Chapter 6.2) was an anthropogenic impact on the landslides surface resulting in a permanent shift of a scarp downslope and the development of a new one slightly above (see Fig. 65). The accumulation zone at the bulged footslope in 2014 and 2021 is also included in Fig. 65. In 2014, parts of the bulged footslope were situated where parts of the horse pasture are located nowadays. So, the depleted mass was either removed by humans, eroded by rain, compacted by the weight of the horses, or all of the above.

Such mappings of surface features allow further interpretations and discussions of the data as well as drawing conclusions about the processes behind the movements, which will be discussed in the following chapter.

9 Discussion

Having presented all results from the obtained data, this chapter discusses all findings and addresses all three hypotheses as well as the related research questions that have been set prior to the surface investigation. Uncertainties of the surface analysis will be addressed afterwards as well as one concluding subchapter in which weather- and subsurface data is included for the discussion.

9.1 Hypotheses and Research Questions

A total of three hypotheses and seven related research questions, frame the SfM-based surface analysis of the landslide in Gresten. The questions will be discussed and answered while the hypotheses will eventually be verified or falsified in the following.

> H1: "***Repeated SfM methodology can be used to investigate short-period surface dynamics of landslides.***"

The first hypothesis is accompanied by two research questions, Q1.1: "*Can surface dynamics of a landslide be identified by comparing two- or more SfM-generated elevation models?" and,* Q1.2: "*Did certain parts of the surface experience greater movements than others?*".

Comparing two- or more SfM-generated terrain models, means a subtraction in this case – producing a DoD. Multiple DoDs, covering periods from two months to nearly a decade have already been presented in this thesis.

By comparing two- or more SfM-generated terrain models of the Salcher landslide, elevation differences and spatial movement trends can be analyzed and visually displayed, which is shown in Fig. 65. Furthermore, the main scarps can be mapped, and zones of accumulation and depletion be identified on the basis of a DoD.

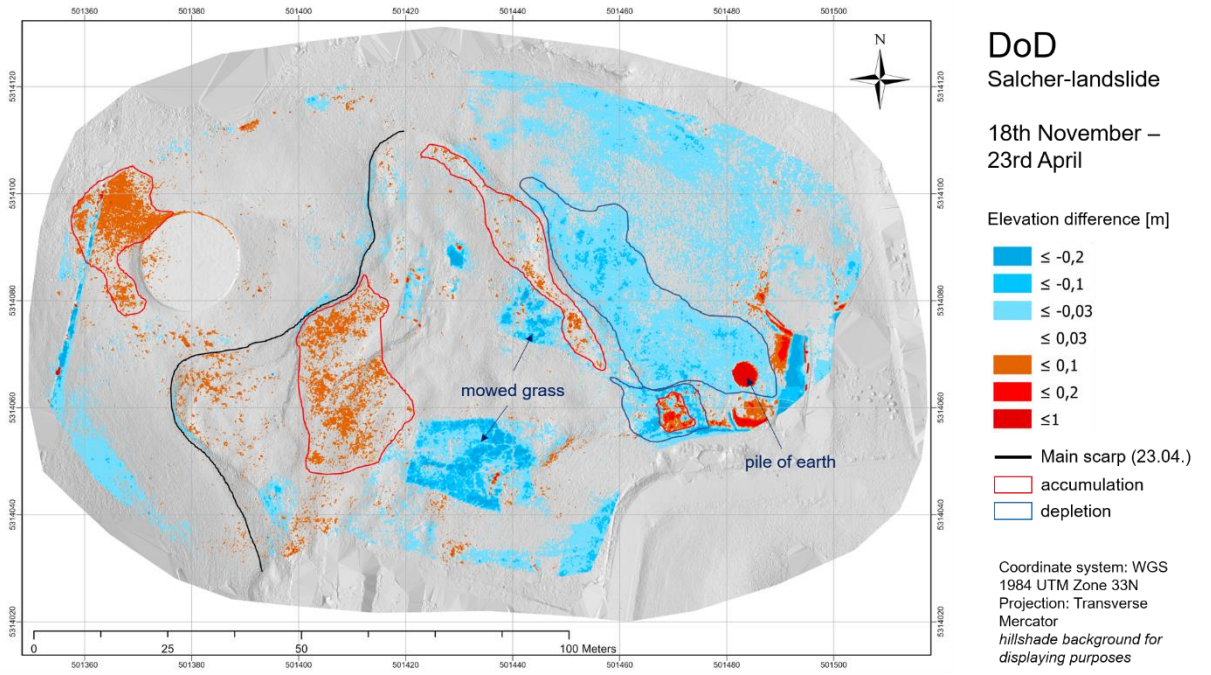

Figure 66: DoD analysis for the observation period November 2020-April 2021

The produced DoDs of the landslide presents interesting spatiotemporal surface information. Data about how and where material has moved in which direction serve as the basis for monitoring investigations and are also the first findings of this thesis. Fig. 67 is a close-up view of the main scarp in southwestern direction taken from the DoD displaying elevation differences between 18th of November and 23rd of April.

Figure 67: Close-up view of main scarp, southwest direction; DoD 18.11-23.04 (left) and photography taken on the 22.02.2021 (right)

An image of the main scarp, taken the day, the second UAV-flight was carried out, was added to illustrate how the data of DoDs display elevation differences along a scarp.

Here, the top of the scarp has subsided by up to 10 cm, while the head of the landslide, right beneath the scarp has gained height. By logic argumentation, two possible explanations apply here: Either material of the upper edge of the scarp has come loose (e.g.: erosion processes) and slid/fell onto the head of the landslide, or a rotational/tilting movement occurred here, which would explain the loss at the scarp on the one hand and gains of height on the other hand around the head (more information about slope movement Chapter 3.1).

Regardless of what was the real driving force behind this surface movement, this specific example showed how pure surface data allows a discussion of its dynamics and changes. Having this spatiotemporal information about surface dynamics, further discussions, and conclusions about internal movements of the ground can be drawn from here. DoDs are therefore a helpful tool to investigate surface dynamics (GODONE et al. 2020).

So, the answer the first research question related to the first hypothesis, Q1.1 "*can surface dynamics of the landslide be identified by comparing two- or more SfM-generated terrain models?"* is simply yes - and is presented above in Fig. 66 and its discussion.

The second research question is, Q1.2. **"***Did certain parts of the surface experience greater movements than others?***"**. As seen in Fig. 66, areas where movement has been detected are unevenly distributed across the research area. For areas, which experienced movements, the range of elevation difference varies mainly between 3 cm up to 20 cm in both, positive and negative direction. Maximum gained and lost elevation is approx. -1,06 to +1,18 m, but is related to anthropogenic changes between the two surveys.

During the observation period, certain parts of the surface experienced greater movements than others. This can be seen especially for the horse pasture area and the toe of the landslide where depleted mass is moved downslope and piles up. So not the whole slope is moving but certain areas experience both, up- and downward movements. There is, however, a tendency that the upper part of the slope is mainly gaining height, while the lower part mainly loses elevation, at least during the observation period. So yes, certain parts of the surface experienced more movements

than others and the landslide does not move as one body, nor does the slope move as a whole.

Coming back to the hypothesis H1. Repeated UAV-surveys and the subsequent creation of elevation models for investigation purposes often cover a period of a year or even more (see SAMODRA et al. 2020; ROSSI et al. 2018; TURNER et al. 2015). In this thesis, a comparably short observation period of about five months (156 days) was used to carry out three surveys, with only 60 days in between the second and third date in the field. However, even between this period, results of the SfM- methodology revealed surface dynamics of the landslide in Gresten (see Fig. 67). Many SfM-related research approaches analyzed landslides before and after their (re-) activation (like WARRICK et al. 2019; KOWALSKI et al. 2018 and GODONE et al. 2020), whereas the investigation for this master thesis focused on monitoring the surface a slow-moving landslide (see STUMVOLL et al. 2020). The presented results above proved that this methodological approach delivers promising outcomes and can serve as a basis for comprehensive further investigations.

So even for slower moving landslides, surface dynamics can be investigated by obtaining and processing UAV-data in short-periods and the hypothesis H1 "***Repeated SfM methodology can be used to investigate short-period surface dynamics of landslides***" is thereby verified.

H2: "***Digital Terrain model- and point cloud analysis are both suitable methods to gain information about landslide-surface dynamics.***"

To verify/falsify this statement, two research questions have been posed. Firstly, Q2.1: "*How do the results of the elevation model- and dense point cloud analysis differ?*" and secondly Q2.2 "*Is one of the approaches more suitable for surface investigations of landslides than the others?".*

In order to answer these questions, three different approaches (two point clouds- and one DTM-analysis) of landslide surface investigation on the basis of UAV gained data have been applied. The presented results in Chapter 8, all provide information about surface dynamics and visually present detected changes of it. The results differ, but in what way?

To answer if Q2.1: "*How do the results of the elevation model- and dense point cloud analysis differ?*". DoDs and point cloud analysis do have in common, that the result is a multidimensional model of the research area with highlighted detected surface changes. Nevertheless, the calculation of differences between two surveys differs due to different used algorithms (see Fig. 68).

To summarise the three methodological approaches that have been applied in this thesis:

- DoDs display the height difference between two points exactly along the z-axis on a pixel-by-pixel basis. Only the vertical distance between two terrain models is measured (see Fig. 68) (LAGUE et al. 2013; SAMODRA et al. 2020).
- C2C-Comparison is a direct method for point clouds without meshing, gridding, or calculations of surface normal. For each point of the "compared" cloud, a closest point can be defined in the "reference" cloud, so simply put, the surface change equals the distance between two closest points (see Fig. 68) (LAGUE et al. 2013). However, improvements can be made by using a model of the "reference" surface (for more details see Chapter 6.4.1), so an algorithm identifies the location of a point via an estimated surface and not purely by the shortest distance between the two point clouds. However, the probably biggest

advantage of this approach is that distances on x-, y-, and z-axis can be calculated independently (CloudCompare 2015).

- M3C2 is the most complex method of the three methods presented. A vector is defined for every point by fitting a plane on the estimated neighbours. Then the distance between the two clouds is calculated with a normal scale selection in relation to surface roughness to identify spatially variable confidence intervals. By setting point cloud-specific parameters, the M3C2 algorithm repeats the steps listed and computes the distances directly between two point clouds (see LAGUE et al. 2013). Since this method does not simply compare the distance of two points but uses a “surface normal”, it is possible to track characteristic features of a surface, especially for steep and complex topography (COOK 2017; WARRICK et al. 2019).

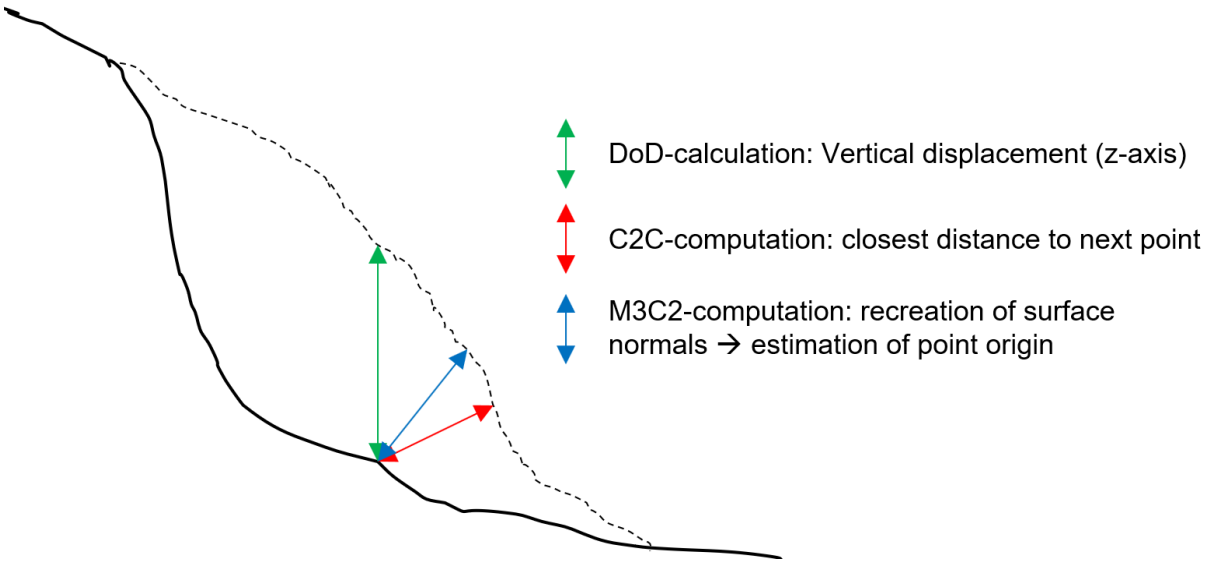

Figure 68: Comparison of distance computation of DoD, C2C and M3C2-method

Fig. 68 displays the main difference of distance computation between either point clouds or raster-datasets. This illustration is for the understanding of the different distance calculations. It is therefore simplified and overexaggerated.

Digital Terrain model- and point cloud analysis are both methods to detect surface dynamics and changes of landslides, however, they differ in their processing, accuracy, and the generated results (WARRICK et al. 2019; GODONE et al. 2020). A general statement about one of these two approaches being more accurate than the other cannot be made. Generally, DoDs tend to be less accurate due to the processing, which requires a point cloud being meshed to produce a digital surface. Usually,

Information gets lost during this step, but surface roughness related errors are reduced (SAMODRA et al. 2020; LAGUE et al. 2013). However, point clouds are more susceptible to errors due to partially unlinked points, roughness, and outliers (see EKER et al. 2017). So, careful on-site data acquisition plays an important role to minimise errors related to position uncertainties since all post-processing methods can only deliver results as good as the data itself.

Even though all produced results looked very similar and visibly display areas of accumulation as well as depletion, the computation differs and hence the results do as well, even if just a little.

So, Q2.2: "*Is one of the approaches more suitable for surface investigations of landslides?".*

As described, the main difference between the methods is their distance computation, so it really depends on the type of movement of a slope that needs to be investigated.

The C2C-Method is used very little in the literature regarding landslide investigation. FUAD et al. (2018) suggests making use of either the Iterative Closest Point or the Least Square Plane method and not exclusively use the C2C-Method, when analyzing landslide surface changes. They also state that the M3C2 method provided better results in displacement measurement than C2C. So, the pure C2C-computation between points is rarely used and the main argument for its application is its simple usage and fast calculation (LAGUE et al. 2013).

DoD-analysis and the M3C2 on the other hand are commonly applied for landslide surface change detection (CLAPUYT et al. 2016; COOK. 2017; EKER et al. 2017; WARRICK et al. 2019; GODONE et al. 2020). As seen in Fig. 68, these two approaches calculate surface movement in a different way. While in this figure a generic landslide is displayed, movements can occur in various forms (see Chapter 3.1). With that being said, none of the presented methods is the "best" or "worst" for surface investigations. It primarily depends on the desired information and the research area, hence the landslide itself.

So as DoDs are a method to detect vertical changes of a surface, this approach is best suited for landslides, where high elevation losses are expected (GODONE et al. 2020). This applies especially for movement types of topple and fast sliding and larger

landslides in general. The M3C2 algorithm finds its application for slower moving landslides and complex topography, since features of the “reference” surface can be tracked, and changes detected (COOK et al. 2017).

However, the M3C2 does have three major advantages over the DoD and C2C method according to LAGUE et al (2013). The M3C2 algorithm (i) does not require gridding or meshing of a point cloud which usually results in loss of resolution and accuracy, (ii) estimates its local accuracy by using an estimate of the local average position of the reference and compared cloud and (iii) operates in 3D, which allows to detect changes for steep slopes, cliffs, and overhangs.

So, Q2.2 “*is one of the approaches more suitable for surface investigations of landslides?”* – Yes, the M3C2 algorithm, implemented into the opensource software CloudCompare, proved to be a useful tool for surface change detection. Its advantage over the other approaches makes this application the best fitting for surface investigations of landslides, especially the slow-moving one surveyed in Gresten. Nonetheless, the DoD results provide similar information about surface movement as well, so the second hypothesis “***Digital Terrain model- and point cloud analysis are both suitable methods to gain information about landslide-surface dynamics***” is verified.

H3: "***The landslide has been continuously moving for more than a decade since the last reactivation.***"

In addition to the hypothesis, the three research questions, Q3.1 *"to what extent did the main scarps and features of the landslide change?"*, Q3.2 *"are there any differences in surface movement during winter and spring?"* and Q3.3 *"can the processes, mainly responsible for movements in Gresten be identified with a surface analysis?*" will be answered.

Although there have been a few reactivations recently, this hypothesis refers to the last major one, which took place in August 2006 (STUMVOLL et al. 2020). The complete surface of the Salcher landslide has been surveyed since then in irregular intervals; starting in 2007 (TLS survey by the GBA), 2009 (ALS survey of the Federal State of Lower Austria), 2014 (TLS survey by the ENGAGE research group) and finally 2020/2021 the UAV-survey carried out for this master thesis. Covering more than a decade, surface dynamics and changes of surface features have been monitored and tracked. To understand more about the movements that occurred over the last decade, a DoD was created, displaying elevation changes of the Salcher landslide between 2009 and April 2021 (see Fig. 60). Height differences range from -1.08 to 1.26 m resulting in an average surface change of 0.195 m per year for the most active zones of the slope. For the period from 2007 to 2014, the largest elevation gain was 0.84 m (12 cm/a) while from 2009 to 2021 the highest uplift was 1.26 m (10.5 cm/a). An average surface movement of 0.22 m per year was determined for the period from 2007 to 2014 (see Chapter 6.4). According to this calculation, the movement rate of the landslide seemed to have decreased since 2014. However, no precise statement can be made from here, since the measurements are purely based on z-axis changes, which means that possible sliding movements without major height differences are not considered in the calculation and calculated movement rates only apply for specific points.

So, regarding Q3.1 "*To what extent did the main scarps and features of the landslide change?"*

To answer this research question, the expanded surface investigation needs to be included. The morphological map, displaying the position of the main scarps and bulged footslope from 2007 until 2021 already provides information for the response. However, to further illustrate the surface changes, parts from three of the topographical profiles (see chapter 8.3.2) were added onto the morphological map, to not only show the horizontal displacement, but also the elevation differences at these points (see Fig. 69).

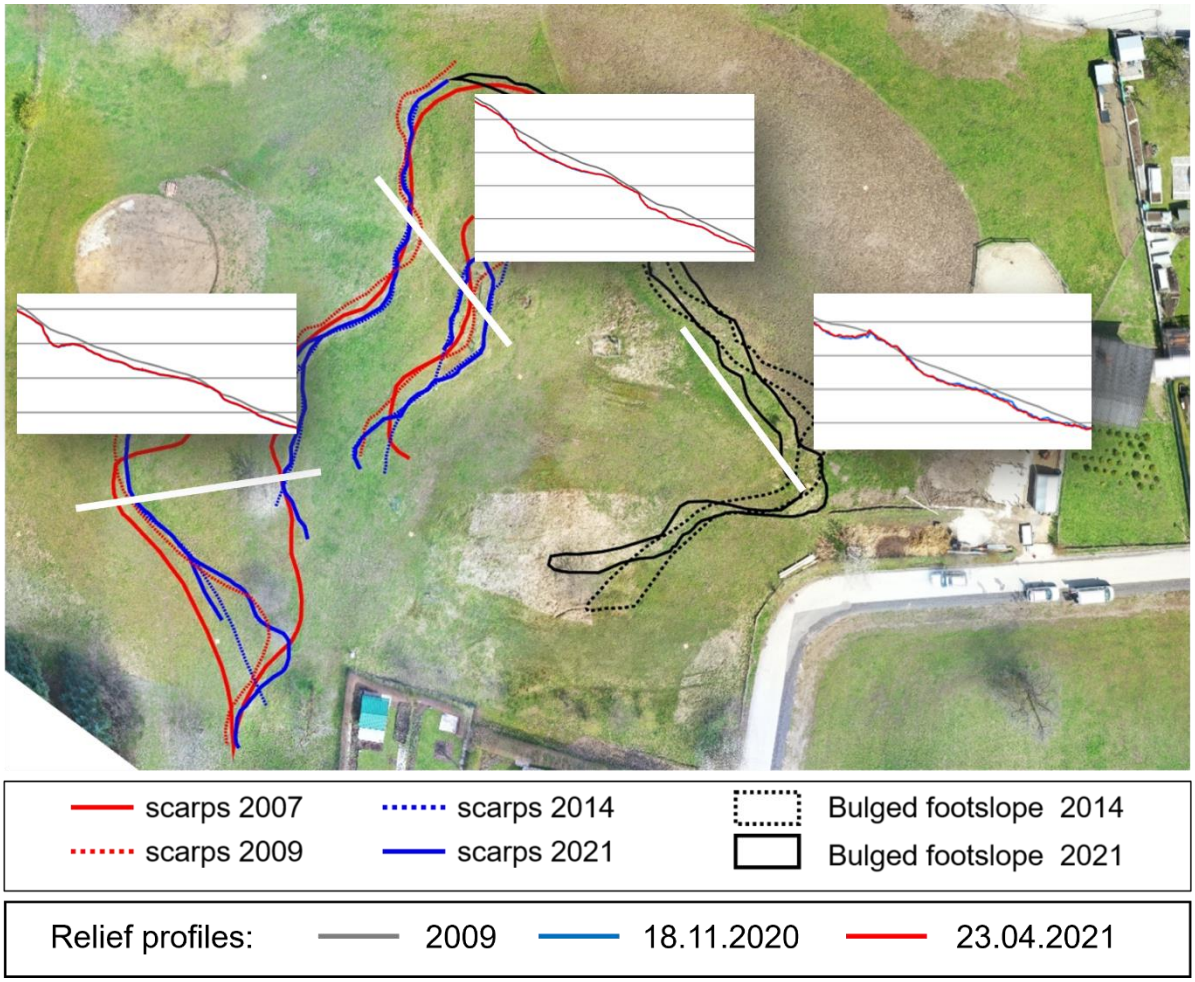

Figure 69: Morphological mapping crossed with topographical profiles

As seen in Fig. 69, no homogeneous movements of the main scarps can be detected. On the contrary, while in some places the scarps seem to have "shifted" downslope, in other parts, the position of the scarp moved upslope. By looking at the three samples from the relief profiles, it can be conducted that there is always a deepening right beneath the scarp. At the upper edges of the scarps, little has changed in terms of

elevation since 2009. However, it is quite different with the head of the landslides below. Here, a loss of height can be observed in multiple places.

So how did the main scarps and features change? The spatial position of the scarps has changed, with variations, up to 7-8 m since the beginning of the surface investigations in 2007. The greatest changes are observed south of the circular plane at the crown of the landslide, at the meteorological station and near the adjacent slope southwest near the private property (see Fig. 69).

The second research question Q3.2 "*Are there any differences in surface movement during winter and spring?*"

To answer this question, two DoDs need to be analyzed and compared. The DoD covering the winter period from November to February (Fig. 57) and the DoD covering spring from February to April (Fig. 58) display different elevation developments of the surface. For the winter period, mainly areas of depletion were identified. An accumulation in the upper part beneath the main scarp did not exceed more than 10 cm and the bulged footslope near the toe, which is usually a zone of accumulation for this landslide (see JOCHUM et al. 2008; STUMVOLL et al. 2020) and for rotational landslides generally (CRUDEN & VARNES 1996), does not show any height development. During spring however, the bulged footslope and toe gained partially up to 20 cm in elevation. The crown of the landslide also seemed to have lifted significantly compared to the winter period. This specific part of the landslide is displayed in Fig. 70 comparing the winter- to the spring period.

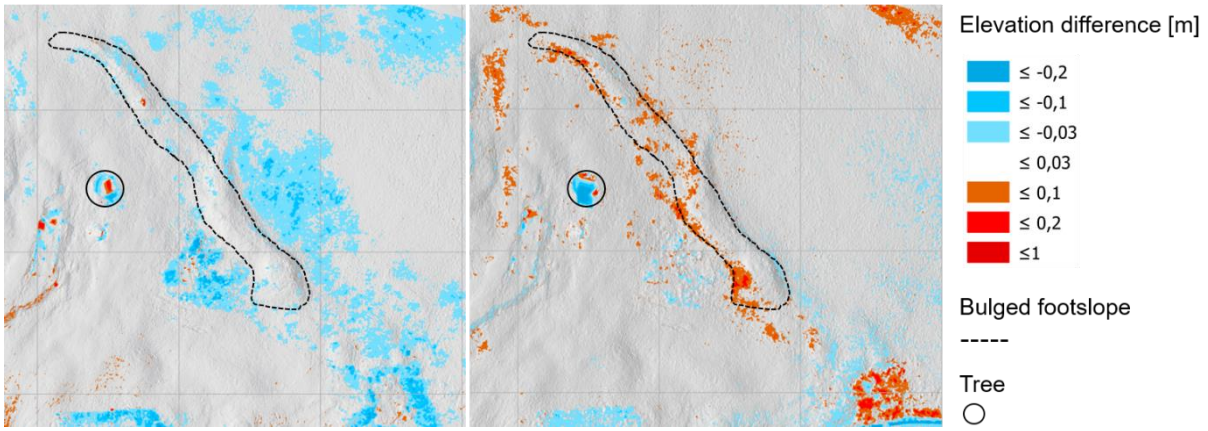

Figure 70: Elevation development of the zone of accumulation during winter (left) and spring (right)

It can be seen in Fig. 70 that during spring, an increasement of elevation occurred slightly uphill of the bulged footslope. This observation concludes that the depleted mass transferred downslope has enlarged and piles up at the zone of accumulation. So, during the winter period, fewer surface dynamics were observed for this certain part of the landslide than during spring. Whether there is a connection of surface movement with precipitation for these periods will be discussed further in chapter 9.3, by validating the SfM-results with data from the meteorological station. To answer the second research question related to the first hypothesis, slightly more movement was observed during spring, especially in the lower part of the landslide. However, during winter, the surface along the scarps in the upper part of the landslide experienced uplifting movements. An interesting result here is how parts of the landslide moved differently in winter and spring. However, the blue line in the topographical profiles is difficult to recognise, as it is only visible for certain spots and is covered by the red, most recent cross-section line. This already suggests that there were no extreme elevation changes during the winter of 2020/2021.The surface has developed very heterogeneous dynamics and does not move as a whole body.

So, Q3.3 *“Can the processes, mainly responsible for movements in Gresten be identified with a surface analysis?”*

As known from previous investigations, there is an approx. up to 4 m deep recent active sliding mass situated on a layer with presumably little to no active movements with a high-water content, which makes it susceptible for sliding movements (JOCHUM et al. 2008; STUMVOLL et al. 2020). Information about the subsurface is difficult to obtain from remote sensing without the necessary sensors, but the results obtained so far allow conclusions to be drawn about the processes responsible for movements. The analysis of the main scarp locations between 2007 and 2021 revealed that there is no linear sliding process at the study site. Some scarps have moved downslope as the entire mass below has probably slid, while other scarps have “migrated” upslope presumably due to retrogressive erosion processes. And the investigation of the cross-section profiles led to the assumption that compaction processes are, at least partly, responsible for the decrease of elevation for the upper parts of the Salcher landslide. So - yes, processes responsible for movement of the landslide in Gresten can be identified purely with a surface analysis. However, most of the findings are only

assumptions that need to be confirmed by on-site data collection and analysis. Nevertheless, this surface dynamic analysis has proved that remote sensing with optical-, RGB-sensors is a good basis to draw conclusions about processes below and on the surface.

However, this does not verify the third hypothesis H3 "***the landslide has been continuously moving for more than a decade since the last reactivation***". On the contrary, it is wrong. According to the main scarps in Fig 69, there seem to have been greater movements between 2007 and 2009 than between 2014 and 2021. Furthermore, no linear movement or trend of main scarp movements can be observed here. This finding falsifies the third hypothesis. The landslide has not been continuously moving for more than a decade since the last reactivation. Movements seem to occur irregularly, probably after rainfall events and water infiltration (see CROZIER 1989: DIKAU & GLADE 2002 for landslide triggers).

9.2 Uncertainties

Having previously discussed the three hypotheses and related research questions set for this master thesis, uncertainties of the used methods for surface analysis will be addressed in the following.

The post-processing, mainly done with the commercial software Pix4DMapper 4.6.4, generates a quality report with various information about the project. To provide highest accuracy possible, selected GCPs are used as check points to determine the location of the generated point cloud compared to the known "real" points on the ground (see GOMEZ & PURDIE 2016). For the SfM-processing, the mean RMSE after georeferencing ranged from 9-14 mm., which is more than acceptable, since grasses and smaller vegetation also distorts even more. However, this means that the results cannot be used to make measurements or statements about surface movements in the millimeter range.

Regarding point cloud analysis, LAGUE et al. (2013: 6) identifies three main sources of uncertainties; (i) position uncertainty of point clouds, (ii) registration uncertainty between the point clouds and (iii) surface roughness related errors. The noise related position uncertainty of point clouds was reduced by applying a noise- and cloth

simulation filter. Registration uncertainty between the different point clouds was reduced by placing at least two GCPs on the same spot for a repeated survey. However, there is still a small deviation so minor errors (millimeter range) for point cloud comparison cannot be ruled out. Same applies to uncertainties due to surface roughness. As already explained (see Chapter 7.2), irregularities caused by vegetation and anthropogenic impacts can lead to a misinterpretation of elevation changes. Deviating height values along the edge of the study area can be the result of slightly inaccurate Delaunay triangulation calculations for the periphery areas of the landslide due to lower point density there.

According to the generated quality report of the SfM-software (Pix4D), the GSD for the produced SfM-based DTMs is 1.31 cm/pixel for UAV-I, 1.22 cm/pixel for UAV-II and 1.26 cm/pixel for UAV-III. Z-axis related uncertainties caused by different used coordinate systems were reduced by manually adjusting height values (see Chapter 6.3). In addition, the results must be interpreted with caution when it comes to the results of the periphery areas of the elevation models and point clouds. Here, increased distortions are more likely to occur since these areas are not fixed by surrounding GCPs (ABER et al. 2019).

There are several sources of error that can cause inaccuracies in point cloud- and DoD-analysis, but these uncertainties showed to produce errors of maximum 2-3 cm which can be neglected for surface dynamic investigation and monitoring at the Salcher landslide. It should be noted that this specific SfM approach via UAV-surveys, with used software Pix4D and platform (RGB-camera), is only suitable to detect reliable surface changes of 3 cm or more. Nevertheless, UAV-based SfM has proven to be a cost- and time-efficient as well as accurate method to investigate and monitor landslides (GODONE et al. 2020; CLAPUYT et al. 2016).

9.3 Results interpretation with weather and subsurface data

To get a more extensive understanding of the processes responsible for slope and surface movements at the Salcher landslide, it is helpful to include other measurements and available data.

Since (heavy) rainfall is one of the most common triggers for landslides (CROZIER & GLADE 2004), gathering information and data about precipitation for the observation period is important for further interpretations. Unfortunately, the newer precipitation measurement device for the meteorological station situated on the landslide was installed on the day the second UAV-survey was carried out, so the data in the following graph is taken from a conventional precipitation measurement device (see Chapter 6.2).

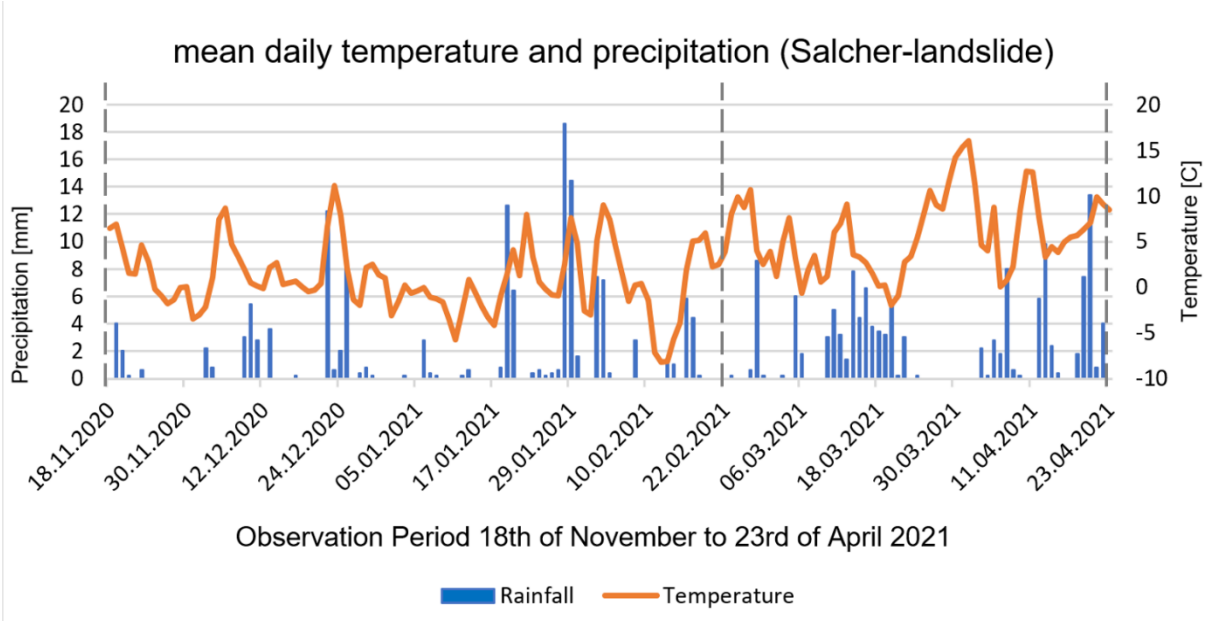

Figure 71: Mean daily temperature and precipitation measured on-site Salcher landslide 18.11.20-23.04.21

Fig. 71 displays the mean daily temperature and precipitation values taken from the meteorological station situated directly on the slope – the three survey dates are marked by a grey dashed line. The average temperature between the 18th of November and the 23rd of April was 2,81°C with 44 days where the mean daily temperature was below freezing. Total precipitation for this period was 271,2 mm (1,73 mm/day), which is a relatively dry winter and spring (see Chapter 5.5). As seen in Fig. 71, especially between UAV I and UAV II the mean daily temperature varied often between negative and positive values. This constant freezing and thawing might have an impact on the

episodic/periodic movement of the landslide. During spring, specifically after UAV II, temperatures increased, and rainfall started to last for several days more often. In this period, the enlargement of the bulged footslope and thus also of the accumulation zone was particularly characteristic. Presumably, the water of the snowmelt is responsible for a movement of depleted mass downslope. Especially during the on-site inspections on the 22.02 and 23.04, the lower part of the landslide was muddy and saturated with water, making it even difficult to walk across certain areas. This waterlogging zone was already identified in previous studies (see Fig. 29) and needs further hydrological investigations, in which the permanent ERT-monitoring plays an important role (see STUMVOLL et al. 2020).

Furthermore, the results of this master thesis can be combined with already examined knowledge about the subsurface of the research area. Fig 72 is a modified representation of the subsurface model already presented in the Chapter about the current knowledge of the Salcher landslide dynamics. The depth and location of shear surfaces was detected by Dynamic Probing, drill core analysis and inclinometer measurements (see Chapter 4.1 and 6.3).

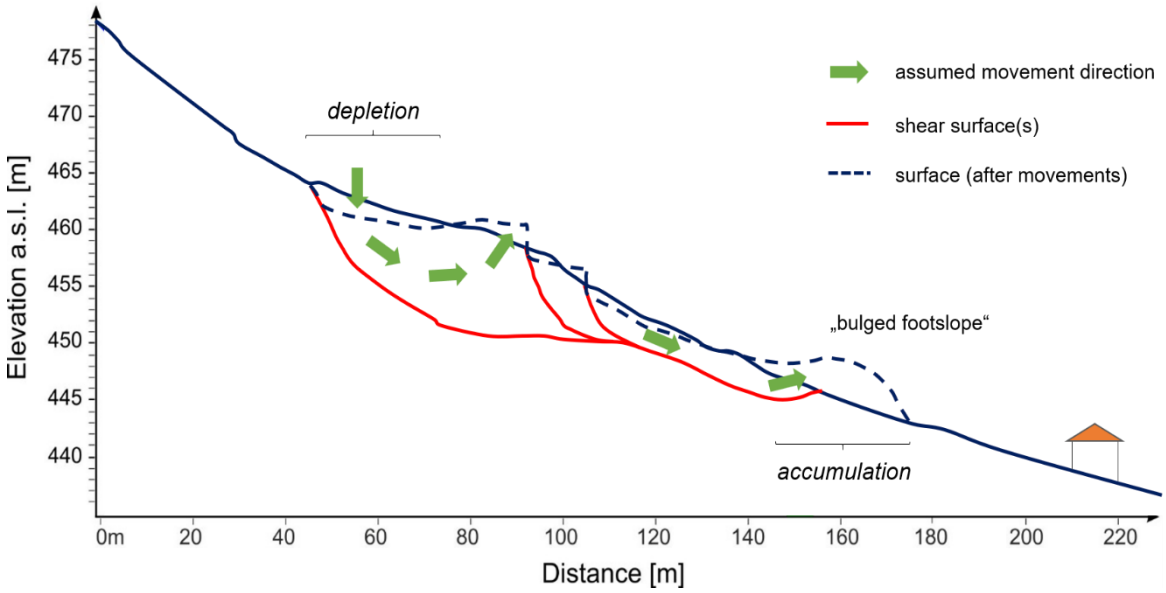

Figure 72: Assumed movement directions along shear surfaces - simplified and exaggerated (changed and adapted from Stumvoll et al. 2020: 1845)

Based on the results of the surface analysis of this master thesis, assumed movement directions were added. In an overexaggerated way, this depiction displays the (rotational) movements of the Salcher landslide, along the slope for at least three different areas, along shear surfaces. Fig. 72 is a simplified representation of a

subsurface model and does not display the elevation changes to scale. However, this figure elucidates how complex this landslide is. At least three sections, which together form the main body of the landslide, are slowly moving downslope, pushing up material and creating an accumulation at the toe. What is special here is, that each of these bodies, between two shear surfaces, seem to do rotational movements nearly independently. At least this would explain why the results of the DoD-analysis revealed that the scarps tend to subside while the head beneath partially gains elevation.

In any case, the type of movement of the Salcher landslide is not easy to define due to the complex geology and resulting characteristics. The surface analysis combined with subsurface and weather data allows further insights about the “behaviour” of the slope and their results can be used for further research and investigation.

10 Conclusion

This master thesis analyzed and investigated surface dynamics of an active slope in Gresten, Lower Austria – situated in a region susceptible for landslides. For this purpose, three aerial surveys were carried out between the 18th of November 2020 and 23rd of April 2021 using a UAV.

The movement processes at the landslide are to be classified as rotational sliding (see Chapter 5), although investigations assume multiple surfaces of ruptures, which makes the whole sliding area more complex (JOCHUM et al. 2008; STUMVOLL et al. 2020). The results of the surface investigation of the analyzed landslide confirms that movements occurred during the observation period. The first hypothesis is verified as repeated SfM methodology is suitable to investigate short-period surface dynamics of a landslide and movements within 60 days are perfectly visible in the results. The second hypothesis is verified as well, because the results proved that elevation model- and point cloud analysis are both reliable methods to gain information about landslide-surface dynamics". Only the third hypothesis was disproved as the surface does not move continuously but in phasic and episodic ways.

Between the first and last data acquisition, areas of the landslide have lifted and subsided by up to one meter according to the DoD-analysis. Due to misinterpreted trees, vegetation, anthropogenic impacts and single pixels, absolute values should be considered with caution. However, trends and spatial elevation changes are reliable, as the results of this master thesis match and confirm previous findings about the surface movement (see JOCHUM et al. 2008; STUMVOLL et al. 2020).

Within the 153 days observation period, the surface of the investigated Salcher landslide in Lower Austria changed dynamically, meaning no continuous movement was identified, instead episodic and periodic downslope movements characterise this landslide. Multiple approaches of point-cloud and elevation model comparison have been carried out to analyze surface changes in different ways. Closest neighbour, multiscale models, z-axis differences, cross-section profiles as well as geomorphological mapping were applied on basis of SfM-produced high-resolution point clouds of the research area, to investigate, how the surface of the landslide in Gresten has changed. The results provided further insights about the "behaviour" of the sliding slope.

The lower areas of the research area, starting from beneath the landslide toe, have experienced a decrease of elevation. The horse pasture, northeast of the landslides main body, which subsided nearly completely with a few exceptions by at least 3 cm is particularly noticeable here. To what extent this development was caused by either the weight of the horses or movements of the slope needs to be further investigated.

Along the bulged footslope, an increase of elevation was detected, especially on the upslope side (Fig. 66). This accumulation of depleted material seems to be the result of a slow rotational slope movement on multiple shear surfaces. At a maximum rate of ~20cm per year, material gets transferred downslope and accumulates at the toe of the landslide, leading to a magnifying bulged footslope. Its downhill side seems to have been compressed by the horses' hooves, as there is clear "cut" seen on the DoDs exactly where the area of the horse pasture begins. Incidentally, this "horse impact" probably resulted also in a shift of position of the landslide's toe since at least year 2014, as seen Fig. 65. It appears that the accumulating zone is increasing spatially, but movements on the downslope side are limited by the horse pasture area. This also results in ever steeper scarp towards the horse pasture.

While the crown of the landslide has changed only slightly in some places, the head, beneath the main scarps, gained height. This is untypical, since the head of a landslide usually subsides along with the main body due to the rotational movement along a subsurface that is curved and concave (see CRUDEN & VARNES 1996). Whereas depleted mass of rotational landslides normally gains elevation further downslope in the accumulation zone, here the situation is more complex as there are several zones of accumulation and depletion which partially overlap. As previously discussed, this is probably due to the presence of several sliding surfaces at different depths (see STUMVOLL et al. 2020) and disconnected bodies with rotational movements at different rates.

As mentioned before, caution is advised when interpreting the results along the edge of the research area, as this is where the probability of errors is the highest. However, the adjacent slope, southwest of the landslides' active zone, seems to subside slightly. To what extent the decrease of elevation here has an effect on the main body of the landslide is unclear. The same applies to the area above of the circular plane at the crown of the landslide. Here, the area gained elevation as seen in Fig. 52,56 & 59, however no connection to the remaining surface movements can yet be drawn.

JOCHUM et al. (2008) suspects a branch of the main scarp in the upper part of the landslide, right beneath the circular plane. As seen in Fig. 29, the scarp runs in a north-western direction, along the adjacent slope, towards the road "*Hunnenstraße*" and then along the "*Salcherstraße*", which both delimit the research area. The elevation differences near the circular plane could be related to this branch of the main scarp and would explain why there are height changes above the main body of the landslide. However, there is no confirmation about the existence of this extended scarp.

Regarding time-series investigation, there are many indications that the M3C2 method will become more popular and commonly applied than the simpler DoD-analysis. Among other things, the extensive settings of the plugin (WARRICK et al. 2019), the lower processing time, not to be limited on the z-axis (LAGUE et al. 2013, the introduced precision maps since version 2.9 of CloudCompare (JAMES et al. 2017), and a general more accurate change detection (EKER et al. 2017) speak for this.

In conclusion, the SfM-approach for an investigation of a surface is well suited, not only for landslides. The fact that UAVs can be used quickly in inaccessible or dangerous areas, e.g. after a natural hazard, makes them a very interesting and universal tool not only for geomorphology but earth sciences, disaster risk reduction and engineering fields as well. The results obtained can be processed in a variety of ways and combined with other data for interpretation and verification, depending on the research aim. Several things such as vegetation growth and increasing inaccuracy towards peripheral areas need to be considered but overall UAV surveys proved to be a suitable method to investigate and monitor surface dynamics.

11 Perspectives and further research

The results of this thesis are in line with previous investigations and theories on the dynamics of the Salcher landslide in Gresten. With the help of remote sensing data collected by UAV, results indicated that several sliding surfaces in the ground are responsible for this slow rotational movement of the slope (see JOCHUM et al. 2008; STUMVOLL et al. 2020). Individual parts of the entire landslide body, separated along scarps and subsurface layers, are situated and move semi-independently on top of multiple shear surfaces. The term “semi-independently” was deliberately chosen here, since the direction of movement and the velocity of these individual parts are heterogeneous, but each part still supports and stabilises each other. Fig. 72 in chapter 9.3 illustrates this. It was also confirmed that the movements of the surface vary a lot depending on the area and time period, making it almost impossible to make statements about the movement of the whole entire slope. The thesis also proved that SfM-based elevation model analysis can provide unique information about a relief surface and is a universal tool for landslide investigations. Not only digital elevation models and their other variants can be generated, point cloud analysis, morphological mapping, topographical profiles and time-series analysis are just a few of all the possible investigation approaches that are built upon simple RGB-imagery, if its post processed.

Applications of UAVs in remote sensing for geomorphological purposes have been increasing in recent years and this development will certainly continue. Reasons for this are particularly the comparatively low costs and the time savings (see WESTOBY et al. 2012; EKER et al. 2017) as well as constantly improved controls and on-board sensors. Here, the currently emerging RTK drones will probably become a standard as soon as their prices no longer differ that much from conventional drones. Their built-in RTK positioning receiver allows to produce high-resolution point clouds and surface models without distributing and surveying GCPs on site, which reduces the susceptibility to errors and mistakes in the field (FORLANI et al. 2018). In the case of the Salcher landslide on-site data acquisition, the most time-consuming part was indeed the distribution and measurement of the GCPs.

Another method of surface investigation that would certainly bring interesting new insights about the Salcher landslide is the processing and evaluation of the pTLS data

(see CANLI et al. 2015). A suggestion here would be a time series analysis by overlaying every scan on top of each other, creating an animation displaying all captured surface movements. This animation would have an enormous data basis and would give a detailed insight of surface movements since there would be no time gaps in between the surveys.

The most recent publication about the landslide from STUMVOLL et al. (2020) states that hydrology and conclusions on future slope stability are fields that need further investigation. Considering that the landslide is under investigation for more than a decade, threshold- and especially spatiotemporal slope stability analysis are the fields further research activities should focus on. The evaluation of the installed ERT is not yet completed at the time of this thesis but will certainly provide valuable information about water content of the subsurface.

While the results of this thesis have answered some questions - at the same time they have raised new ones:

To what extent do the horses' weight influence the detected elevation loss in the horse pasture or what is the relationship between the sliding movements and erosive processes in terms of the shifted scarps? It is still unclear how great the influence of precipitation is and which role the waterlogged area plays. Likewise unclear is the existence of a branch from the main scarp running above the main active landslide body.

Further investigations here are necessary to understand the sustaining processes, shaping this slope. Especially since movements of the landslides' crown and its upslope area have been detected, an investigation of the adjacent slope south-west of the main body might deliver new insights of the complex movements. Same as for the slope northwest, movements have been detected in this master thesis whereas no connections to other observations can be drawn yet. Also, correlations between heavy rainfall-/snowmelt events and surface movements have not yet been found, even though they are commonly knowing for triggering a slope failure and presumably already led to the movements documented in the 1970s by SCHWENK (1976).

To conclude this chapter with an outlook. Determining threshold values for slope stability and the correlation of precipitation and surface movements would be the goal of the long-term monitoring project, however, multiple investigations need to be carried out.

As now shown several times, repeated UAV-based remote sensing with optical sensors and the subsequent photogrammetric image processing methodology SfM is a quick, suitable, and accurate surface investigation and monitoring method which certainly will be used for further research.

Statements about when and how the slope might fail in the future cannot be made at this point. The slope experienced various movements since the 1970s, damaging surrounding residential buildings and piled up material which blocked pathways and streets (SCHWEIGL 2013; SCHWENK 1978 and 1979). However, after several years of monitoring, there are no direct indications of a slope failure in the near future, which would threaten local residents. Nevertheless, the slope is slowly moving downhill, depleted material is accumulating, which can create new instabilities. Possibly displaced material from the adjacent western slope may well mobilise smaller landslides or debris flows like the one reported in 2007, but there is no evidence of a connection to the main body of the Salcher landlide itself (see JOCHUM et al. 2008).

Subsequent edit [28th of July 2021]**:**

Major floods in Germany and Belgium between the 13th and 15th of July destroyed various critical infrastructure and residential buildings. With a death toll of over 200 people, this flood event is the worst natural hazard in Germany since 1962.

The same depression causing these floods led to precipitation measures going up to 200mm in parts of Lower Austria over the weekend 17th/18th of July. These exceptionally large amounts of rain seem to have also caused movements of the Salcher-landslide. Fig. 73 are webcam images taken from noeslide.at, shortly before (14th of July) and after (19th of July) the rainfall events.

Figure 73: Webcam screenshots of the Salcher-landslide 14.07 (left) and 19.07 (right) (University of Vienna 2021)

Within a few days, the pole in Fig. 73 has tilted due to movements of the landslide body. Triggering factor for this development was the massive rain, leading to an oversaturated ground and therefore higher driving force which results in surface changes. If an UAV-survey is now carried out, the results of the surface analysis will probably display further surface changes between April 2021 and July 2021. However, this analysis would fall outside of the time frame of this thesis, which is the reason, this subsequent edit is included here. Nevertheless, this once more proves, further investigations here will provide interesting insights about the slope.

12 References:

ABER J. S., MARZOLFF I. & RIES J. B. (2010): Small-Format Aerial Photography: Principles, Techniques and Geoscience Applications. Elsevier B.V., Amsterdam & Oxford.

ArcGIS Pro (ed.) (n.d.): Project Raster (Data Management). URL: https://pro.arcgis.com/en/pro-app/latest/tool-reference/data-management/project-raster.htm [18.05.2021].

AVANZI G. D., DUCHI G., GALANTI Y., GIANNECCHINI R., LO PRESTI D. C. & MARCHETTI D. (2013): DP Test in Geotechnical Characterization of Shallow Landslides Source Area: Results and Perspectives. -In: MARGOTTINI C., CANUTI P. & SASSA K. (Ed.): Landslide Science and Practice: Landslide Inventory and Susceptibility and Hazards Zoning.1: p. 249-255.

BALTZER A. (1875): Ueber Bergstürze in den Alpen. Verlag der Schabelitz'schen Buchhandlung (C. Schmidt). Zürich.

BELL R., KRUSE J. E., GARCIA A., GLADE T. & HÖRDT A. (2006): Subsurface investigations of landslides using geophysical methods – geoelectrical applications in the Swabian Alb (Germany). -In: Geographica Helvetica: p. 201-208.

BEV (Ed.) (n.d.): Bundesamt für Eich- und Vermessungswesen: Transformation von Gauß-Krüger (GK)- Koordinaten des Systems MGI in Universal Transversal Mercator (UTM)- Koordinaten des Systems ETRS89. URL: https://portal.bev.gv.at/pls/portal/docs/PAGE/BEV_PORTAL_CONTENT_ALLGEMEIN/0200_PRODUKTE/PDF/TRANSFORMATION_GK_MGI_UTM_ETRS89.PDF [18.05.2021].

BFW (Ed.) (2021): Bundesforschungszentrum für Wald: eBod Digitale Bodenkarte. Beschreibung der Bodenform – ID 58 | KB 196 | Bodentyp K. URL: https://bodenkarte.at/#/center/15.01932,47.97953/zoom/18.5 [11.04.2021].

BMLRT (Ed.) (2021a): Bundesministerium für Land - und Forstwirtschaft, Umwelt- und Wasserwirtschaft. Portal für hydrographische Daten Osterreichs. eHYD NLV Messstelle 109041 Gresten. Vienna, Austria. URL: https://ehyd.gv.at/ [24.03.2021].

BMLRT (Ed.) (2021b): Bundesministerium für Land - und Forstwirtschaft, Umwelt- und Wasserwirtschaft. Portal für hydrographische Daten Osterreichs. eHYD OWF Messstelle 209817 Wang. Vienna, Austria. URL: https://ehyd.gv.at/ [24.03.2021].

CANLI E., HÖFLE B., HÄMMERLE M., THIEBES B. & GLADE T. (2015): Permanent 3D laser scanning system for an active landslide in Gresten (Austria). European Geoscience Union General Assembly Vol 17., Vienna, Austria.

CLAGUE J. J. & ROBERTS N. J. (2012): Landslide hazard and risk. -In: CLAGUE J. J. & STEAD D. (Ed.): Landslides: Types, Mechanisms and Modeling. Cambridge University Press. New York: p. 1-9.

CLAPUYT F., VANACKER V. & OOST K. V. (2016): Reproducibility of UAV-based earth topography reconstructions based on Structure-from-Motion algorithms. -In: Geomorphology 260: p. 4-15.

CloudCompare (Ed.) (2015): Cloud-to-cloud Distance. URL: https://www.cloudcompare.org/doc/wiki/index.php?title=Cloud-to-Cloud_Distance [12.05.2021].

CloudCompare (Ed.) (2019): M3C3 (plugin). URL: https://www.cloudcompare.org/doc/wiki/index.php?title=M3C2_(plugin) [12.05.2021].

COE J. A., ELLIS W. L., GODT J. W., SAVAGE W. Z., SAVAGE J. E., MICHAEL J. A., KIBLER J. D., POWERS P. S., LIDKE D. J. & DEBRAY S. (2003): Seasonal movement of the Slumgullion landslide determined from Global Positioning System surveys and field instrumentation July 1998 - March 2002. -In: Engineering Geology 68: p. 67-101.

COMERT R., AVDAN U., GORUM T. & NEFESLIOGLU H. A. (2019): Mapping of shallow landslides with object-based image analysis from unmanned aerial vehicle data. -In: Engineering Geology 260: 105264.

COOK K. (2017): An evaluation of the effectiveness of low-cost UAVs and structure from motion for geomorphic change detection. -In: Geomorphology 278: p. 195-208.

CROZIER M. J. (1986): Landslides: causes, consequences & environment. Croom Helm. London.

CROZIER M. J. & GLADE T. (2004): Landslide Hazard and Risk: Issues, Concepts and Approach. -In: GLADE T., ANDERSON M. & CROZIER M. J. (Ed.): Landslide Hazard and Risk. John Wiley & Sons Ltd. Chichester: p. 1-41.

CRUDEN D. M. (1991): A simple definition of a landslide. -In: Bulletin of the International Association of Engineering Geology, 43 (1): p. 27-29.

CRUDEN D. M. & VARNES D. J. (1996): Landslide types and processes. -In: Turner A. K. & Schuster (Ed.): Landslides: Investigation and mitigation. Washington D.C., Special Report, 247: p. 36-75.

DEMEK J. (1972): Manual of detailed geomophological mapping. -In: International Geographical Union, Commission on Geomophological Survey and Mapping. Academica. Prague

DEMOULIN A. & GLADE T. (2004): Recent landslide activity in Manaihan, East Belgium. -In: Landslides 1: p. 305-310.

DIKAU R, BRUNSDEN D, SCHROTT L, IBSEN M-L (Ed.) (1996): Landslide recognition: Identification, movement, and causes. Wiley, New York, 1996.

DIKAU R. & GLADE T. (2002): Gefahren und Risiken durch Massenbewegungen. -In: Geographische Rundschau, 54: p. 38-45.

DIKAU R., EIBISCH K., EICHEL J., MEßENZEHL K. & SCHLUMMER-HELD (2019): Geomorphologie. Springer Spektrum. Berlin.

DJI (Ed.) (2021): DJI Mavic 2 Specs. URL: https://www.dji.com/uk/mavic-2/info [24.04.2021].

EBERHARDT E. (2012): Landslide monitoring: The role of investigative monitoring to improve understanding and early warning of failure. -In: CLAGUE J. J. & STEAD D. (Ed.): Landslides: Types, Mechanisms and Modeling. Cambridge University Press. New York: p. 222-234.

EECKHAUT M. VAN DEN, POESEM J., VERSTRAETEN G., VANACKER V., NYSSEN J., MOEYERSONS J., BEEK L. P. H. VAN, VANDEKERCKHOVE L. (2007): Use of LIDAR-derived images for mapping old landslides under forest. -In: Earth Surface Processes and Landforms 32: p. 754-769.

EKER R., AYDIN A. & HÜBL J. (2017): Unmanned aerial vehicle (UAV)-based monitoring of a landslide: Gallenzerkogel landslide (Ybbs-Lower Austria) case study. – In: Environmental Monitoring Assessments (190) 28: p. 1-14.

ELLIS E. C. (2020): Anthropozän: Das Zeitalter des Menschen – eine Einführung. Oekom Verlag. München.

European Committee for Standardization (Ed.) (2005): ISO 22476-2:2005 Geotechnical investigation and testing – Field testing – Part 2: Dynamic Probing. URL: https://www.iso.org/obp/ui/#iso:std:iso:22476:-2:ed-1:v1:en [17.03.2021].

Federal State of Lower Austria (Ed.) (2021): Wasserstandsnachrichten und Hochwasserprognosen. Messstellendaten 209817 Wang Kleine Erlauf. URL: https://www.noe.gv.at/wasserstand/#/de/Messstellen/Details/209817/Durchfluss/Jahr [26.03.2021].

FLORINSKY I. V. (2016): Digital Terrain Analysis in Soil Science and Geology. 2nd Edition. Academic Press. Elsevier. London, San Diego, Cambridge & Oxford.

FORLANI G., ASTA E. D., DIOTRI F., DI CELLA U. M., RONCELLA R. & SANTISE M. (2018): Quality Assessment of DSMs Produced from UAV Flights Georeferences with On-Board RTK Positioning. -In: remote sensing (10) 311: p. 1-22.

FUAD N. A., YUSOFF A. R., ISMAIL Z. & MAJID Z. (2018): Comparing the performance of point cloud registration methods for landslide monitoring using mobile laser scanning data. -In: International Conference on Geomatics and Geospatial Technology (GGT 2018), 3-5. September, Kuala Lumpur, Malaysia: p.11-21.

GALI J. A., COROMINAS J. & RIUS J. (2000): Using global positioning system techniques in landslide monitoring. -In: Engineering Geology 55: p. 167-192.

GALLISTL J., WEIGAND M., STUMVOLL M., OTTOWITZ D., GLADE T. & OROZCO A. F. (2018): Delineation of subsurface variability in clay-rich landslides through spectral induced polarization imaging and electromagnetic methods. -In: Engineering Geology 245: p. 292-308.

GARIANO S. L. & GUZZETTI F. (2016): Landslides in a changing climate. -In: Earth-Science Reviews 162: p. 227-252.

GATTINGER T. E. (1980): Hydrogeologie. -In: Geologische Bundesanstalt (GBS) (Ed.): Der geologische Aufbau Österreichs. Wien: p. 580-593.

GINDRAUX S., BOESCH R. & FARINOTTI D. (2017): Accuracy Assessment of Digital Surface Models from Unmanned Aerial Vehicles' Imagery on Glaciers. -In: Remote Sensing (9) 186: p. 1-15.

GLADE T. & CROZIER M. J. (2005): The Nature of Landslide Hazard Impact. -In: GLADE T., ANDERSON M. & CROZIER M. J. (Ed.): Landslide Hazard and Risk. John Wiley & Sons Ltd. Chichester: p. 41-74.

GLADE T., STUMVOLL M. J. & FAHRNGRUBER R. (2019): Projekt [NoeSLIDE] Multi-Parameter Monitoring von unterschiedlichen Typen gravitativer Massenbewegungen in Niederösterreich. Projektpräsentation on the 11th of October 2019 – Gemeindesaal Gresten, Scheibbs, Niederösterreich.

GLADE T. & ZANGERL C. (2020): Gravitative Massenbewegungen – Terminologie und Charakteristika. -In: GLADE T., MERGILI M. & SATTLER K. (Ed.): ExtremA 2019. Aktueller Wissensstand zu Extremereignissen alpiner Naturgefahren in Österreich. Vienna University Press: p. 367-382.

GODONE D., ALLAISIA P., BORRELLI L. & GULLÀ G. (2020): UAV and Structure from Motion Approach to Monitor the Maierato Landslide Evolution. -In: remote sensing 12: p. 1-18.

GOMEZ C. & PURDIE H. (2016): UAV- based Photogrammetry and Geocomputing for Hazards and Disaster Risk Monitoring – A Review. -In: Geoenvironmental Disasters (3) 23: p. 1-11.

Government of Lower Austria (Ed.) (2021): Wasserstandsnachrichten und Hochwasserprognosen. Messdatenstelle Wang. URL: https://www.noe.gv.at/wasserstand/#/de/Messstellen/Details/209817/Durchfluss/Jahr [21.05.2021].

HASTAOGLU K. O., POYRAZ F., TURK T., YILMAZ I., KOCBULUT F., DEMIREL M., SANIL U., DUMAN H. & BALIK-SANIL F. (2018): Investigation of the success of monitoring slow motion landslides using Persistent Scatterer Inferometry and GNSS methods. -In: Survey Review 50 (363): p. 475-486.

HAUCK C., STUMVOLL M. J., JOCHUM B., GUARDIANI C. & GLADE T. (2018): The influence of hydro-meteorological conditions on landslide dynamics – an application to the Salcher landslide in Gresten, Lower Austria. NH3.1/HS2.3.10. EGU General Assembly 2018, Vienna, Austria.

HELENO S., MATIAS M., PINA P. & SOUSA A. J. (2016): Semiautomated object-based classification of rain-induced landslides with VHR multispectral images on Madeira Island. -In: Natural Hazards and Earth System Sciences 16: p. 1035- 1048.

HERRERA G., TOMÁS R., VICENTE F., LOPEZ-SANCHEZ J. M., MALLORQUÍ J. J. & MULAS J. (2010): Mapping ground movement in open pit mining areas using differential SAR interferometry. -In: International Journal of Rock Mechanics & Mining Sciences 47: p. 1114-1125.

HIGHLAND L. M. & BOBROWSKY P. (2008): The landslide handbook: a guide to understanding landslides; United States Geological Survey (USGS), Circular 1325.

HÖCK V., ANDRZEJ Ś., GASIŃSKI M. A. & BĄK. M. (2005): Konradsheim limestone of the Gresten Klippen Zone (Austria): new insight into its stratigraphic and paleogeographic setting. -In: Geologica Carpathica 56: p. 237-244.

HUGGEL C., CLAGUE J. J. & KORUP O. (2012): Is climate change responsible for changing landslide activity in high mountains?. -In: Earth Surface Processes and Landforms 37: p. 77-91.

HUNGR O., LEROUEIL S. & PICARELLI L. (2014): The Varnes classification of landslide types, an update. -In: Landslides 11(2): p. 167-194.

IFRC (International Federation of Red Cross) (2020): World Disasters Report 2020 – Tackling the humanitarian impacts of the climate crisis together. URL: https://media.ifrc.org/ifrc/wp-content/uploads/2020/11/20201116_WorldDisasters_Full.pdf [14.06.2021].

JABOYEDOFF M., OPPIKOFER T. ABELLÁN A., DERRON M. H., LOYS A., METZGER R. & PEDRAZZINI A. (2012): Use of LIDAR in landslide investigations: a review. -In: Natural Hazards 61: p. 5-28.

JAFARI B., KHALOO A. & LATTANZI D. (2017): Deformation Tracking in 3D Point Clouds via Statistical Sampling of Direct Cloud-to-Cloud Distances. -In: Journal of Nondestructive Evaluation 36:65: p. 1-10.

JAMES M. R., ROBSON S. & SMITH M. W. (2017): 3-D uncertainty-ased topographic change detection with structure-from-motion photogrammetry: precision maps for ground control and directly georeferenced surveys. -In: Earth Surface Processes and Landforms 42 (12): p. 1769-1788.

JOCHUM B., LOTTER M., OTTNER F. & TIEFENBACH K. (2008): Geophysikalische und ingenieurgeologische Methoden zur Untersuchung von durch Massenbewegungen bedingte Bauschäden in Niederösterreich. BBK-Projekt NC-62/F (2007) und ÜLG-35

(2007). Endbericht zur Fallstudie Gresten (NÖ). Geological Survey of Austria (GBA); University of Natural Resources and Life Sciences (BOKU), Vienna, Austria.

JOHNSON C., AFFOLTER M. D., INKENBRANDT P. & MOSHER C. (2017): An Introduction to Geology. Salt Lake Community College. Opengeology.org.

KLEIN A. (2006): Remote sensing in Geomorphology. -In: GOUDIE A. (Ed.): Encyclopedia of Geomorphology. Routledge Ltd. New York: p. 884-846.

KORUP O. (2012): Landslides in the Earth System. -In: CLAGUE J. J. & STEAD D. (Ed.): Landslides: Types, Mechanisms and Modeling. Cambridge University Press. New York: p. 10-23.

KOTTEK M., GRIESER J., BECK C., RUDOLF B. & RUBEL F. (2006): World Map of the Köppen-Geiger climate classification updated. -In: Meteorologische Zeitschrift 15 (3): p. 259-263.

KOWALSKI A., WAJS J. & KASZA D. (2018): Monitoring of anthropogenic landslide activity with combined UAV and LiDAR-derived DEMs – A case study of the Czerwony Wawoz landslide (SW Poland, Western Sudetes). -In: Acta Geodyn. Geomater. 15 (2): p. 117-129.

LAGUE D., BRODU N. & LEROUX J. (2013): Accurate 3D comparison of complex topography with terrestrial laser scanner: Application to the Rangitikei canyon (N-Z). -In: ISPRS Journal of Photogrammetry and Remote Sensing 82: p. 10-26.

LARGE A. R. G. & HERITAGE G. L. (2009): Principles of 3D Laser Scanning. -In: HERITAGE G. L. & LARGE A. R. G. (Ed.): Laser Scanning for the Environmental Sciences. Blackwell Publishing. Chichester: p. 21-34.

LESER H. & STÄBLEIN G. (Ed.) (1975): Geomorphologische Kartierung: Richtlinien zur Herstellung geomorphologischer Karten 1:25.000. Institut für Physische Geographie der Freien Universität Berlin.

LI Z., ZHU Q. & GOLD C. (2005): Digital Terrain Modelling – Principles and Methodology. CRC Press. Boca Raton, London, New York & Washington D.C..

LIN J., WANG M., YANG J. & YANG Q. (2017): Landslide Identification and Information Extraction Based on Optical and Multispectral UAV Remote Sensing Imagery. -In: IOP Conference Series: Earth and Environmental Science 57: 012017.

LINDNER G., SCHRAML K., MANSBERGER R. & HÜBL J. (2016): UAV monitoring and documentation of large landslide. – In: Applied Geomatics 8: p. 1-11.

LISSAK C., BARTSCH A., MICHELE M. D., GOMEZ C., MAQUAIRE O., RAUCOULES D. & ROULLAND T. (2020): Remote Sensing for Assessing Landslides and Associated Hazards. -In: Surveys in Geophysics 41: p. 1391-1435.

LUCIEER A., DE JONG S. M. & TURNER D. (2014): Mapping landslide displacements using Structure from Motion (SfM) and image correlation of multi-temporal UAV photography. – In: Progress in Physical Geography 38 (1): p. 97-116.

MATESE A., GENNARO S. F. DI & BERTON A. (2016): Assessment of a canopy height model (CHM) in a vineyard using UAV-based multispectral imaging. -In: International Journal of Remote Sensing 8-10 (38): p. 2150-2160.

MCCOLL S. T. (2015): Landslide Causes and Triggers. -In: SHRODER J. F. & DAVIES T. (Ed.): Landslide Hazards, Risks and Disasters. Elsevier, Amsterdam & Oxford :p. 17-42.

MESSENZEHL K., HOFFMAN T. & DIKAU R. (2014): Sediment connectivity in the high-alpine valley of Val Müschauns, Swiss National Park – linking geomorphic field mapping with geomophometric modelling. -In: Geomorphology 221: p. 215-229.

METTERNICHT G., HURNI L. & GOGU R. (2005): Remote Sensing of Landslides: An analysis of the potential contribution to geo-spatial systems for hazard assessment in mountainous environments. -In: Remote Sensing of Environment 98: p. 284-303.

MERGILI M., JABOYEDOFF M., PULLARELLO J. & PUDASAINI S. P. (2020): Back calculation of the 2017 Piz Cengalo-Bondo Landslide cascade with r.avaflow: what we can do and what we can learn. -In: Natural Hazards and Earth System Sciences 20: p. 505-520.

NUR S. M. A. W., NG W. K., NOR H. H. A., ANAS I., MOHD R. A. M., BADRUL N. I., ROZAINI R. & SYAHIRAH M. (2016): Potential Of Time Domain Reflectometry As Early Warning System In Slope Stability Monitoring Project: A Review. -In: AIP Confcerence Proceedings 1774, 030016: p. 1-7.

NYIMBILI P. H., DEMIREL H., SEKER D. Z. & ERDEN T. (2016): Structure from Motion (SFM) – Approaches & Applications. International Scientific Conference on applied Sciences 27-30 September 2016. Antalya. Turkey.

OTT HydroMet (Ed.) (2021): OTT Parsivel-2- Laser Weather Sensor. Laser precipitation disdrometer measuring all precipitation types. URL: https://www.ott.com/en-uk/products/meteorological-sensors-101/ott-parsivel2-laser-weather-sensor-2372/ [05.04.2021].

OTTOWITZ D., HOYER S., JOCHUM B., RIEGLER M., PREUNER P., SCOLOBIG A. & SUPPER R. (2018): Long-term landslide monitoring for understanding of underlying dynamic processes as basis for an End-User focused early warning – LAMOND. Endbericht. Wien, Österreich: Geologische Bundesanstalt Fachabteilung Geophysik.

PARISE M. (2000): Landslide Mapping Techniques and Their Use in the Assessment of the Landslide Hazard. -In: Phys. Chem. Earth 26 (9): p. 697-703.

PECKHAM R. J. & JORDAN G. (2007): Digital Terrain Modelling: Development and Applications in a Policy Support Environment. Spinger. Heidelberg & Berlin.

PEEL M. C., FINLAYSON B. L. & MCMAHON T. A. (2007): Updated world map of the Köppen-Geiger climate classification. -In: Hydrology and Earth System Sciences 11: p. 1633-1644.

PERRONE A., LAPENNA V. & PISCITELLI S. (2014): Electrical resistivity tomography technique for landslide investigation: A review. -In: Earth-Science Reviews 135: p. 65-82.

PETERNEL T., KUMELJ S., OSTIR K. & KOMAC M. (2017): Monitoring the Potoska planina landslide (NW Slovenia) using UAV photogrammetry and tachymetric measurements. – In: Landslides 14: p. 395-406.

PETLEY D. (2012a): Global patterns of loss of life from landslides. -In: Geology 40: p. 927–930.

PETLEY D. (2012b): Remote sensing techniques and landslides. -In: CLAGUE J. J. & STEAD D. (Ed.): Landslides: Types, Mechanisms and Modeling. Cambridge University Press. New York: p. 159-171.

PIX4D SA (Ed.) (2021a): Pix4Dmapper Photogrammetry software. Version 4. X.X. URL: https://www.pix4d.com/product/pix4dmapper-photogrammetry-software [03.02.2021].

Pix4D SA (Ed.) (2021b): Processing Steps. URL: https://support.pix4d.com/hc/en-us/articles/115002472186-Processing-steps [05.05.2021].

PREUTH T., GLADE T. & DEMOULIN A. (2010): Stability analysis of a human-influenced landslide in eastern Belgium. -In: Geomorphology 120: p. 38-47.

RAUCOULES D., DE MICHELE M. & AUNAY B. (2020): Landslide displacement mapping based on ALOS-2/PALSAR-2 data using image correlation techniques and SAR interferometry: application to the Hell-Bourg landslide (Salazie Circle, La Réunion Island). -In: Geocarto International 35 (2): p. 113-127.

REES W. G. (2012): Physical Principles of Remote Sensing – Photographic systems. Cambridge University Press: p. 135-163.

ROSSI G., TANTERI L., TOFANI V., VANNOCCI P., MORETTI S. & CASAGLI N. (2018): Multitemporal UAV surveys for landslide mapping and characterization. -In: Landslides 15: p. 1045-1052.

ROTARU A., OAJDEA D. & RAILEANU P. (2007): Analysis of the Landslide Movements. -In: International Journal of Geology 3 (1): p. 70-79.

RUTTNER A. & SCHNABEL W. (1988): Geologische Karte der Republik Österreich 1:50.000 Blatt 71 Ybbsitz. GBA. Wien.

SALAS-ROMERO S., MALEHMIR A., SNOWBALL I., LOUGHEED B. C. & HELLQVIST M. (2016): Identifying landslide preconditions in Swedish quick clays – insights from integration of surface geophysical, core sample- and downhole property measurements. -In: Landslides 13: p. 905-923.

SAMODRA G., RAMADHAN M. F., SARTOHADI J., SETIAWAN M. A., CHRISTANTO N. & SUKMAWIJAYA. (2020): Characterization of displacement and internal structure of landslides from multitemporal UAV and ERT imaging. -In: Landslides 17: p. 2455-2468.

SCHNABEL W. (1999): The Flysch Zone of the Eastern alps vol. 49. Verlag der Geologischen Bundesanstalt (GBA). Wien.

SCHWEIGL J. & HERVÁS J. (2009): Landslide Mapping in Austria. European Commission Joint Research Centre. Institute for Environment and Sustainablility. JRC Scientific and Technical Reports.

SCHWEIGL J. (2013): Gresten, Krause (Gst Nr.1999/1), Bramreiter (Gst.Nr. 1999/6) u. Plank (Gst.Nr. 1999/7) Katastrophenschaden 2006, Rutschung Salcher, geologischer Abschlussbericht zu den Vermessungen. (BD1-G-142/002-2007) (intern). 4. Geological office of the Federal State Government of Lower Austria.

SCHWENK H. (1976): Erhebungsbericht und Gutachten des geologischen Dienstes der Baudirektion. (No. BD-3120/1-1975) (intern). 4. Geological office of the Federal State Government of Lower Austria.

SCHWENK H. (1979): Erhebungsbericht und Gutachten des geologischen Dienstes der Baudirektion. (No. BD-G-78156) (intern). 3. Geological office of the Federal State Government of Lower Austria.

SCHWENK H. (1992): Massenbewegungen in Niederösterreich 1953-1990. -In: Jahrbuch der Geologischen Bundesanstalt 135: p. 567-660.

SHALABY A., ELMOGY M. & EL-FETOUH A. A. (2017): Algorithms and Applications of structure from motion (SfM): A survey. – In: International Journal of Computer and Information Technology 6 (6): p. 358-366.

SMITH J. T. (1979): A History of flying and photography: In the Photogrammetry Division of the National Ocean Survey 1919-1979. U.S. Department of Commerce. National Oceanic and Atmospheric Administration. Washington.

SMITH M. W., CARRIVICK J. L. & QUINCEY D. J. (2016): Structure from motion photogrammetry in physical geography. – In: Progress in Physical Geography 40 (2): p. 247-275.

STANGL R., BUCHAN G. D. & LOISKANDL W. (2009): Field use and calibration of a TDR-based probe for monitoring high-clay landslide soil in Austria. -In: Geoderma 150: p. 23-31.

STARK T. D. & CHOI H. (2008): Slope inclinometers for landslides. In: Landslides 5: p. 339-350.

STUMVOLL M. & GLADE T. (2019): NoeSLIDE II – Monitoring unterschiedlicher Typen gravitativer Massenbewegungen in Niederösterreich. Interner Abschlussbericht für den geologischen Dienst, Land Niederösterreich. Universität Wien, Institut für Geographie und Regionalforschung. Wien.

STUMVOLL M., CANLI E., ENGELS A., THIEBES B., GROISS B., GLADE T., SCHWEIGL J. & BERTAGNOLI M. (2020): The „Salcher“ landslide observatory – experimental long-term monitoring in the Flysch Zone of Lower Austria. -In: Bulletin of Engineering Geology and the Environment 79: p. 1831-1848.

SUPPER R., OTTOWITZ D., JOCHUM B., KIM J. RÖMER A., BARON I., PFEILER S., LOVISOLO M., GRUBER S. & VECCHIOTTI F. (2014): Geoelectrical monitoring: an innovative method to supplement landslide surveillance and early warning. -In: Near Surface Geophysics 12: p. 133-150.

TERHORST B. & KIRSCHHAUSEN D. (2001): Legends for mass movements in the MABIS-Project. -In: Zeitschrift für Geomorphologie 125: p. 177-192.

THIEBES B., BELL R., GLADE T., JÄGER S., MAYER J., ANDERSON M. & HOLCOMBE L. (2014): Integration of a limit-equilibrium model into a landslide early warning system. -In: Landslides 11: p. 859-875.

TOFANI V., VENTISETTE C. D., MORETTI S. & CASAGLI N. (2014): Integration of Remote Sensing Techniques for Intensity Zonation within a Landslide Area: A case study in the Northern Apennines, Italy. -In: remote sensing 6 (2): p. 907-924.

UNDRR (United Nations Office for Disaster Risk Reduction) (2018): Economic losses, poverty & disasters: 1998-2017. URL: https://www.preventionweb.net/files/61119_credeconomiclosses.pdf [14.06.2021].

UNESCO – WP/WLI (1990): A suggested method for a reporting a landslide. -In: Bulletin of the International Association of Engineering Geology, 41: p. 5–12.

UNESCO – WP/WLI (1991): A suggested method for a landslide summary. -In: Bulletin of the International Association of Engineering Geology, 43: p. 101–110.

UNESCO – WP/WLI (1993a): A suggested method for describing the activity of a landslide. -In: Bulletin of the International Association of Engineering Geology, 47: p. 53–57.

UNESCO – WP/WLI (1993b): A multi-lingual landslide glossary. International Geotechnical Societies. UNESCO Working Party on World Landslide Inventory, BiTech Publishers Ltd., Vancouver.

University Vienna (Ed.) (2021): NoeSlide: Salcher – landslide – observatory. URL: https://www.noeslide.at/index.php/de/Salcher landslide-observatory [04.06.2021].

VARNES D. J. (1954): Landslide types and processes. -In: Eckel E. B. (ed.) Landslides and engineering practice, special report 28. Highway research board. National Academy of Sciences, Washington, DC: p. 20-47.

VARNES D. J. (1978): Slope movement types and processes. -In: Schuster RL, Krizek RJ (ed.) Landslides, analysis and control, special report 176: Transportation research board, National Academy of Sciences, Washington, DC.: p. 11-33.

WANG G., KEARNS T. J., YU J. & SAENZ G. (2014): A stable reference frame for landslide monitoring using GPS in the Puerto Rico and Virgin Islands region. -In: Landslides 11: p. 119-129.

WARRICK J. A., RITCHIE A. C., SCHMIDT K. M., REID M. E. & LOGAN L. (2019): Characterizing the catastrophic 2017 Mud Creek landslide, California, using repeat structure-from-motion (SfM) photogrammetry. -In: Landslides 16: p. 1201-1219.

WESTOBY M. J., BRASINGTON J., GLASSER N. F., HAMBREY M. J. & REYNOLDS J. M. (2012): Structure-from-Motion photogrammetry: A low-cost, effective tool for geoscience applications. – In: Geomorphology 179: p. 300-314.

WIDDER R. W. (1988): Zur Stratigraphie, Fazies und Tektonik der Grestener Klippenzone zwischen Ma. Neustift und Pechgraben/OÖ. -In: Oberösterreichs M-uf (Ed.) Oberösterreichische GEO-Nachrichten, Beiträge zur Geologie, Mineralogie und Paläontologie von Öberösterreich vol. 3: p. 11-55.

WILLIAMS R. D. (2012): DEMs of Difference. -In: Geomorphological Techniques, 2, (3.2).

WOLTER A., GISCHIG V., STEAD D. & CLAGUE J. J. (2016): Investigation of Geomorphic and Seidmic Effects on the 1959 Madison Canyon, Montana, Landslide Using an Integrated Field Engineering Geomorphology Mapping, and Numerical Modelling Approach. -In: Rock Mechanics and Rock Engineering 49: p. 2479-2501.

ZAMG (Ed.) (n.d.): Zentralanstalt für Meteorologie und Geodynamik. Klimadaten von Österreich 1971-2000. URL: https://www.zamg.ac.at/fix/klima/oe71-00/klima2000/klimadaten_oesterreich_1971_frame1.htm [25.03.2021.]

ZAMG (Ed.) (2012): Zentralanstalt für Meteorologie und Geodynamik. Klimanormalperiode 1981-2010. URL: https://www.zamg.ac.at/cms/de/forschung/klima/datensaetze/klimanormalperiode-198120132010 [24.03.2021].

ZHANG W. QI J., WAN P., WANG H., XIE D. & YAN G. (2016): An Easy-to-Use Airborne LiDAR Data Filtering Method Based on Cloth Simulation. -In: Remote Sensing 8 (6): 501.

ZHAO C. & LU Z. (2018): Remote Sensing of Landslides - A Review. -In: remote sensing 279 (10). p: 1-6.

13 ANNEX

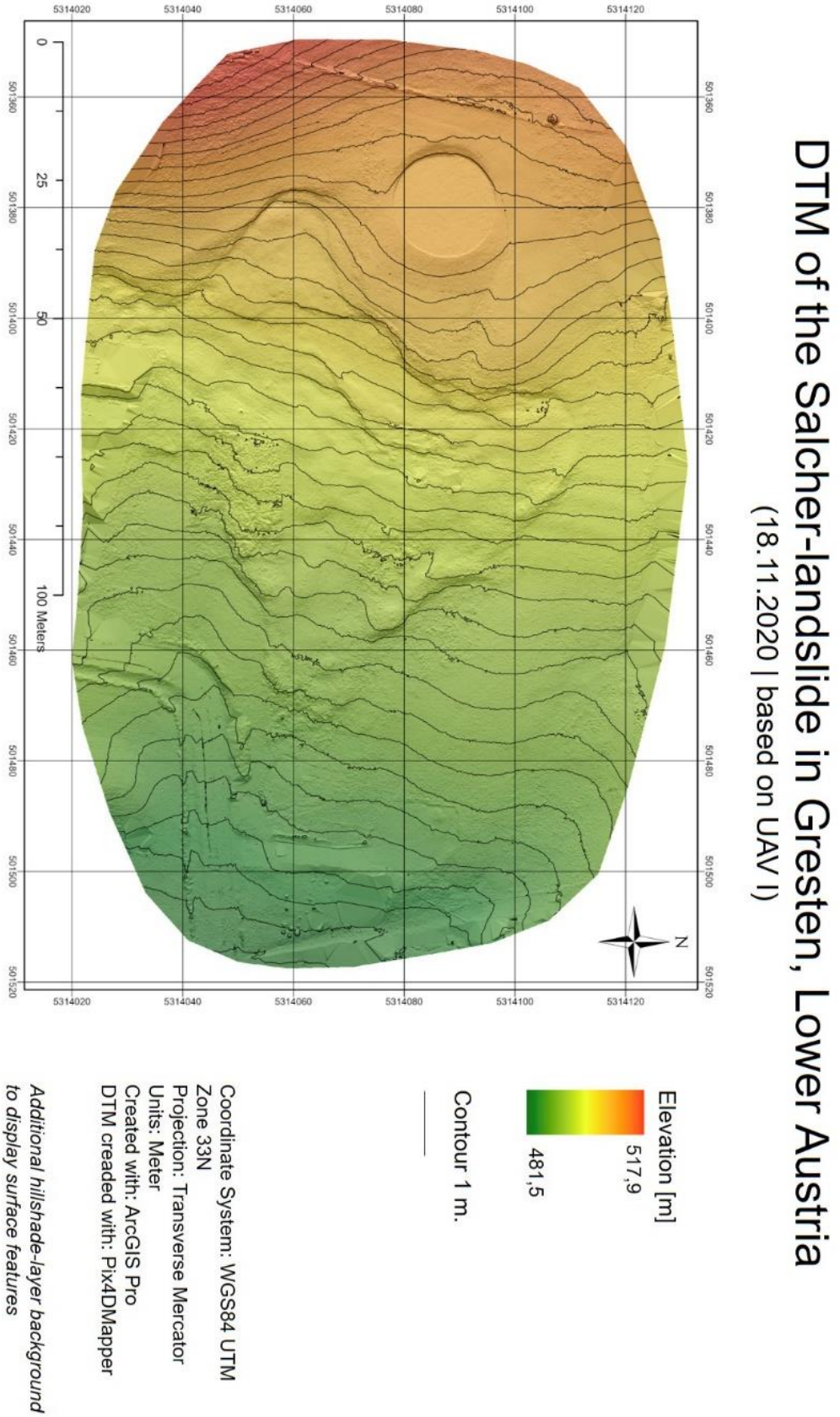
DTM of the Salcher-landslide in Gresten, Lower Austria
(18.11.2020 | based on UAV I)
5314020
5314040
5314060
5314080
5314100
5314120
501360
501380
501400
501420
501440
501460
501480
501500
501520
0
25
50
100 Meters
N
Elevation [m]
517,9
481,5
Contour 1 m.
Coordinate System: WGS84 UTM
Zone 33N
Projection: Transverse Mercator
Units: Meter
Created with: ArcGIS Pro
DTM creaded with: Pix4DMapper
Additional hillshade-layer background
to display surface features

DTM of the Salcher-landslide in Gresten, Lower Austria

(22.02.2021 | based on UAV II)

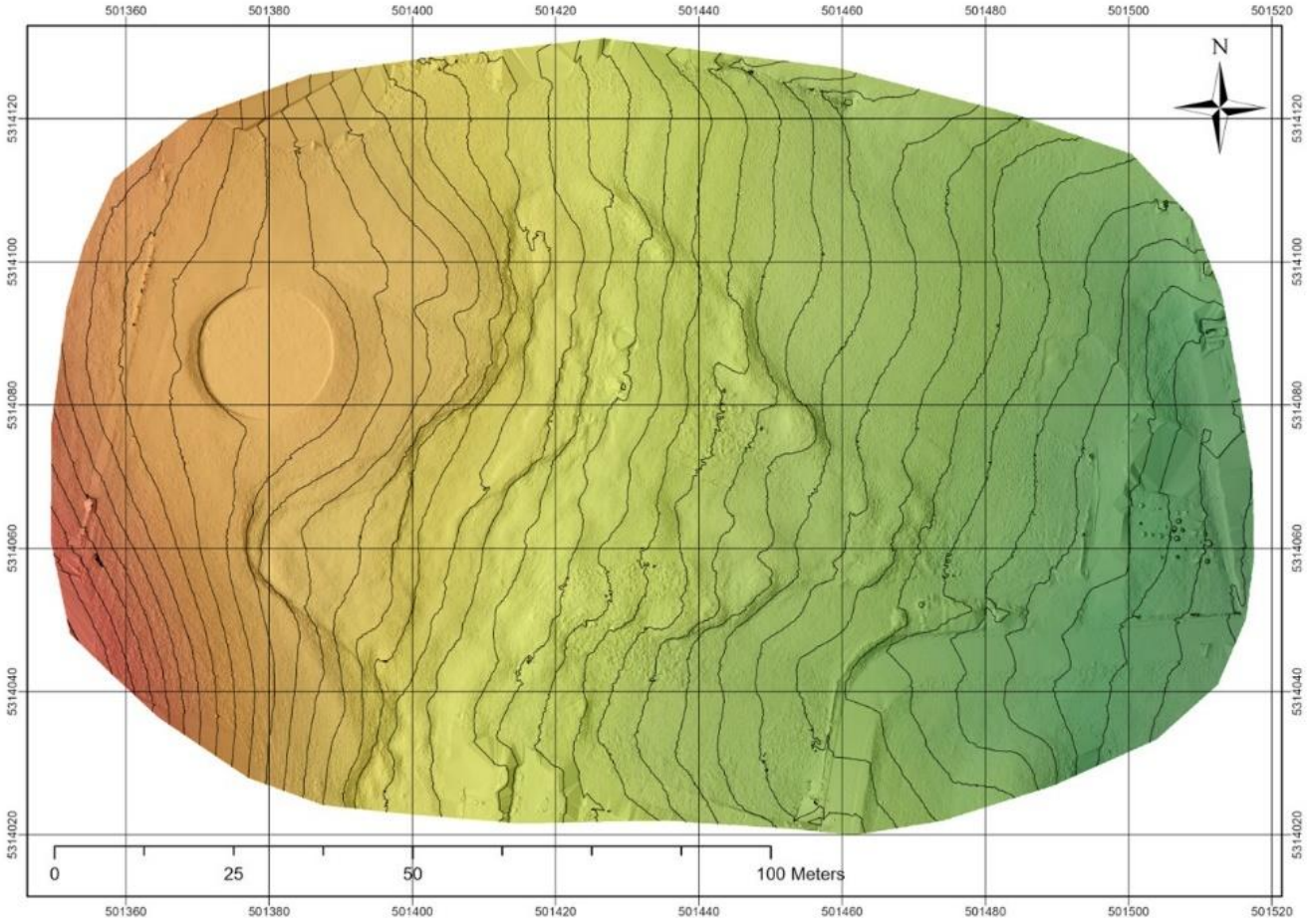

Elevation [m]

517,2

481,6

Contour 1 m.

Coordinate System: WGS84 UTM
Zone 33N
Projection: Transverse Mercator
Units: Meter
Created with: ArcGIS Pro
DTM creaded with: Pix4DMapper

Additional hillshade-layer background to display surface features

DTM of the Salcher-landslide in Gresten, Lower Austria

(23.04.2021 | based on UAV III)

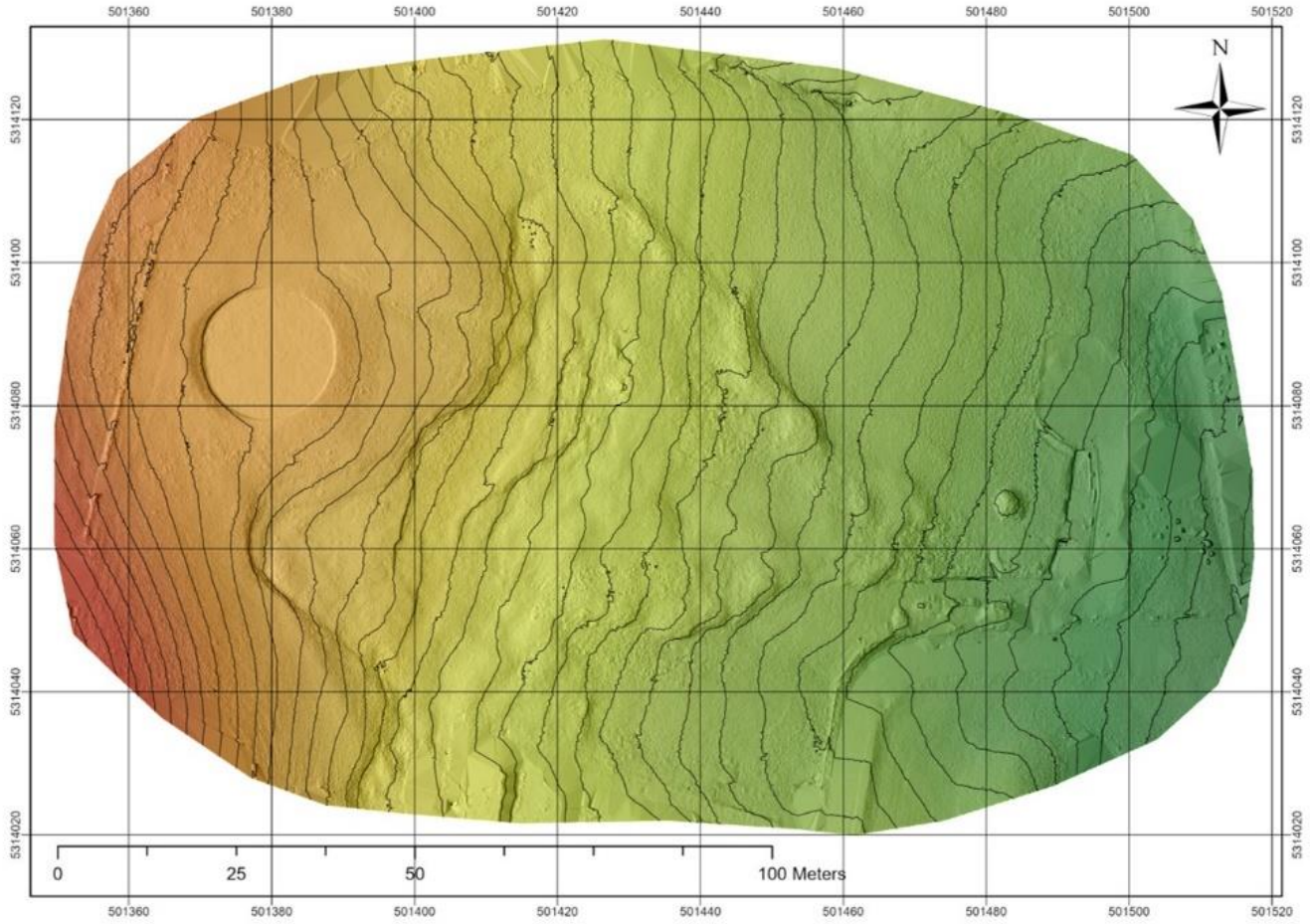

Elevation [m]

517,5

481,5

Contour 1 m.

Coordinate System: WGS84 UTM
Zone 33N
Projection: Transverse Mercator
Units: Meter
Created with: ArcGIS Pro
DTM creaded with: Pix4DMapper

Additional hillshade-layer background to display surface features

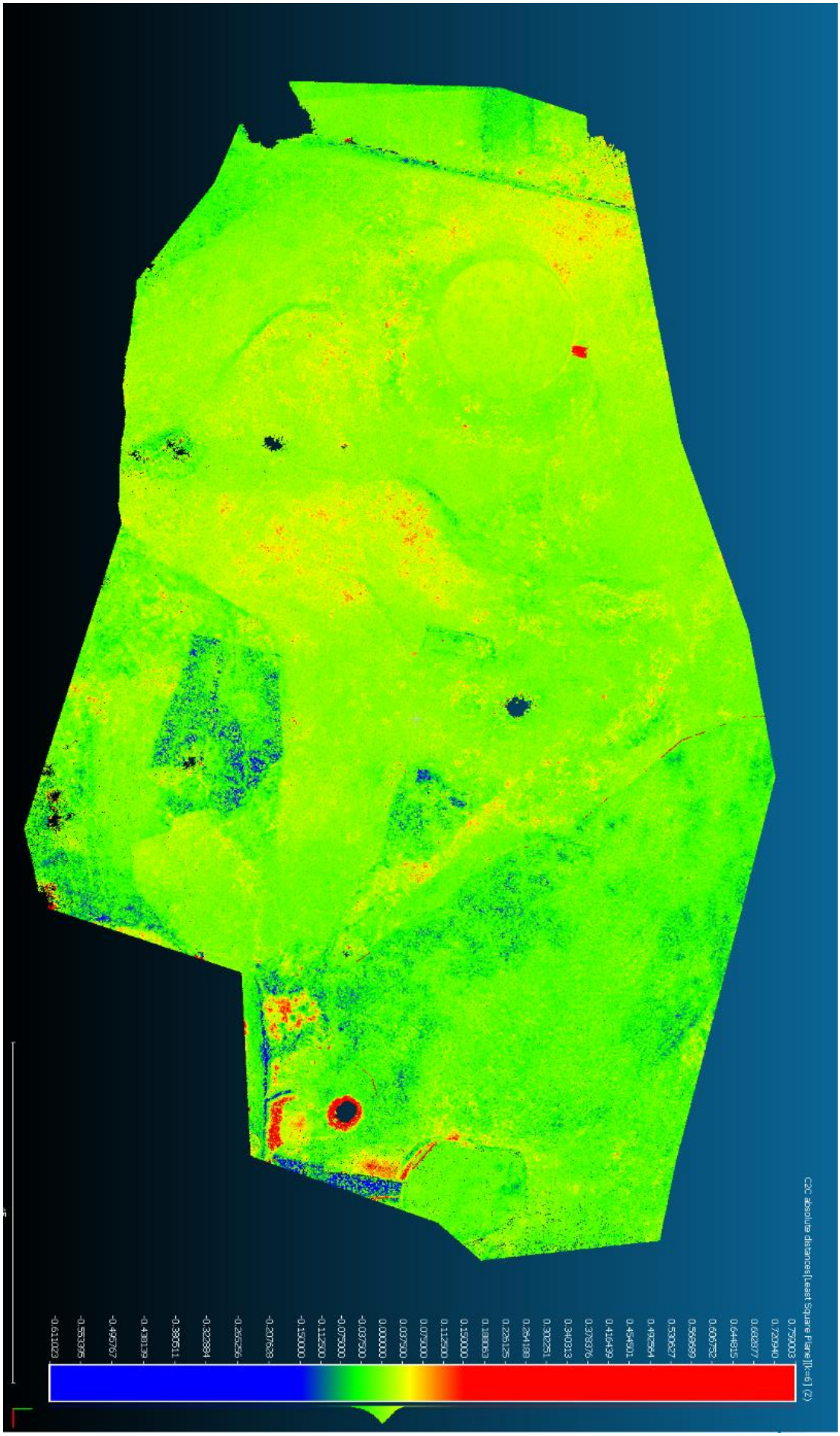
C2C absolute distances[Least Square Plane][i=6] (2)
0.759003
0.722940
0.686877
0.644815
0.608752
0.569689
0.530627
0.495564
0.454501
0.416439
0.378376
0.340313
0.302251
0.264188
0.226125
0.188063
0.150000
0.112500
0.075000
0.037500
0.000000
-0.037500
-0.075000
-0.112500
-0.150000
-0.188063
-0.226125
-0.264188
-0.302251
-0.340313
-0.378376
-0.416439
-0.454501
-0.495564
-0.530627
-0.569689
-0.608752
-0.644815
-0.686877
-0.722940
-0.759003

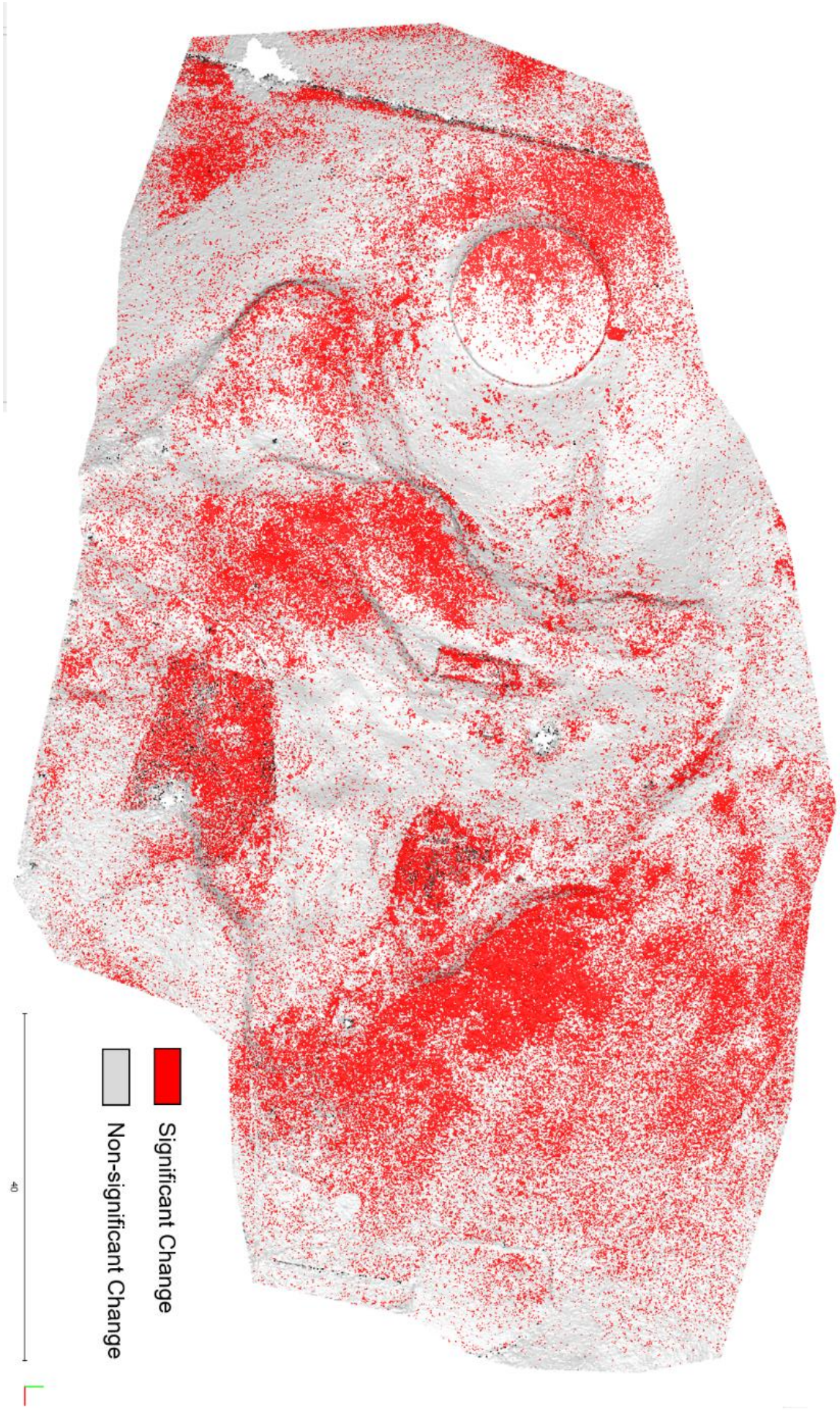
Significant Change
Non-significant Change

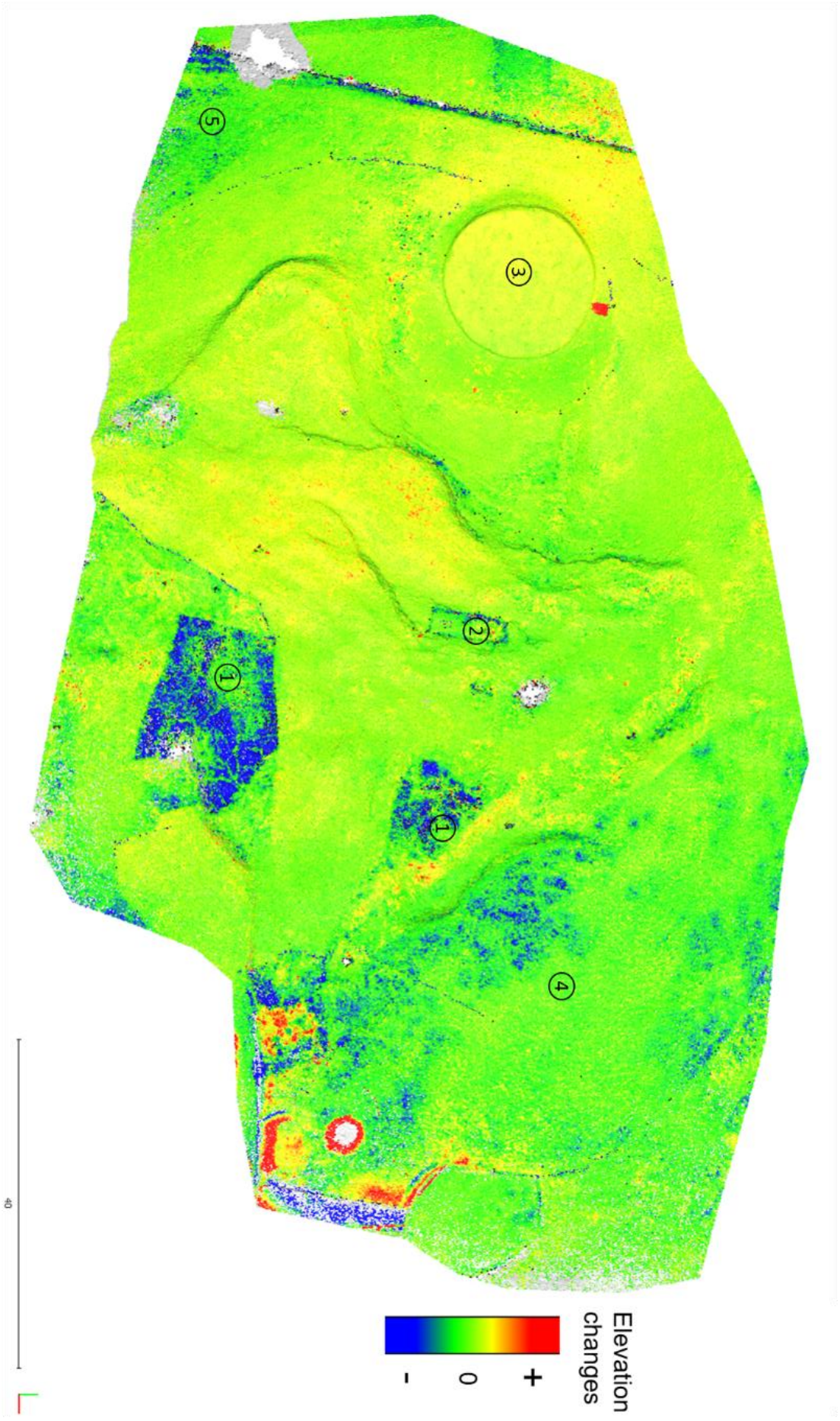
5
3
2
1
1
4
40
Elevation changes
-
0
+

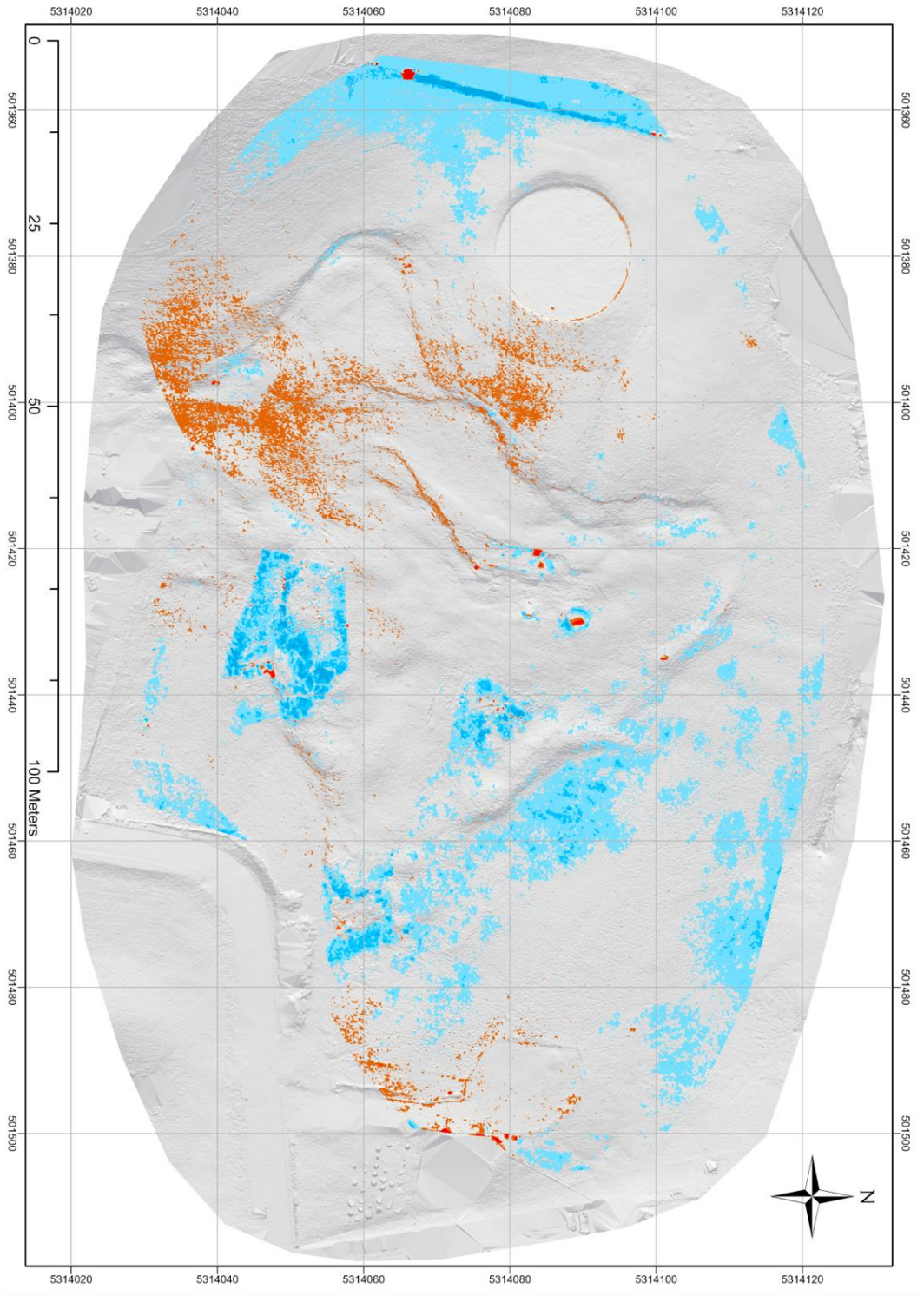

DoD
Salcher-landslide

18th November – 22nd February

Elevation difference [m]

- ≤ -0,2
- ≤ -0,1
- ≤ -0,03
- ≤ 0,03
- ≤ 0,1
- ≤ 0,2
- ≤1

Coordinate system: WGS 1984 UTM Zone 33N
Projection: Transverse Mercator

hillshade background for displaying purposes

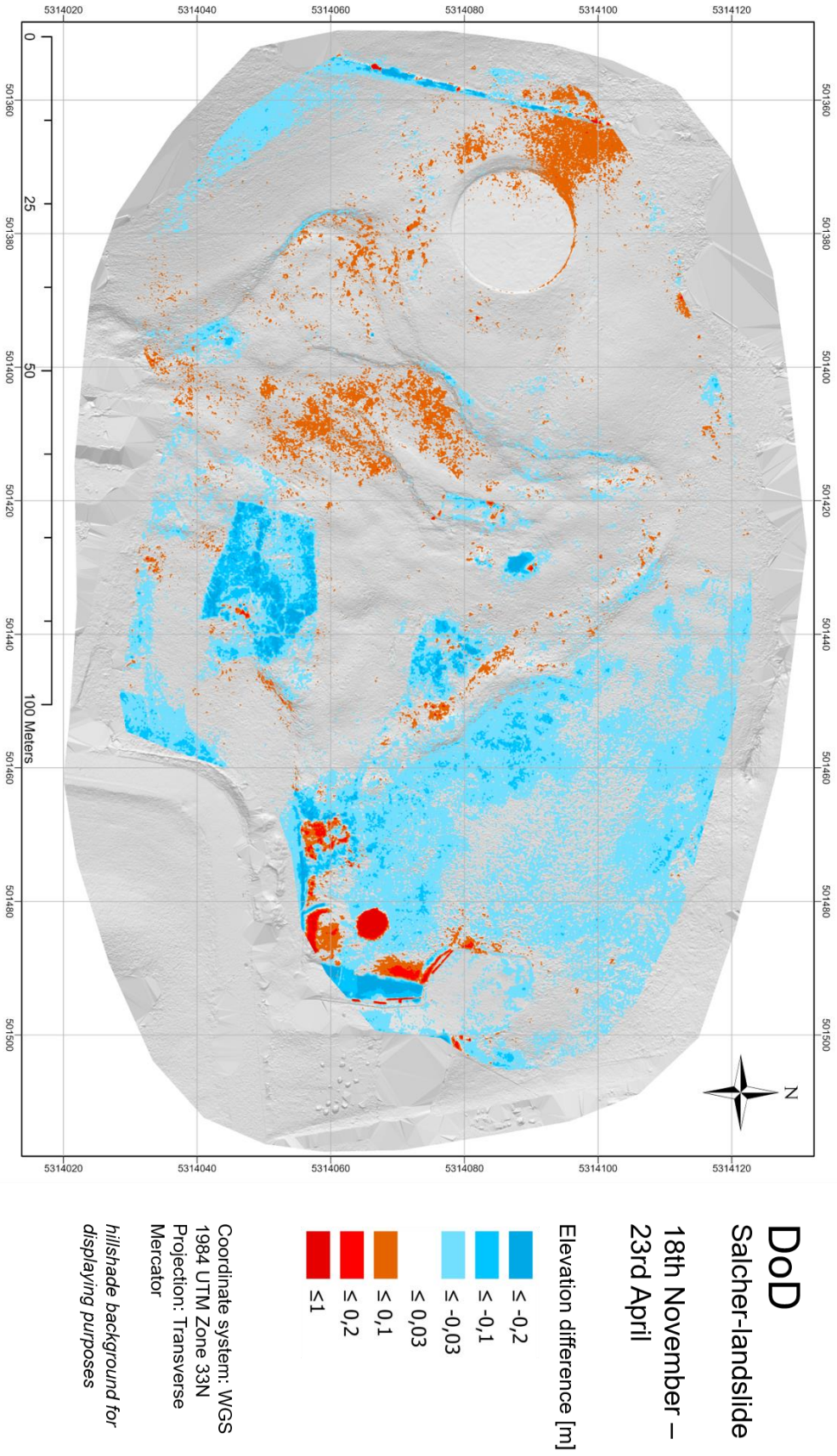
5314020
5314040
5314060
5314080
5314100
5314120
501360
501380
501400
501420
501440
501460
501480
501500
0
25
50
100 Meters
N
DoD
Salcher-landslide
18th November – 23rd April
Elevation difference [m]
≤ -0,2
≤ -0,1
≤ -0,03
≤ 0,03
≤ 0,1
≤ 0,2
≤1
Coordinate system: WGS 1984 UTM Zone 33N
Projection: Transverse Mercator
hillshade background for displaying purposes

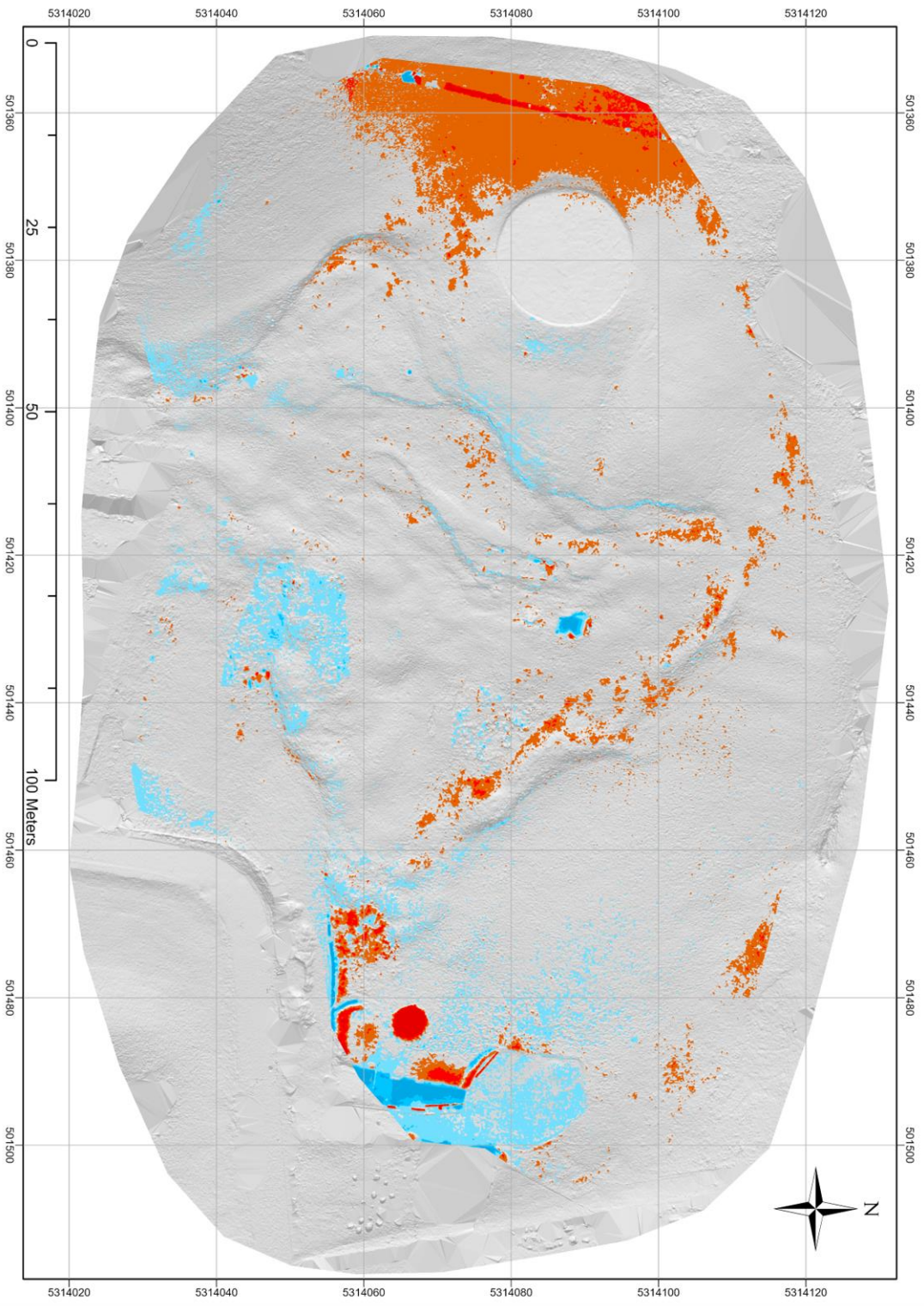

DoD
Salcher-landslide
22nd February – 23rd April

Elevation difference [m]

- ≤ -0,2
- ≤ -0,1
- ≤ -0,03
- ≤ 0,03
- ≤ 0,1
- ≤ 0,2
- ≤1

Coordinate system: WGS 1984 UTM Zone 33N
Projection: Transverse Mercator

hillshade background for displaying purposes

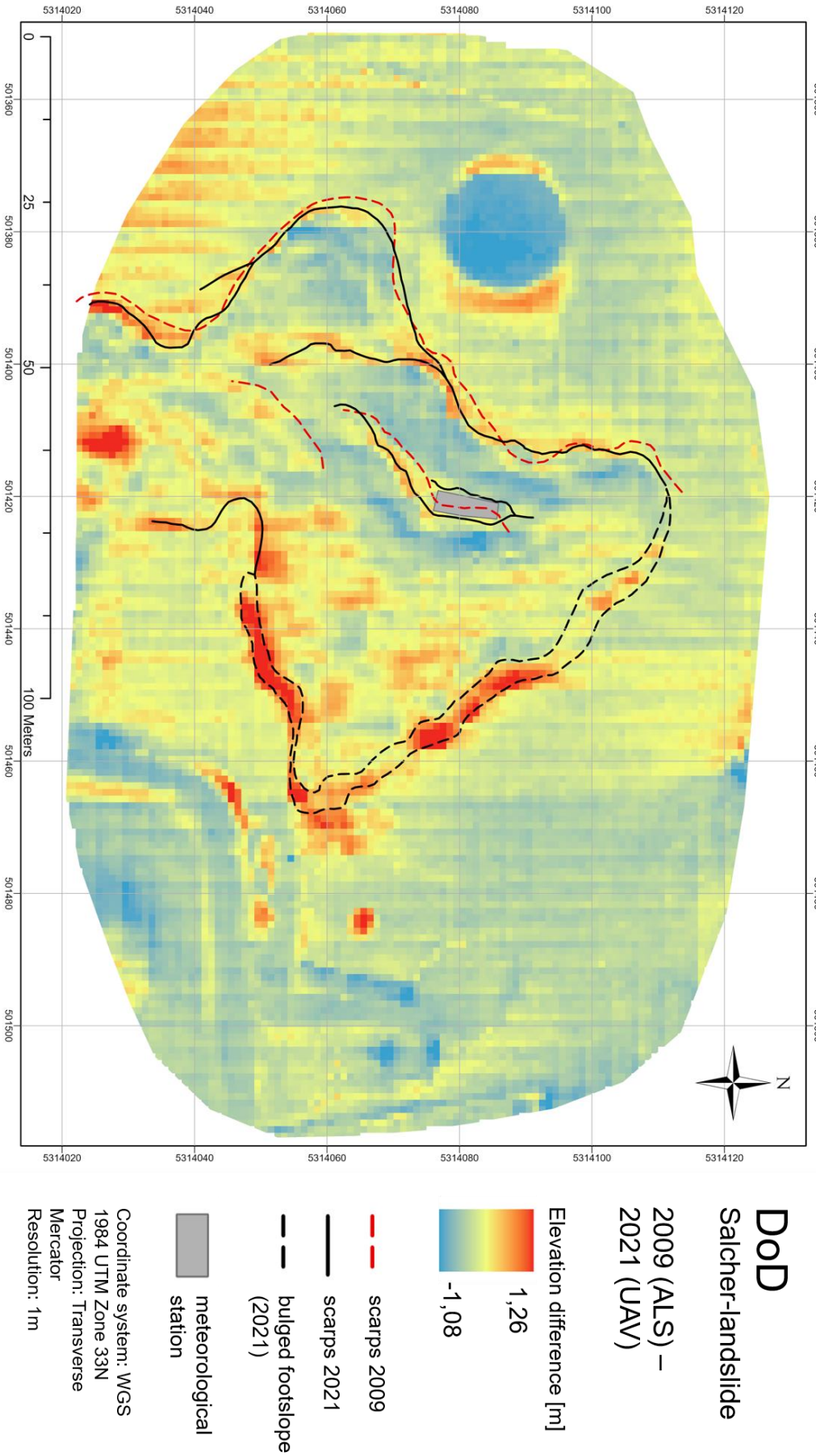
5314020
5314040
5314060
5314080
5314100
5314120
501360
501380
501400
501420
501440
501460
501480
501500
0
25
50
100 Meters
N
DoD
Salcher-landslide
2009 (ALS) –
2021 (UAV)
Elevation difference [m]
1,26
-1,08
scarps 2009
scarps 2021
bulged footslope
(2021)
meteorological
station
Coordinate system: WGS
1984 UTM Zone 33N
Projection: Transverse
Mercator
Resolution: 1m

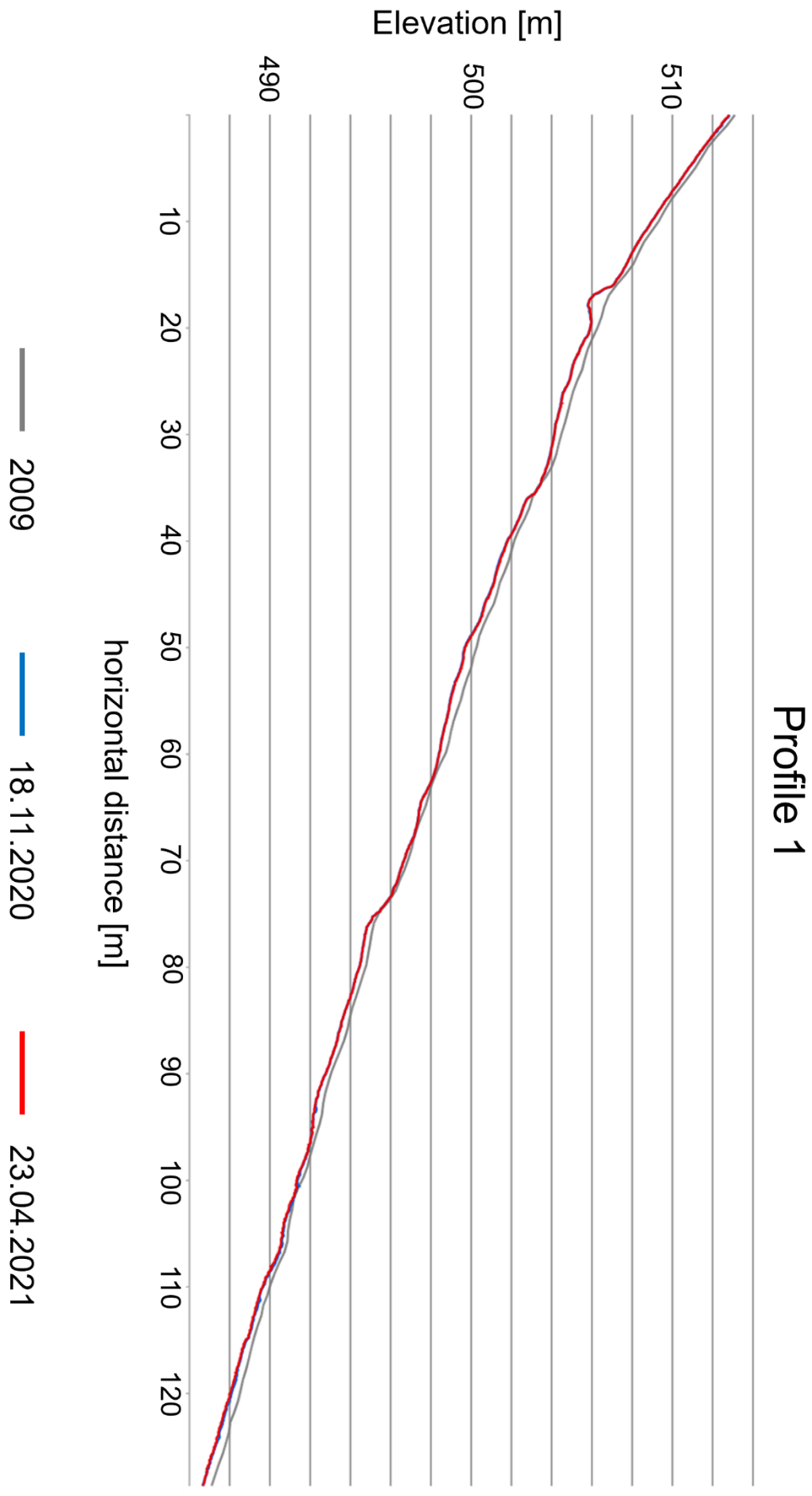
Profile 1
Elevation [m]
490
500
510
horizontal distance [m]
10
20
30
40
50
60
70
80
90
100
110
120
2009
18.11.2020
23.04.2021

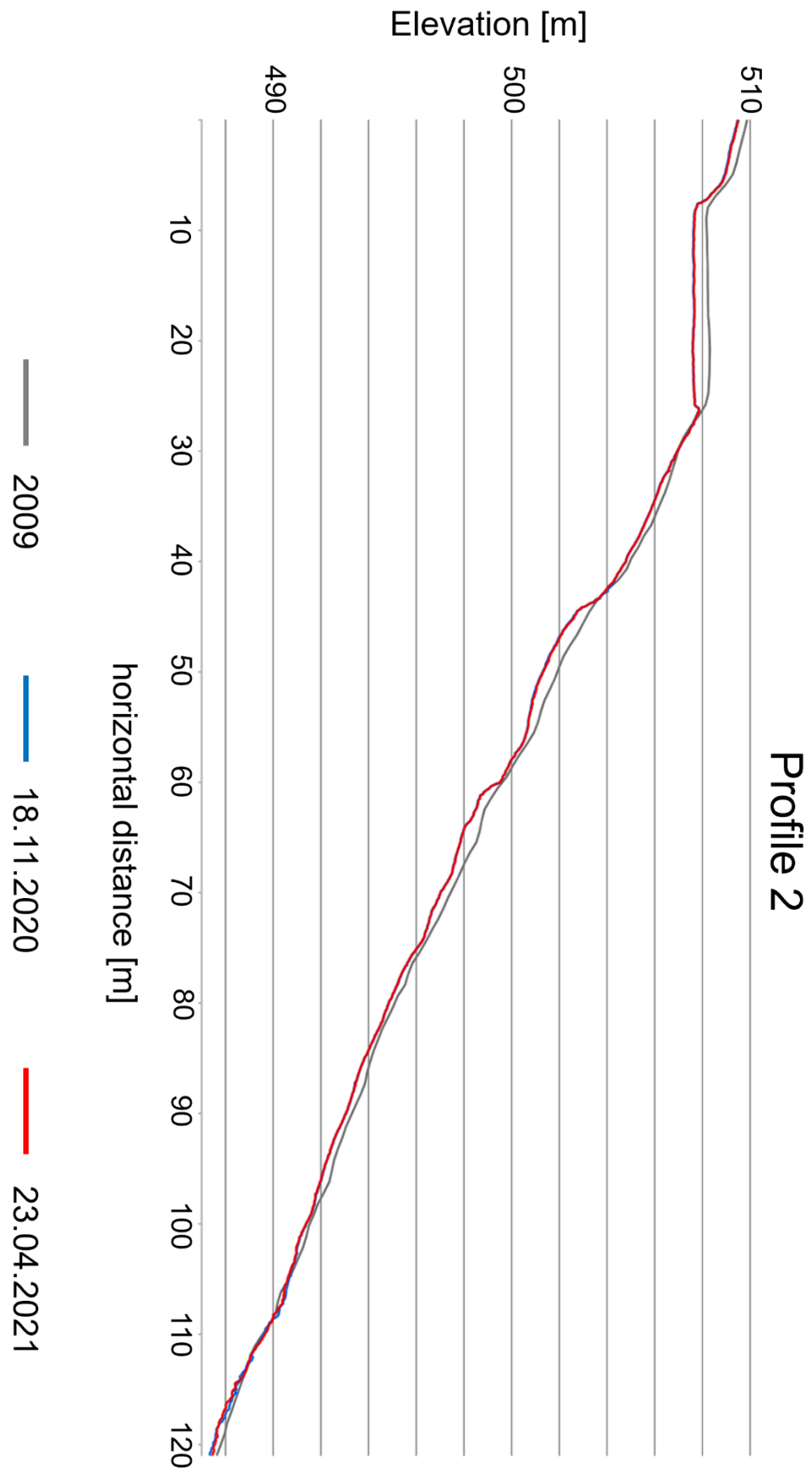
Profile 2
Elevation [m]
510
500
490
horizontal distance [m]
10
20
30
40
50
60
70
80
90
100
110
120
2009
18.11.2020
23.04.2021

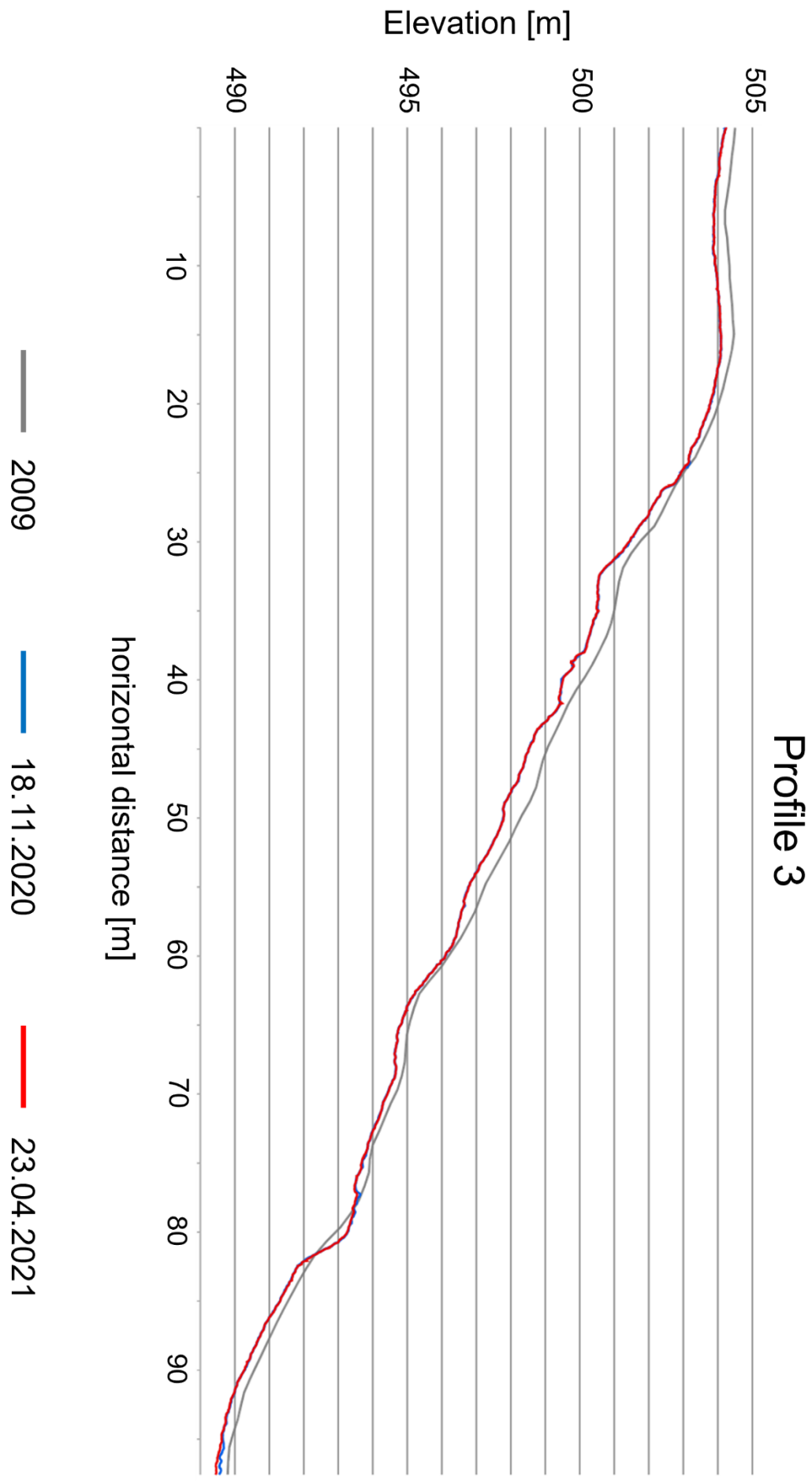
Profile 3
Elevation [m]
505
500
495
490
horizontal distance [m]
10
20
30
40
50
60
70
80
90
2009
18.11.2020
23.04.2021

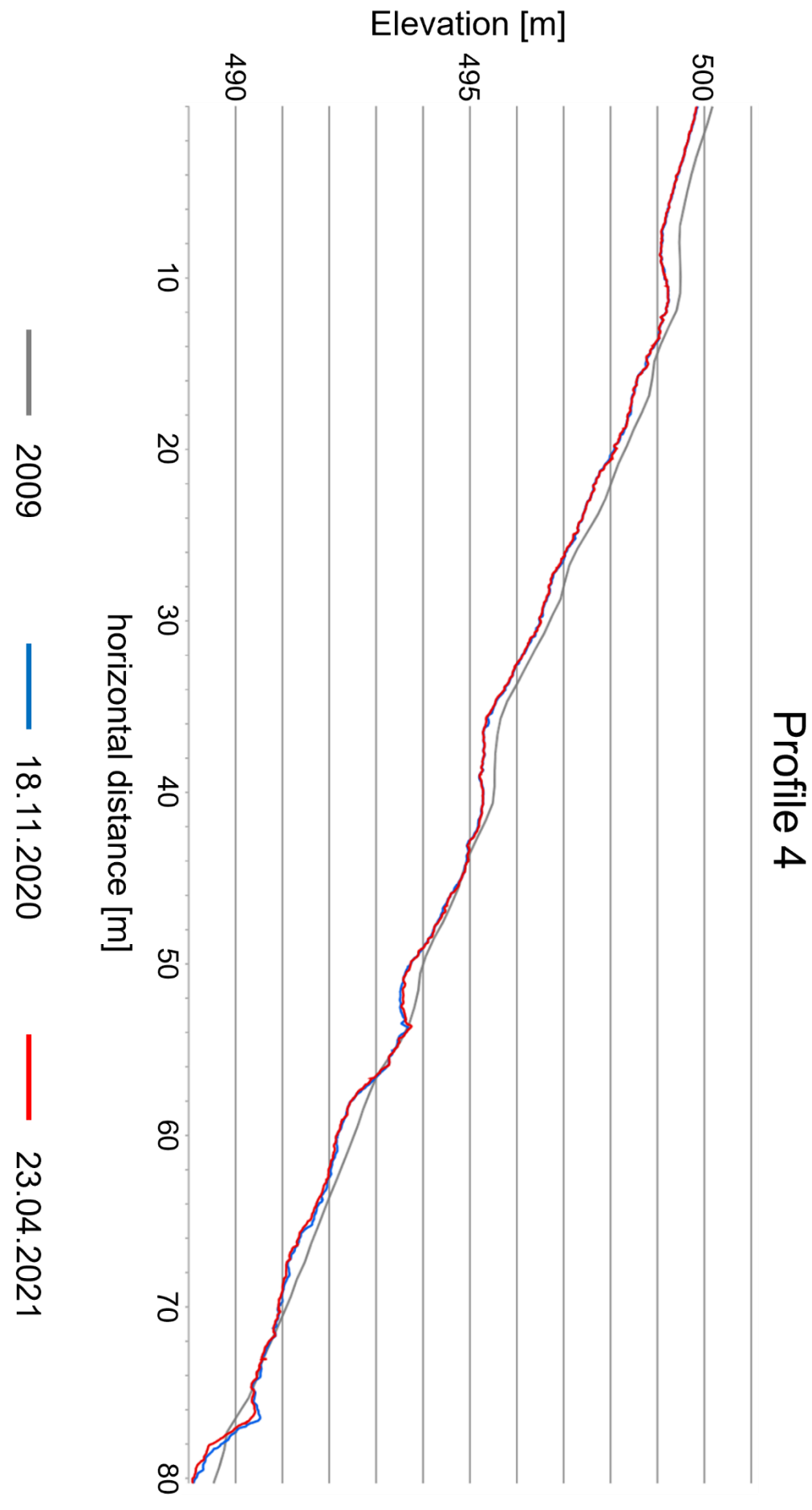
Profile 4
Elevation [m]
500
495
490
horizontal distance [m]
10
20
30
40
50
60
70
80
2009
18.11.2020
23.04.2021

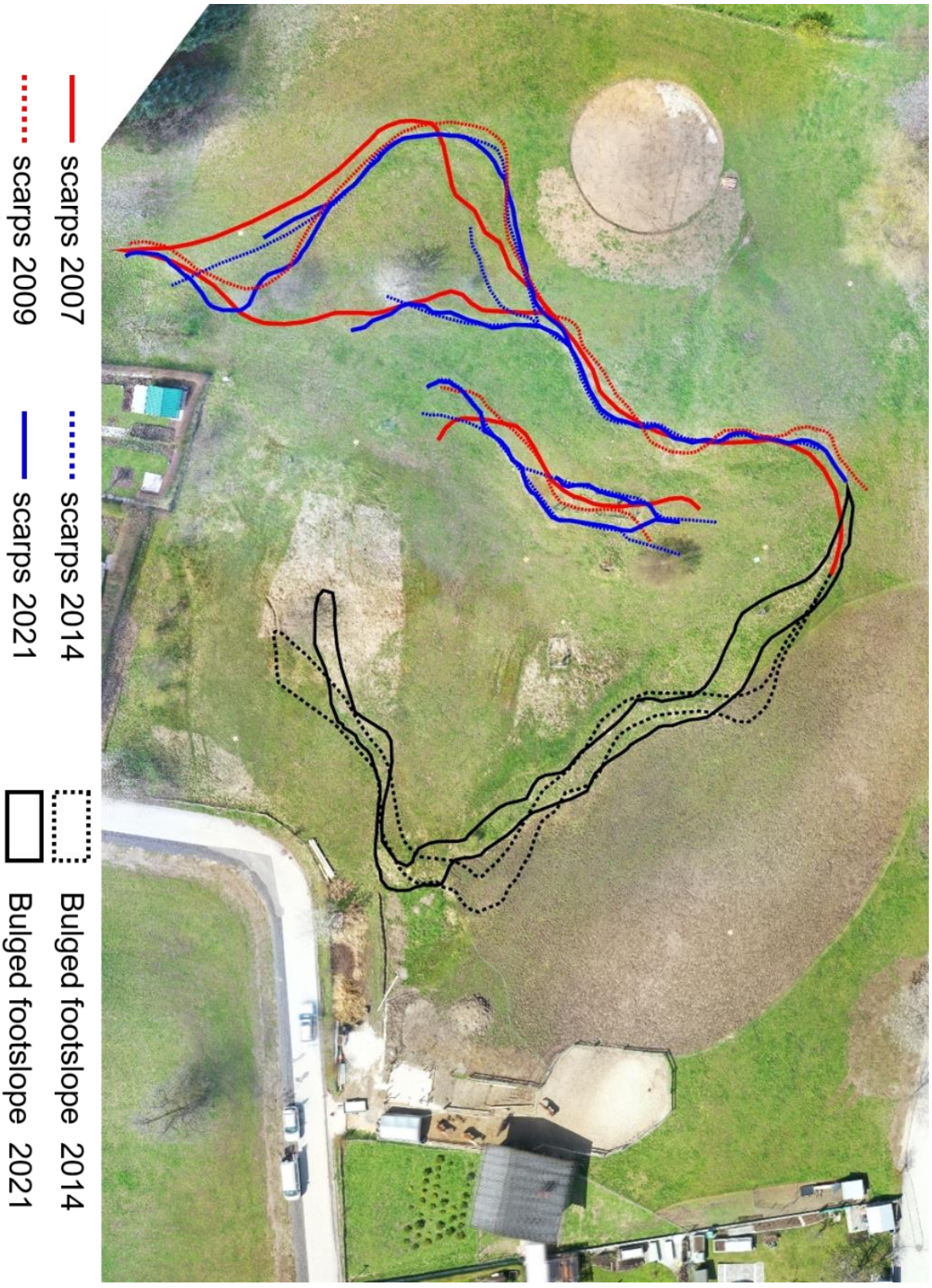
scarps 2007
scarps 2009
scarps 2014
scarps 2021
Bulged footslope 2014
Bulged footslope 2021